o

Thesis for the degree
of Candidatus Scientiarum

Thor Lichtenthaler

Ordering of oxygen vacancies in reduced phases of $CaMnO_{3-x}$ and $SrMnO_{3-x}$.

DEPARTMENT OF CHEMISTRY
FACULTY OF MATHEMATICS
AND NATURAL SCIENCES
UNIVERSITY OF OSLO 11/2005

Preface:

The work done in this thesis has been carried out at the Department of Chemistry at the University of Oslo and has been preformed under the supervision of Professor Helmer Fjellvåg and Doctor Ole Henrik Hansteen.

I wish to thank Helmer Fjellvåg and Ole Henrik Hansteen for guidance both theoretically and practically in the laboratory and theoretical work performed. I also wish to thank the scientific staff that has helped me and the students in my reading hall that I have shared so many excellent experiences with through this period. I would in particular like to thank Ole Bjørn Karlsen for always being willing to help me.

I would also like to thank all my friends who have encouraged me too push on.

At last and most importantly I wish to thank my family for the interest and enthusiasm you have showed on my behalf and for never giving up but always believing in me and encouraging me to complete my work. Without you it would not have been possible.

"Life is not measured in years, but by the deeds of Men"

Blindern, Oslo, November 2005

Thor Lichtenthaler

Abstract:

The structures of various $CaMnO_{3-x}$ and $SrMnO_{3-x}$ oxygen deficient compounds have been attempted solved from experimental diffraction patterns by Rietveld refinement. All samples used for this purpose have been synthesized with metallic manganese and $SrCO_3$ or $CaCO_3$ as starting materials. Samples of $CaMnO_3$ and $SrMnO_3$ have been produced with the Citric acid sol gel process. These samples have further been reduced by zirconium reduction in closed ampoules in order to obtain reduced phases. The zirconium added controls the oxygen content in the samples. Reoxidation of the totally reduced phases $SrMnO_{2.5}$ and $CaMnO_{2.5}$ in TGA furnaces show that the samples reoxidize fully between 400-600˚C when heated in air. The sample lose oxygen at temperatures above 800˚C

The refinement calculations have been based on various reported structural information in literature. The results show that only a few well defined structures exist with a high degree of certainty. These are $CaMnO_3$, $CaMnO_{2.5}$, $CaMnO_{2.75}$, $SrMnO_3$ and $Sr_2Mn_2O_5$. In the case of $CaMnO_{2.75}$ it is clear that the structure is not entirely solved. The extra reflections due to the superstructures are not fully understood and a space group has not been found. What has been verified is the unit cell of $CaMnO_{2.75}$ phase that was proposed in literature. Also, a neutron diffraction pattern of $CaMnO_{2.75}$ at low temperature revealed extra magnetic reflections. These have been assigned hkl values and a magnetic unit cell. A solution for the magnetic structure of the hexagonal $SrMnO_3$ is presented with ordering of the magnetic momentums.

The structures of $CaMnO_{2.8}$, $CaMnO_{2.667}$ and $CaMnO_{2.556}$ are not solved. There is no clear indication form the present work that they exist as separate phases. Nor is there any indication that $CaMnO_3$ samples quenched from temperatures above 1000˚C experience any oxygen deficiency at room temperature. The $SrMnO_{3-x}$ phase that earlier has been reported as a separate orthorhombic phase is presently identified as a mixture between $SrMnO_3$ and $Sr_2Mn_2O_5$.

Table of Contents:

Chapter 1: Introduction

1.1 Introduction

Compounds with the perovskite structure have been the subject for numerous studies through the last forty to fifty years due to the large variety of structural and physical (electrical and magnetic) properties that they inherit. A large group of these perovskites are ternary oxides with the formula ABO_3, and many of these have been investigated thoroughly from a structural point of view. Perovskites that contain B cations that inhabit 3d electrons are of great magnetic and electric interest, and the perovskites $CaMnO_3$ and $SrMnO_3$ are two of these. These perovskites have the ability to retain part of their structural framework when oxygen is removed from the lattice, creating oxygen deficient metastable phases. However, most of the investigations made until now are concentrated on only one, or a few different chemical compositions and structures, and there does not exist any direct understanding that takes into consideration the whole oxygen deficiency range from the phases of $CaMnO_3$ to $Ca_2Mn_2O_5$ and $SrMnO_3$ to $Sr_2Mn_2O_5$, although a few thorough investigations have been carried out. There are also some contradicting reports on structures in the $CaMnO_{3-x}$ and $SrMnO_{3-x}$ systems. The oxygen deficient materials are often referred to as reduced phases, related to the reduction of the B cation, in this case Mn. Both $CaMnO_3$ and $SrMnO_3$ are important end members in quaternary series of A cation substitution compounds $(A,A')MnO_3$, and a thorough investigation of the structures will contribute to improved understanding of their physical properties.

1.2 Background:

1.2.1: Cubic Perovskite:

"Perovskite" is originally the name of the mineral $CaTiO_3$. Today the term is generally used for oxides with the same type of atom arrangement as this mineral. The general formula for perovskite type structure is ABX_3, where A typically is an alkaline earth or rare earth cation and B typically a transition metal cation. The anion X is typically

oxygen, but perovskites with halogens, nitrogen and hydrogen are also known to exist. The ideal perovskite structure is cubic, and can be described as A cations surrounded by 12 O anions (12 coordination), and B cations in octahedral holes created by the oxygen lattice. The B ions are thus coordinated by 6 oxygen atoms. The space group of the ideal cubic perovskite structure is $Pm\bar{3}m$. In the ideal perovskite structure the BO_6 octahedra are all sharing corners. The cubic perovskite can also be described as a cubic ccp stacking of AO_3 layers. An illustration of the perovskite type structure is shown in figure 1.1

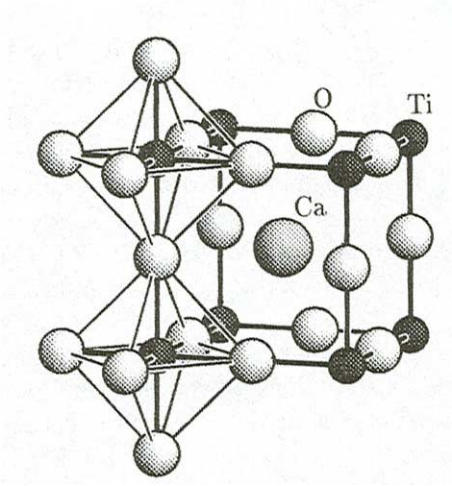

Figure 1.1: A schematic illustration of the perovskite type structure. 12 coordinated Ca and 6 coordinated Ti in O octahedra.

1.2.2 Hexagonal perovskite:

There exist perovskites that have hexagonal stacking of the AO_3 layers. This means packing sequences of AB, AC (hexagonal stacking is also denoted h) or both of the AO_3 layers. These are referred to as hexagonal perovskites. This term is used for all hexagonal perovskites even though both hexagonal and cubic stacking sequences of AO_3 layers occur. The exception to this is the ideal 2 layered hexagonal perovskite that has only hexagonal stacking. The ideal space group for hexagonal perovskites is $P6_3/mmc$. The tolerance factor, equation 1.1 which is discussed in chapter 1.3 (page 7) is higher for hexagonal perovskites. This implies that they are normally favoured when the A cation ionic radii (and A/B ratio) is large like Ba or Sr (i.e. $BaNiO_3$, $BaTiO_3$ and $SrMnO_3$).

1.2.3 Orthorhombic and Tetragonal perovskites:

Orthorhombic and tetragonal perovskites are modifications of cubic perovskites with tilted or distorted octahedra due to either cation interactions or oxygen vacancies. These can modify the axis lengths and bring the perovskite to lower symmetry. Perovskites like these are often referred to as pseudo cubic or pseudo tetragonal to indicate that they only have minor differences from these symmetries. Orthorhombic and tetragonal unit cells can be seen in figure 1.3 under chapter 1.4, superstructures.

1.3 Non-stoichiometry:

Most perovskite oxides inhabit non-stoichiometry to a smaller or larger extent, and this has great influence on their properties. The most common type of non-stoichiometry in $CaMnO_3$ or $SrMnO_3$ is anion vacancies. Removal of one oxygen atom will lead to the reduction of two Mn^{4+} atoms to Mn^{3+} atoms. Two MnO_6 octahedra will at the same time turn into MnO_5 square pyramids. When oxygen is removed from the structure, it is possible for the vacancies to order into stable or metastable structures, of partly reduced phases. Figure 1.2a, 1.2b and 1.2c show how two MnO_6 octahedra change into two MnO_5 square pyramids by the removal of one oxygen atom. The right illustration (figure 1.2c) shows the structure that appears when all Mn^{4+} ions are reduced to Mn^{3+}.

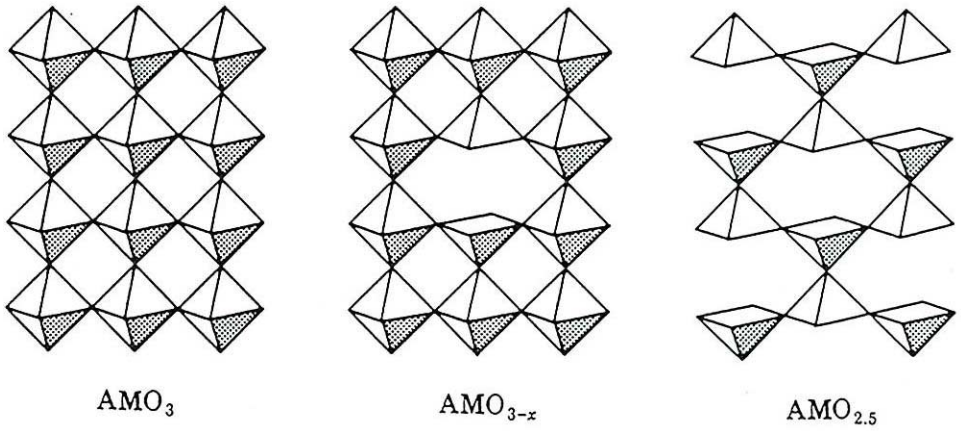

Figure 1.2a, 1.2b and 1.2c: Illustration of the removal of one oxygen atom from MnO_6 octahedra to form two MnO_5 square pyramids (1.2a and 1.2b), and the condition where this has happened to every MnO_6 octahedra.

In the ideal cubic perovskite type structure the cations must be of adequate size in order to favour the 6 and 12 coordination provided by the oxygen sub lattice. In most cases of perovskites or perovskite like structures investigated, the radii of the cations differ from those required by the ideal structure, and the structures become distorted. A correlation between ion radii and the perovskite structure was proposed by Goldschmidt and is expressed in terms of the tolerance factor t:

$$t = (r_A + r_O)/\sqrt{2}(r_B + r_O) \qquad \text{Equation 1.1}$$

where r_A, r_B and r_O are the radii of the A, B and O ions. The perovskite structures occur only when the tolerance factor is between 0,75 and 1,00. In addition the cations must be stable in twelve fold (12, 8+4 or 6+6) coordination. This limits the radius of the cations to $r_A > 0{,}09$ Å and $r_B > 0{,}51$ Å, respectively. The mentioned structural distortion can be viewed as a rotation of the BO_6 octahedra along one or more crystallographic directions or as a slight displacement of one or more of the cations from their ideal positions, leading to lower symmetry.

1.4 Superstructures:

Perovskite materials can in many respects be said to show superstructures. A superstructure has an enlarged unit cell, but has the same basic structural building principle as the material it is a superstructure to. In $CaMnO_3$ and $SrMnO_3$ oxygen vacancies give rise to doubling of one, two or three edges of the unit cell, thus creating superstructures. A relevant example is Reller et al [1] who observed superstructures for reduced phases of the parent compound $CaMnO_3$. The superstructures are often given as factors of the cubic unit cell length a_c (a_c = 3.73 Ångstrøm) and an angle of rotation of the unit cell by an angle R. In example a tetragonal unit cell can have an orthorhombic superstructure. In figure 1.3 cubic, tetragonal and orthorhombic unit cells are shown in projection of the x-y plane. The tetragonal unit cell (b) can be described as $\sqrt{5}a_c$ x $\sqrt{5}a_c$ R= 30° and the orthorhombic (c) can be described as$\sqrt{2}a_c$ x $2\sqrt{2}a_c$ R= 45° in terms of the cubic perovskite.

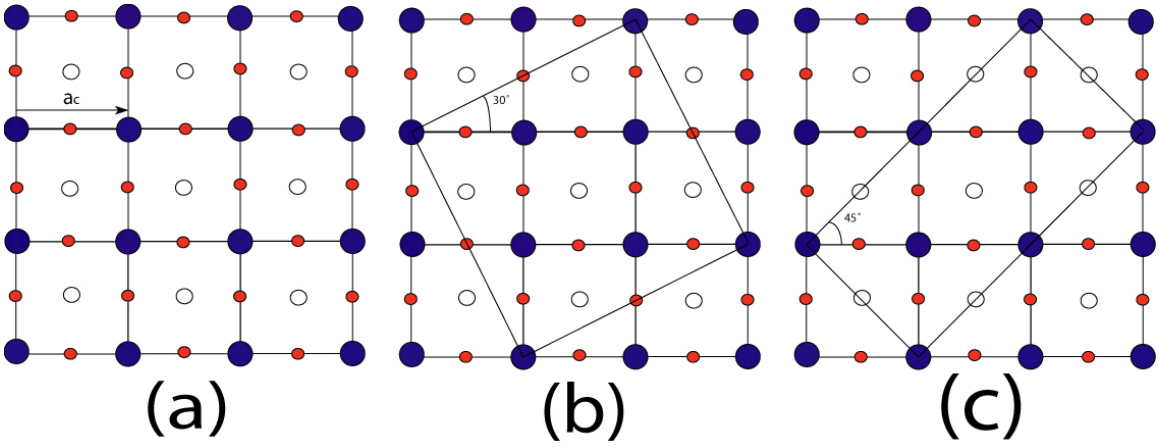

Figure 1.3: Cubic (a), tetragonal (b) and orthorhombic (c) unit cells. The tetragonal and orthorhombic cells can be described in terms of the cubic unit cell. Ca is blue, Mn white and oxygen red. Oxygen above and below Mn are not drawn.

1.5 Earlier work on structural properties of $CaMnO_3$ and $SrMnO_3$:

An enhanced interest in ABO_3 perovskites was probably initiated by Jonker and Van Saten [2] with their discovery of ferromagnetism in manganese compounds with perovskite structures in 1950. They investigated a number of perovskites with manganese

as the B cation, including $CaMnO_3$ and $SrMnO_3$, and pointed out important novel features related to exchange interactions between Mn^{3+} and Mn^{4+}. The fact that Mn^{3+} and Mn^{4+} exist simultaneously, and that their ratio can be tuned chemically, gave rise to great interest in the ABO_3 and reduced perovskite structures. Investigations with the aim to describe the structures in detail therefore began. In the $CaMnO_3$-$CaMnO_{2.5}$ oxygen deficiency range both Poeppelmeier and Reller made investigations, and sought to discover new structures. Their work and others are described in this chapter. Here follows a brief summary of the results reported.

1.5.1 $CaMnO_3$ – $CaMnO_{2.5}$

1.5.1.1 $CaMnO_3$:

In a magnetic study of manganese phases, MacChesney et al [3] reported lattice constants for $CaMnO_3$. They determined the oxygen content to $CaMnO_{2,98}$ in his phase. No detailed structural investigation was made. The first structural investigation was made by Poeppelmeier et al [4]. They prepared single crystals up to 0.5 mm in dimension. The lattice parameters where refined from 25 reflections. Poeppelmeier found the space group Pnma. Atom positions where also determined. Reller et al [1] also found the unit cell of this phase by using high resolution electron microscopy (HREM). They found slight cation displacements to the framework from cubic symmetry. The displacement could be described as an orthorhombic phase which also was in agreement with the finding of MacChesney et al [3]. Reller also claimed to have observed a tetragonal unit cell for $CaMnO_3$. Table 1.1 below summarises the results.

	a (Å)	b (Å)	c (Å)
MacChesney[3]	5.270	7.64	2.75
Poeppelmeier[4]	5.279	7.448	5.264
Reller (orthorhombic)[1]	5.275	7.46	5.275
Reller (tetragonal)[1]	7.46	7.46	3.73

Table 1.1: Reported unit cell dimensions of $CaMnO_3$.

1.5.1.2 $Ca_2Mn_2O_5$:

Poeppelmeier [5] et al first investigated the ordered oxygen defect phase $Ca_2Mn_2O_5$ by x-ray diffraction and found an orthorhombic unit cell. The findings were confirmed with neutron data by Poeppelmeier et al [4] in a later publication. The space group found was Pbam, atom positions, bond lengths and lattice constants were reported. Reller et al [1] also observed the unit cell dimensions in his HREM study, but claimed to also see three other types of oxygen orderings in addition to the one found by Poeppelmeier. In this study Reller et al expressed the structures as superstructures in terms of the ideal cubic perovskite as described under chapter 1.4. For this composition the angle of rotation was 45°. The results are summarized in table 1.2.

	a (Å)	b (Å)	c (Å)
Poeppelmeier[4]	5.424	10.230	3.735
Reller[1]	$\sqrt{2}$ x $a_c \approx 5{,}275$	$2\sqrt{2}$ x $a_c \approx 10.55$	$a_c \approx 3.73$
Reller[1]	$\sqrt{2}$ x $a_c \approx 5{,}275$	$3\sqrt{2}$ x $a_c \approx 15{,}825$	$a_c \approx 3{,}73$
Reller[1]	$\sqrt{2}$ x $a_c \approx 5.275$	$4\sqrt{2}$ x $a_c \approx 21{,}1$	$a_c \approx 3{,}73$

Table 1.2: Summary of the reported unit cell dimensions for $Ca_2Mn_2O_5$.

1.5.1.3 $CaMnO_{2.75}$:

In the HREM study by Reller et al [1] a proposed structure for $CaMnO_{2.75}$ was made up of 50% of MnO_6 octahedra and 50% MnO_5 square pyramids. HREM studies revealed orthorhombic symmetry. Another structural investigation by Chiang –Poeppelmeier et al [6] using x-ray and neutron data analysis was done some years later. They also found an orthorhombic structure, but with doubled b axis. The x-ray diffraction pattern contained some impurities of the phase $Ca_2Mn_2O_5$ and these where subtracted from the scan. Chiang-Poeppelmeier also studied a neutron data set. They used the space group $Pmc2_1$ and it gave a good fit to the observed neutron powder diffraction pattern. The bond lengths and thermal parameters he obtained were not meaningful, however, and he concluded that space group could not be correct. The unit cell dimensions reported for this composition are summarized in table 1.3.

	a (Å)	b (Å)	c (Å)
Reller[1]	5,35	10,50	7,46
Poeppelmeier[4]	5,35	20,96	7,47

Table 1.3: Unit cells dimensions for $CaMnO_{2.75}$.

The compositions $CaMnO_3$, $Ca_2Mn_2O_5$ and $CaMnO_{2.75}$ are those that have been studied most intensively.

1.5.1.4 Other reported $CaMnO_{3-x}$ phases:

Reller et al [1] reported more metastable phases in their HREM study. The phases they obtained by heating in oxygen free atmospheres. These phases were expressed as superstructures of the cubic perovskite as described in 1.5.1.2 for the $Ca_2Mn_2O_5$ phase. In example, the lattice constants for the phase $CaMnO_{2.8}$ were given as $\sqrt{5}a_c$ x $\sqrt{5}a_c$ x R26.5° where a_c = 3,73Å (a_c being the idealized lattice constant of the cubic perovskite). As already mentioned Reller et al [1] had described phases of $CaMnO_3$, $Ca_2Mn_2O_5$ and $CaMnO_{2.75}$. The new phases reported by Reller et al [1] are summarized in table 1.4:

	a (x a_c)	b (x a_c)	Angle of rotation (°)
$CaMnO_{2.8}$	$\sqrt{5}$	$\sqrt{5}$	26.5
$CaMnO_{2.667}$	$\sqrt{2}$	$3\sqrt{2}$	45

Table 1.4: Observed new phases by Reller et al [1] observed in HREM.

In addition Reller et al [1] predicted another phase, $CaMnO_{2.556}$, and expressed the unit cell as given in table 1.5.

	a (x a_c)	b (x a_c)	Angle of rotation (°)
$CaMnO_{2.556}$	$3\sqrt{3}$ a_c	$3\sqrt{3}$ a_c	45

Table 1.5: Theoretically described phase by Reller et al [1].

Other $CaMnO_{3-x}$ compositions have been proposed with different oxygen contents. No attempts to solve the structures of any of these $CaMnO_{3-x}$ compositions have been preformed. In 1985 Taguchi et al [7] reported phases with the oxygen content $CaMnO_{2.92}$

and $CaMnO_{2.85}$. In 1998 Taguchi et al [8] reported new phases again. This time he reported the phases $CaMnO_{2.65}$ and $CaMnO_{2.56}$ which he had obtained by high temperature x-ray measurements at the temperatures of 920°C and 900°C respectively. No attempt to solve the structure was done in either publication and no x-ray patterns were presented. Except from oxygen content measurements no indication that these compositions exist as structures at normal conditions was presented. In 1998 Britacio et al [9] attempted to produce the compositions $CaMnO_{2.84,}$ $CaMnO_{2.75}$ and $CaMnO_{2.66}$. No approach to solve the structures was performed, and they could not conclude that the oxygen content they found in each sample reflected a new phase. Zeng and Greenbladt et al [10] quenched samples from 1100°C and 1000°C and found these to be $CaMnO_{2.89}$ and $CaMnO_{2.94}$ respectively. Again no x-ray diffraction patterns or structure models were provided, and Zeng and Greenbladt viewed them as belonging to the $CaMnO_3$ orthorhombic phase.

1.5.2 $SrMnO_3$ – $SrMnO_{2.5}$

1.5.2.1 $SrMnO_{3-x}$:

In 1968 Syono et al [11] reported two structures for $SrMnO_3$. They reported both a normal and high pressure form and called them $SrMnO_3$ I and $SrMnO_3$ II. Both of these structures where indexed as hexagonal. They proposed abac stacking of the SrO_3 units for $SrMnO_3$ I, and abcacb stacking for $SrMnO_3$ II. These forms were also given the names hexagonal 4H (four layer) and hexagonal 6H (six layer) respectively with reference to their hexagonal stacking order. The unit cells are listed in table 1.6

	a (Å)	b (Å)	c (Å)
$SrMnO_3$ I	5,449		9,055
$SrMnO_3$ II	5,431		13,396

Table 1.6: Unit cell dimensions for $SrMnO_3$ high and low pressure form found by Syono et al [11].

Chamberland et al [12] also studied the high and low pressure forms of $SrMnO_3$, and confirmed the same stacking sequence as Syono et al. They also studied the magnetic

susceptibility of the two phases. They found that the six layered high pressure form was antiferromagnetic with an ordering temperature of 90K. The four layered low pressure form showed completely different behaviour and did not obey any Currie –Weiss law under 800K.

It was Negas and Roth [13] who first contributed extensively with an investigation of the $SrMnO_{3-x}$ system. They discovered that four layered $SrMnO_3$ heated in air retains its composition until 1035°C. At this temperature $SrMnO_3$ begins to give away oxygen until 1400°C where it reaches the composition of $SrMnO_{2.89}$, and a phase transition occurs. A homogeneity range of different oxygen contents exists in this temperature range, while the framework is still intact. The cubic perovskite has ABC stacking of the AO_3 units. $SrMnO_3$ keeps the four layered hexagonal perovskite like structure build up of four close packed layers of SrO_3 units stacked in ABAC sequence until about 1169°C. Phases between 1170°C and 1400°C Negas and Roth indexed on the basis of an orthorhombic distortion of the hexagonal structure. At 1400°C a discontinuity in the oxygen loss was found and the following reaction was presumed to happen.

$$SrMnO_{2.89} \leftrightarrow SrMnO_{2.74} + 0.075O_2 \qquad \text{Equation 1.2}$$

Above 1400°C they found a new homogeneity range to exist from $SrMnO_{2.74}$ until melting point at 1740°C where the composition reaches $SrMnO_{2.62}$. In this range the powder pattern was indexed as an orthorhombic distortion of the hexagonal perovskite like $SrMnO_{3-x}$ phase with axis lengths changing with the oxygen content. Near the melting point the diffraction patterns of the quenched specimen became poor. Negas and Roth noted, however, that by decreasing the oxygen pressure and temperature, the orthorhombic perovskite like phases could be prepared with even lower oxygen content than $SrMnO_{2.62}$. These diffraction patterns were considerably better. Negas and Roth also discovered quite interestingly that if the high temperature quenched phases where allowed to reoxidize metastably at lower temperature the distorted perovskite converts rapidly into cubic perovskite. Temperatures as low as 150° C and times as short as 10 minutes were sufficient. The diffraction pattern of the cubic perovskite was indexed and

reported together with d values, intensities and hkl numbers. The unit cell dimensions are summarized in table 1.7

Structure	Temperature Range (˚C)	a (Å)	b (Å)	c (Å)
4L hexagonal	0-1035	5,669		9,38
Orthorhombic 4L-hex like	1035-1400	9,452	5,467	9,105
Orthorhombic perovskite like	1400-1700	5,43	3,81	5,44
Cubic	Reox. 150	3,806		

Table 1.7: Unit cells dimensions and experimental temperatures for the structures found for $SrMnO_{3-x}$ found by Negas and Roth [13].

Kuroda et al [14] investigated thoroughly the four layer hexagonal $SrMnO_3$ phase, that had been investigated earlier [11]. From single crystal x- ray they found the space group $P6_3/mmc$, but also discovered that the Sr (1) atom was distorted along the c axis statistically as half atoms with z = 0.012. This model gave a better fit to the observed diffraction pattern than the earlier models.

Kriegel et al [15] confirmed the 4H $SrMnO_3$ structure that had been described earlier by Syono [11], Negas and Roth [13] and Kuroda [14] and also investigated the cubic $SrMnO_3$ together with an orthorhombic reduced phase. Their results are summarized beneath in table 1.8.

	Space group	a (Å)	b (Å)	c (Å)
$SrMnO_3$ hexagonal	$P6_3/mmc$	5,4437		9,0685
$SrMnO_3$ Cubic	$Pm\bar{3}m$	3,8037		
$SrMnO_{2.58}$ Orthorhombic		5,5168	10,7650	3,8091

Table 1.8: Space groups and unit cell dimensions found by Kriegel et al [15].

A reinvestigation of $SrMnO_3$ was done by Battle and Gibb [16] in 1987 with neutron diffraction and Moessbauer spectroscopy. They confirmed the space group $P6_3/mmc$, but refined the unit cell parameters. They also tested the half atom Sr(1) model of Kuroda et al [14], but this did not improve the refinement They where able to reproduce the

magnetic results found by Chamberland et al, but their interpretation of the data was different. Battle and Gibb interpreted the data to short range antiferromagnetic ordering only, and not long range like Chamberlain et al had proposed. The results are shown in table 1.9.

	Space group	a (Å)	b (Å)	c (Å)
$SrMnO_3$ 4H	$P6_3$ /mmc	5,4434		9,0704

Table 1.9: The results of Battle and Gibb [16].

In 1991 Shibahara [17] published synthesis procedures of the different $SrMnO_3$ phases together with x-ray diffraction patterns and HREM studies. He reproduced the results of Negas and Roth [13]. He also described a model for how the 4H $SrMnO_3$ phase transformed into the non-stoichiometric state by a displacement of the face sharing octahedra caused by the oxygen defects. The stacking sequence where the displacement took place, by a displacement vector of ± [110], gave rise to corner sharing octahedra. Eventually this displacement resulted in formation of a cubic stacking.

In 2003 Sedmidubsky et al [18] reported single crystal x-ray diffraction that revealed that the $SrMnO_{3-x}$ phase could be indexed as pseudo-orthorhombic with 25 formula units per unit cell and space group Pm. They also found a smaller unit cell containing 5 formula units within the larger unit cell. This unit cell was also pseudo orthorhombic. The results are listed in table 1.10

	a (Å)	b (Å)	c (Å)
Pseudo Orthorhombic	19,244	3,813	19,299
Smaller Pseudo Orthorhombic	8,601	3,813	8,606

Table 1.10: Two pseudo orthorhombic unit cells found for $SrMnO_{3-x}$ by Sedmidubsky [18].

1.5.2.2 $Sr_2Mn_2O_5$:

In 1985 Caignaert et al [19] managed to obtain the phase $Sr_2Mn_2O_5$. They used zirconium in a closed ampoule to obtain adequate loss of oxygen at 500°C. The diffraction pattern

yielded an orthorhombic cell with the space group Pbam which unit cell could be described by the idealized cubic perovskite. The structure was the same as that found for $Ca_2Mn_2O_5$. They also found an antiferromagnetic behaviour at low temperature, with an ordering temperature T_N at 380 ± 10K. They noted however that some impurities might be present, and to a small degree increase the sucsesibility at low temperatures. The unit cell is listed in table 1.11.

	a	b	c
$Sr_2Mn_2O_5$	5,523	10,761	3,811
In terms of a_c	$a_c \sqrt{2}$	$2 \sqrt{2}a_c$	a_c

Table 1.11: The unit cell of $Sr_2Mn_2O_5$ reported by Caignaert [19]. The cell dimensions are given both in axis lengths and in terms of idealized perovskite.

In Caignaert et al's [20] next work, a HREM study on the same compound, the lattice constants were confirmed. Caignaert also noticed differently oriented domains in the crystals. At the boundaries of these domains face sharing octahedra were observed.

In 1999 Mori et al [21] made a neutron study of $Sr_2Mn_2O_5$. Mori used the symmetry predicted by Caignaert, and found very good results for the crystal structure. They performed neutron studies at 20K, and found additional reflections that were purely magnetic. The new unit cell had changed by a doubling of the c axis in regard to the crystallographic cell. The results are summarized in table 1.12:

	Space group	a (Å)	b (Å)	c (Å)
Crystal	Pbam	5,5307	10,7829	3,8145
Magnetic	Pnnm	5,499	10,737	7,600

Table 1.12: Space groups and unit cells of the crystal and the magnetic unit cell of $Sr_2Mn_2O_5$ found by Mori et al [21].

1.6 Objective:

There is good reason to believe that there exist well ordered oxygen deficient structures in both the systems of $CaMnO_{3-x}$ and $SrMnO_{3-x}$. By controlling the amount of manganese

that is to be reduced it is possible to attempt to draw structures where every second, third or fourth and so on oxygen position is vacant. The manganese can then be reduced to the desired content. By this theoretical approach it is my wish to investigate the phases that can retain their oxygen deficiency at standard conditions, and to determine their structures by modelling the x-ray and neutron diffraction patterns they yield with the Rietveld GSAS refinement pack. The different diffraction patterns collected are home XRD, synchrotron XRD and neutron. These patterns can when solved give information on both the crystal and magnetic space group and unit cell in addition to the atom positions.

Chapter 2: Materials and Experimental Methods

2.1 Synthesis of $CaMnO_3$ and $SrMnO_3$

The single phase synthesis of the $SrMnO_3$ and $CaMnO_3$ perovskites that were later used as starting materials for reduction was performed using the Citric acid sol-gel process. When synthesising complex oxides it is important to choose a route that involves good mixing of the reactants. Ideally the mixture should be on an atomic scale in order to reduce the diffusion length, time of temperation, need for crushing and repeated annealing. Starting materials, $CaCO_3$ and $SrCO_3$ are mixed in melted citric acid under the addition of water. The carbonates are always heated at 200˚C before use so that internal moisture is removed. Table 2.1 lists the materials used

Distributor/ Brand	Name	Chemical Formula	Purity
Fluka	Strontium Carbonate	$SrCO_3 \bullet H_2O$	98%
Fluka	Calcium Carbonate	$CaCO_3 \bullet H_2O$	98%
Goodfellow	Manganese (Flake)	Mn	99.98%
Prolabo p. a quality	Citric Acid	$C_6H_8O_7$	99.7 %

Table 2.1: The starting materials, their origin and purity.

Metallic manganese is washed in 1:1 hydrochloric acid and ethanol. This removes any oxygen from surface layers. It is then and dissolved in 1:1 nitric acid before it is added to the melted citric acid. The solution is slight yellow in colour at this point, and a colloidal suspension or sol is obtained. It is important to prevent the citric acid from polymerizing since this will lower the ability to bind the metal ions severely. The mixture is then heated at 250°C for at least 24 hours while the water and carbon dioxide evaporate off to the gas phase and a xerogel is obtained. The xerogel is cooled to room temperature and then grinded in an ashat mortar until a fine powder is obtained. The powder is then pressed in an iron anvil (200 Bar) so that the distance between the particles is reduced. This will improve solid state diffusion. The pellets are heated at 400°C for two days, before being cooled and grinded to fine powder again. The powder is then for a second time pressured into pellets and reheated at 1000°C for a week. The heat treatment is

carried out in alumina boats in order to minimize reaction with the sample at high temperatures. The obtained material is finally grinded to powder. The powder is gathered in small glass containers and stored in a desicator containing silica gel for water free conditions.

2.2 Methods used for reduction of $CaMnO_3$ and $SrMnO_3$:

2.2.1 Zirconium Reduction:

To obtain the reduced $CaMnO_3$ and $SrMnO_3$ phases, zirconium metal is used as a reducing agent (oxygen getter). The method uses zirconium's ability to easily be oxidised at very low partial O_2 pressures. When zirconium is oxidized, each atom gives away four electrons, and ZrO_2 is formed.

$$Zr \rightarrow Zr^{4+} + 4e- \qquad \text{Equation 2.1}$$

The manganese ions in Ca/$SrMnO_3$ are reduced from Mn^{4+} to Mn^{3+}.

$$Mn^{4+} + e^{-} \rightarrow Mn^{3+} \qquad \text{Equation 2.2}$$

Thus only ¼ of the zirconium is needed of the amount of manganese that is to be reduced. In the case of complete reduction we have the following reaction:

$$CaMnO_3 + \frac{1}{4}Zr \rightarrow Ca_2Mn_2O_5 + \frac{1}{4}ZrO_2 \qquad \text{Equation 2.3}$$

The zirconium used is shown in table 2.2:

Distributor	Name	Chemical Formula	Purity
Goodfellow	Zirconium (turnings from rod)	Zr	99.8%

Table 2.2: Zirconium used for reduction.

Because of these abilities zirconium can be used to reduce less stable oxides. An appropriate amount of zirconium is put in a quartz glass ampoule with a diameter of about 16 mm. The sample material is put in a smaller and shorter glass tube of 10mm

diameter and placed on top of the zirconium. The opening of the outer ampoule is then reduced over a H_2/O_2 flame until it is 1-2 mm wide. The outer glass ampoule is after evacuation, using a vacuum pump, closed over the H_2/O_2 flame. Figure 2.1 shows an illustration of the closed ampoule.

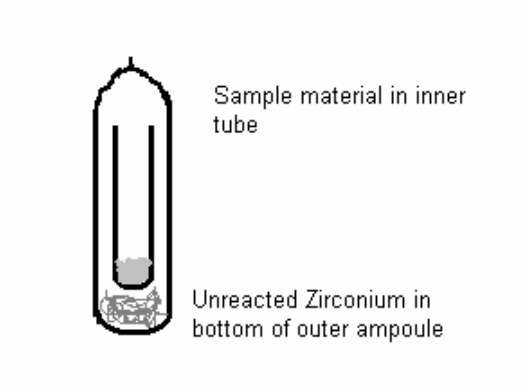

Figure 2.1: Closed ampoule with zirconium and sample material.

The ampoule is then heated in an oven so that the temperatures commonly are between 550˚C and 650˚C. The heating periods usually last for one week or more. Upon cooling it may be possible to preserve the reduced (possibly metastable) phase even after the ampoule is opened in normal atmosphere. Depending on the reactivity and stability of the reduced phases it may be necessary to quench the ampoule in ice-water mixture and store the sample under inert conditions in order to prevent the reduced phases to reoxidize to more oxygen stable compounds.

2.2.2 Reduction Furnace:

Reduced phases where furthermore obtained by heating a sample in controlled atmosphere. A cylindered oven is placed horizontally with the sample container placed in the middle. Gas with controlled pO_2 was flowed over the sample. Both ends are then closed and a gas valve is opened so that the desired gas (or gases) can flow through the cylinder. The gas (or gases) is let out on the other end to ensure continuous flow and transportation of released O_2 gas from the sample. The sample is kept at this temperature from one to two weeks before the temperature is gradually reduced to room temperature.

2.3 Characterisation

Various methods were used to characterise the samples. These methods are summarized below.

2.3.1: X-rays and x-ray diffraction (XRD):

The definition of an x-ray beam is that it is electromagnetic radiation with a wavelength between 0.1 and 100Å. When used for experimental diffractometric purposes it is commonly in the region of 0.5-3Å, and is usually created in a way that leads to monochromatic x-rays. In an x-ray tube a beam of electrons are accelerated through the tube by a voltage of example 30kV and fired at a metal target, usually copper. When the incident electrons hit the target metal, also called the anode metal, some of the 1s electrons of the k shell are ionized. Outer orbital electrons then drop to occupy the vacant 1s orbital, and the relaxation energy released appears as x-radiation. This transition has a fixed energy value, and thus a characteristic spectrum of radiation exists for every element. The 2p-1s transition has due to the two possible spin states two almost identical wavelengths named $K_{\alpha 1}$ and $K_{\alpha 2}$. In copper these $K_{\alpha 1}$ and $K_{\alpha 2}$ have wavelengths of 1.54051Å and 1.54433Å respectively. Figure 2.2 shows a typical x-radiation emission spectrum.

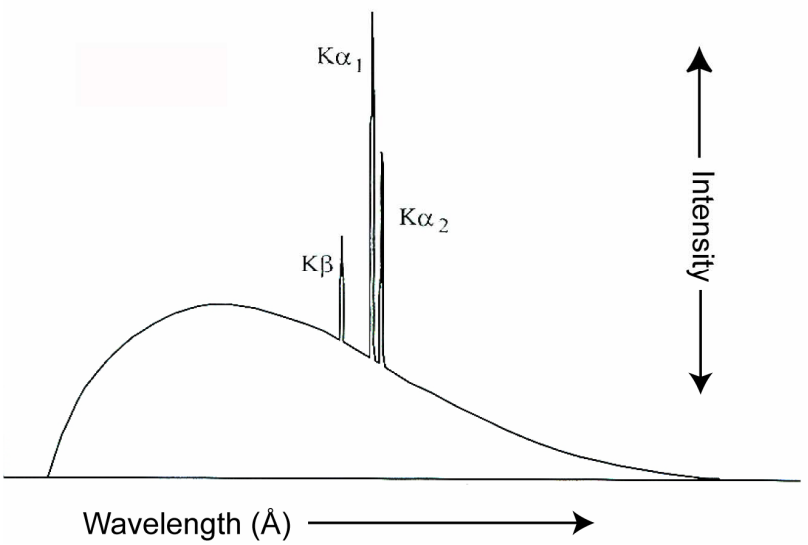

Figure 2.2: Typical x-ray emission spectra.

The basic principle for powder x-ray diffraction is that a monochromatic converging or diverging x-ray beam hits a thoroughly grinded crystalline powder sample. The sample itself rotates, and it is presumed that there exists crystals and lattice planes for every direction possible allowed by the space group of the system. Figure 2.3 below shows the basic principle of a diffractometer.

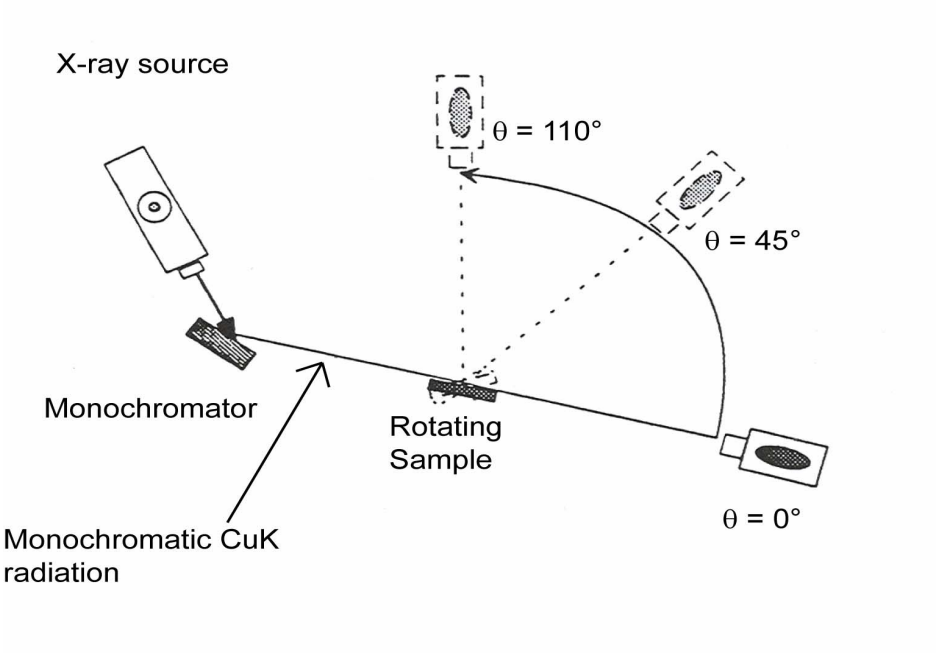

Figure 2.3: Basic principle of a diffractometer.

The sample will then reflect the monochromatic ray in every direction that satisfies Bragg's law:

Braggs Law: $2d\sin\theta = n\lambda$ Equation 2.4

d = distance between two lattice
θ = angle between ray and plane
n = order of diffraction
λ = wavelength of x – ray

This formula can be understood by studying figure 2.4.

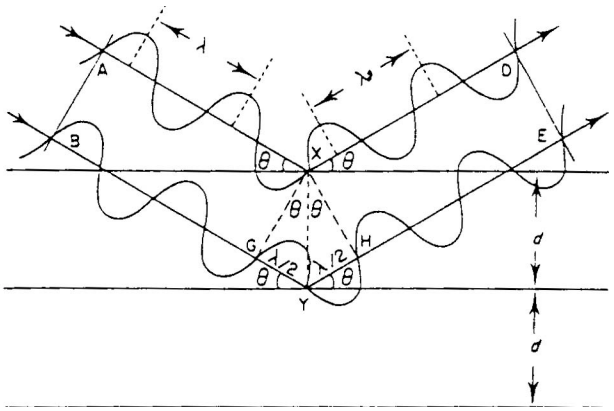

Figure 2.4: X-rays being reflected by crystallographic planes.

In this figure two incident beams with wavelengths λ are reflected by crystallographic planes with a distance d. The angle between the incident beams and the planes is θ. The distance between G and Y (GY) and Y and H (YH) can be expressed by the incident angle.

$d\sin\theta = GY = HY$ Equation 2.5

This implies that:

$$GY + HY = 2d \sin\theta \qquad \text{Equation 2.6}$$

But the sum of the distances GY and HY can also be expressed by any number of whole wavelengths.

$$GY + HY = n \cdot \lambda \qquad \text{Equation 2.7}$$

This gives us Braggs Law:

$$2d \sin\theta = n\lambda \qquad \text{Equation 2.8}$$

All crystalline compounds have their own characteristic powder x-ray diffractometer pattern, characterized by angle of reflection and intensity of each reflection. It is therefore possible to use powder x-ray diffraction for phase identification together with determination of homogeneity, crystal structure and unit cell dimensions. The distance between the planes (d) can be described by the lattice constants a, b, c, α, β and γ, and the miller indexes h, k and l. Due to this, if we know the lattice constants, it is possible to find the d values, and from that the angle θ for every plane of reflection. The angle of dispersment is characteristic for every substance, as is the distribution of the intensities. The intensity I(hkl) of a reflected beam is dependent on two major factors:

First, from the reflection from a set of planes with indices (hkl), we can find a phase difference δ. This distance is between atoms at the origin and a position with fractional coordinates (xyz), and is given by $\delta = 2\pi(hx+ky+lz)$. This implies that some planes with specific miller indices will have reflections that are out of phase with other plane reflections, and complete cancellation will occur.

Second, the intensity is reversed proportional with the square of the so called structure factor F(hkl). All atoms contribute to the structure factor in the following manner:

$$F(hkl) = \sum f_n \exp 2\pi i(hx_n + ky_n + lz_n) \qquad \text{Equation 2.9}$$

where f_n (the atom factor) is dependent on the number of electrons in the atom n and the dispersion angle. The sum is taken over all N atoms in the unit cell.

Both the intensities and angles of the reflections are thus important in analysing and in characterisation of the substances. As an internal standard, Silica is commonly added to the measured compounds. The number of lines created by the materials increase with decreasing degree of symmetry. This is due to the multiplicity in high symmetry phases. In these cases the lines appear on top of each other.

A detector is used to detect the diffracted x-ray beams. This detector may be an x-ray sensitive film or an x-ray counter. The scattering of the beam is measured in θ or 2θ. Powder x-ray diffraction can give multiple types of information about the sample. The characterisation method has its advantages when evaluating problems like homogeneity, contamination phases or defining axis lengths or crystal structure. Two different types of x-ray data where recorded on two different diffractometers. Both are Siemens/Braun D5000 diffractometers with monochromatic CuKα_1 radiation and Braun PSD detectors. The main difference is that the diffractometer 1 can use transmission sample holders that create less background. Many cycles must be performed, and for most identification experiments the diffractometer 3 with multiple sample holders gives sufficient quality diffraction patterns. The diffractometer 3 creates notably more background however and diffraction patterns from this instrument usually disqualify quickly when the data is used for refining structures.

2.3.2: Powder Neutron Diffraction (PND):

The basic principle of powder neutron diffraction is the same as for powder x-ray diffraction, except the fact that neutrons are used instead of x-rays. The neutrons have neutral charge, and are not scattered by the electron cloud around atoms, like electron and x-ray beams are. Instead they are scattered by the atom nuclei and unpaired inner electrons. The neutrons have magnetic momentum that can reveal any cooperative magnetic properties of the compound being hit by the neutron beam. In a ferromagnetic substance the magnetic momentums are ordered in the same direction, and if such a sample is hit by a monochromatic neutron beam the unit cell will appear identical to the one observed by x-ray diffraction. If the magnetic momentums of the compound are ordered in opposite directions, such as is the case in ferri and antiferromagnetic compounds, then the unit cell will be different in neutron diffraction and x-ray diffraction. Neutron diffraction has some advantages over x-ray diffraction. Scattering caused by x-rays is a function of the square of the number of electrons, and therefore increases with atomic number. Thus light atoms do not diffract x-rays to a large extent. The neutrons however are scattered by the nuclei of the atoms, and neutron diffraction from light atoms can be equally strong as the diffraction obtained from the heavier elements. It is also possible to use neutron diffraction to determine the magnetic ordering at low temperature. If the sample is ordered magnetically at temperatures as low as 9 K, the neutron diffraction pattern recorded at that temperature will show changes in regard to the one recorded at room temperature.

2.3.3 Synchrotron X-ray Diffraction:

Another diffractometer resource used was the European Synchrotron Radiation Facility (ESRF) in Grenoble at the SNBL (Swiss-Norwegian Beam Line). Synchrotron radiation is emitted from electrons that have been accelerated up to near light speed before they are ejected into a large ring. Here the electrons are moved through the ring by great curving magnets. When these electrons change direction in the ring, electromagnetic radiation is released, and directed towards the experimental instrumental stations. An illustration of the beam line is shown in figure 2.5.

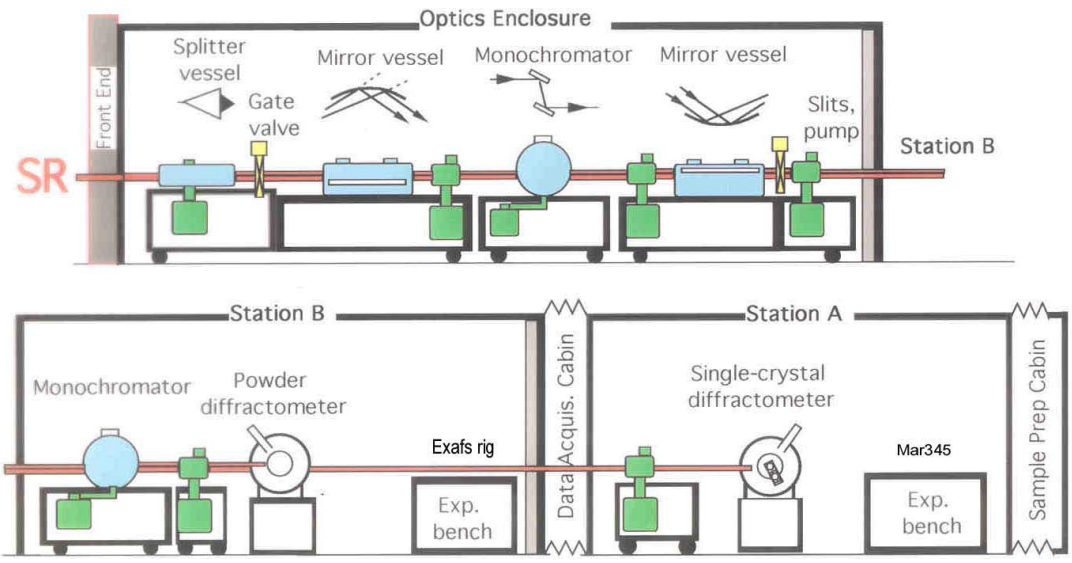

Figure 2.5: A schematic illustration of the Swiss Norwegian Beam Line stations B and A in Grenoble.

The x-rays from a synchrotron radiation source have intensities several million times that of a normal x-ray source. Long collimators give good resolution without losing much intensity. The high resolution x-ray diffractometer at station B has a Si (111) crystal monochromator in front of each detector. There are six different detectors with a small angular offset of 1.1 degrees. This makes it possible to collect six different diffraction patterns at the same time, and reduces the total measuring time greatly. Transmission (capillary) measurements can be performed between 5 and 1273 K. This because the beam line is equipped with both a He cryostat for temperature ranges from 5 to 350 K, and a furnace from room temperature to 1000°C.

2.3.4 Thermo gravimetric analysis, TGA:

Thermo-gravimetry is a technique for measuring weight change of a substance as a function of temperature in a controlled atmosphere. The samples commonly have masses from 5-100mg, and must be fine powdered. The instrument used was a Perkin Elmer

TGA 7. The system consists of a control unit (Perkin Elmer TAC 7/DX) which governs the system and a computer that records and adjusts the data. The heat flow can be controlled and made to vary from 0.1°C per minute to 100°C per minute. The sample containers are small quartz ampoules that have been preheated at 1100°C to remove any adsorbed water on the ampoule. The atmosphere of the instrument is controlled by direct supply of the wanted gas or gas mixture by a reduction valve. When the reduced samples are heated in normal or oxygen atmosphere they will reoxidize with temperature. The weight of the sample is continuously measured, and the weight gain can be calculated into the amount of oxygen that has been absorbed. If there are intermediate phases it will be possible to see these as areas were no weight change is obtained over a temperature interval and a weight loss/gain between them.

2.3.5 Electron diffraction from Transmission Electron Microscopy:

Electron diffraction is a single crystal diffraction method that makes use of the wave properties of electrons. Electrons are fired from an electron gun on a small single crystal, commonly on nm scale and diffracted by the sample. The method has the great advantage that it can be used on small samples since the scattering efficiency of electrons is high. The results obtained are displayed as patterns of spots on photographic film that displays the reciprocal space of the actual unit cell. This makes it a very useful technique for obtaining unit cell and space group information. In this case it was used on one of the $CaMnO_{2.75}$ samples in order to look for systematic extinctions. Electron diffraction experiments can be performed with transmission electron microscopes. The instrument used was a 200 cx by Jeol.

2.4 Refinement

2.4.1 GSAS and Rietveld refinement analysis of the measured diffraction pattern:

The diffraction patterns were refined using the GSAS Rietveld programme package. In the Rietveld method [22] and [23], least square refinements are carried out until the best

fit between the observed diffraction pattern and the calculated pattern is obtained. The observed pattern must be recorded in digitized form with a numerical intensity value y_i at each several thousand step i to be usable in Rietveld refinement method. The calculated pattern is based on models of crystal structure, diffraction optics, instrumental factors and specimen characteristics. The best fit sought for is the best least square refinement simultaneously of all the thousand small intensities y_i at each step i. The quantity minimized is the residual S_y, given in equation 2.10

$$S_y = \sum_i w_i \left(y_i - y_{ci} \right)^2 \qquad \text{Equation 2.10}$$

where $w_i = 1/y_i$,
y_i = observed intensity at step i
y_{ci} = calculated intensity at step i

GSAS (General Structure Analysis System) is a set of programs developed for processing and analysing both powder and single crystal patterns from x- ray and neutron diffraction. Many parameters in GSAS can be changed in order to create a good calculated pattern that can model the pattern of the measured sample. It is therefore important to obtain understanding of what kind of scattering leads to what kind of contributions in the actual measured diffraction pattern.

First of all it is important to create a good background definition for the calculated pattern which is as equal as possible to the observed one. In Rietveld refinement the observed diffraction intensities $y_{obs}(Q)$ can be modelled by summing the contributions from crystalline Bragg scattering and background scattering.

$$y_{obs}(Q) = y_{cx}(Q) + y_b(Q) \qquad \text{Equation 2.11}$$

Where y_{cx} is the calculated crystalline intensities and y_b is the calculated background intensities and Q is the magnitude of the scattering factor.

$$Q = 4\pi \cdot \sin\frac{\theta}{\lambda}$$ Equation 2.12

The background intensities can often be fitted with low order polynomial functions. Other contributions to the background cannot be accounted for by these functions. These contributions can in many diffraction experiments be the reason for the patterns to contain additional non crystalline scattering components. This scattering can be thermal diffuse scattering, scattering from containers, incompletely crystallized samples and separate phases. A successful refinement of the crystalline structure requires a precise modelling of these non crystalline contributions. This can be expressed by an additional sum:

$$y_{obs}(Q) = y_{cx}(Q) + y_b(Q) + y_{ca}(Q)$$ Equation 2.13

Where y_{ca} is the non crystalline scattering.

To accomplish modelling for these contributions it is possible to use empirical functions such as high order polynomials. Alternatively they can be removed from the diffraction pattern by extracting useful structural information from non crystalline scattering. Two such methods are Fourier filtering or Direct modelling.

Another important issue when analysing the diffraction profile is the fit of the intensity peaks and the origin of the peaks themselves. In neutron diffraction, peaks are Gaussian and symmetric, and not very complicated to analyse. In x-ray diffraction however peaks are much more asymmetric, and a better understanding of the x-ray diffraction peaks and their creation is helpful.

The diffraction profile can be divided into three contribution categories. These are intrinsic profile, special distribution and instrumental distribution. The intrinsic profile comes from the diffraction of the sample itself. A perfect crystal produces a reflection

with an inherent width called Darwin width. This relies on the fact that a photon in a crystal is restricted in a small but existent volume. Other intrinsic contributions that broaden the peaks are crystallite sizes less than 1μm and micro strain in the crystal. The spectral distribution comes from the x-ray beam. Even monochromatic x-ray beams have a width that is shown to have a Lorentzian and slightly asymmetric peak. At high angles this can contribute to the diffraction profiles, making peaks broader and more symmetric. Instrumental contributions are contributions that come from the instruments used. The monochromator and the focusing optics greatly increase the intensity, but also create significant symmetric broadening. Also a flat sample holder will create an out of focus condition. Since the focusing circle continuously changes radius with the reflection angle 2θ, most experiments use flat specimen holders that will produce a small asymmetric contribution. Other instrumental contributions are the axial divergence of the incident beams and specimen transparency. When modelling x-ray diffraction profiles, peaks can have both symmetric and asymmetric parts. Functions that can describe both Gaussian and Lorentzian peaks must be used. Two types of functions that do this are the Voight and the split-Pearson function. These functions can range from both types of peaks and can describe peaks as fractions of both Gaussian and Lorentzian.

The quality of the fitted pattern is given as R-factors, developed by Rietveld. These R-factors are quality error factors that are minimized as the fitted pattern approaches the experimental pattern. The R-values used in this thesis are R_p and R_{wp}. Both compare the fitted pattern to the experimental one, but the R_{wp} is weighted. The R-factors are given in equation 2.14 and 2.15

$$R_p = \frac{\sum y_i(obs) - y_i(calc)}{\sum y_i(obs)} \qquad \text{Equation 2.14}$$

$$R_{wp} = \left(\frac{\sum w_i (y_i(obs) - y_i(calc))^2}{\sum w_i (y_i(obs))^2} \right)^{1/2} \qquad \text{Equation 2.15}$$

where $w_i = 1/y_i$,

$y_i(obs)$ = observed intensity at step i

$y_i(calc)$ = calculated intensity at step i

The third quality factor used to describe the refinement in this thesis is the χ^2 (chi squared). Chi squared is given in equation 2.16.

$$\chi^2 = \left(\frac{R_{wp}}{R_{\exp}} \right)^2 \qquad \text{Equation 2.16}$$

This factor is a measure between the actual R_{wp} and the expected profile R-factor for a perfect fit R_{exp} [24]. R_{exp} is given by equation 2.17

$$R_{\exp} = \left(\frac{N - P}{\sum w_i \left(y_i(\ obs \ ) \right)^2} \right)^{1/2} \qquad \text{Equation 2.17}$$

where $w_i = 1/y_i$,

$y_i(obs)$ = observed intensity at step i

$y_i(calc)$ = calculated intensity at step i

N = number of observations (data points)

P = number of parameters used

The chi squared is also known as goodness of fit and is in the case of ideal refinement equal to 1.

2.4.2 Le Bail method:

The Le Bail method is a method that was developed by Armel Le Bail [25], and is implemented in the GSAS package as a separate programme. The programme can extract structure factors F (see Equation 2.8) from powder diffraction data by iterating process of full pattern profile fitting. The pattern matching is done by estimating the integrated intensities of the pattern without using least squares optimization. No structure model is

used. The Le Bail method may therefore be useful when determining instrumental parameters and background when little other structural information about the compound is known.

Chapter 3: Results

3.1 Material synthesis results and characterisation:

The samples of $CaMnO_3$ and $SrMnO_3$ that have been synthesized are undistinguishable by sight. Their powders have the same approximate grain size and consistency. They are also black in colour. A total of ten batches of $CaMnO_3$ and a total of six batches of $SrMnO_3$ of variable amount have been produced. The amount of the end product in each batch ranged from 2 to 9 grams. The qualities of the produced samples vary. The diffraction patterns of the first two $CaMnO_3$ samples show that the end product of these batches is not of satisfactory quality. The batches made thereafter however are of good to very good quality in respect to the earlier reported values and the presence of impurities. The exception is the seventh batch which has little resemblance to the other ones and has like the two first not been used for further work. For $SrMnO_3$ none of the first three attempts are of satisfactory quality in regard to the earlier reported patterns. The three latter batches are of very good quality, and are those that have been used for further synthesis and structural work.

The results of the synthesis of the reduced phases are more variable. These results are presented in detail under the different compositions in this chapter. A result of the synthesis of the $CaMnO_{3-x}$ materials and particularly in the reduced compositions is the presence of impurities. These create problems during the refinement. The most common impurities are $CaMn_2O_4$ (Marokite) and $Ca_2(MnO_4)$ in addition to the totally reduced $CaMnO_{2.5}$ phase.

3.2 Analysis of TGA experiments:

Some of the reduced samples were heated in a TGA oven in order to view the reoxidation of the samples as a function of weight gain versus temperature. The samples with compositions of $CaMnO_{2.5}$, $CaMnO_{2.8}$ $CaMnO_{2.665}$ and $Sr_2Mn_2O_5$ were heated in air, while a sample with the composition of $CaMnO_{2.665}$ was also heated in nitrogen atmosphere. The heating rate was 5˚ per minute and the end temperature was 1000˚C.

Some samples were heated to 1100˚C. In figure 3.1 three reoxidation TGA graphs for samples with the $CaMnO_{2.5}$ composition can be seen.

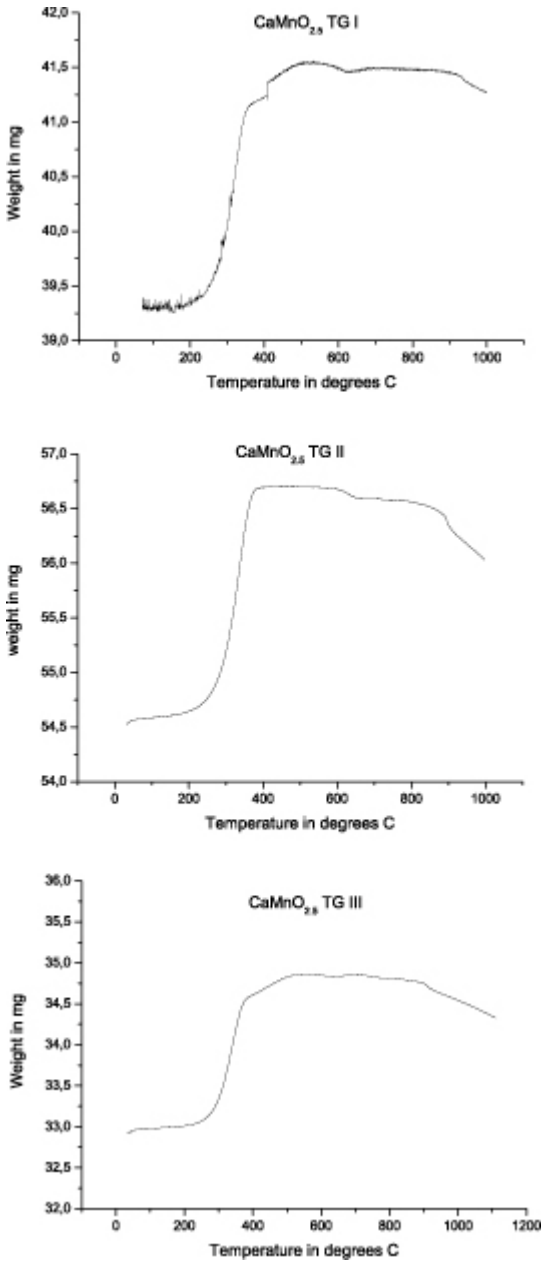

Figure 3.1: Three TGA reoxidation experiments for samples with the $CaMnO_{2.5}$ composition.

Each of these curves show weight gain from room temperature to about 400˚C before the samples start losing weight at about 600˚C up to 1100˚C. The top point, where the TGA curve is flattening, is presumed to be the totally reoxidized $CaMnO_3$ phase. At

approximately 600˚C a small weight loss is seen. This is followed by another relatively flat area without change in weight until the temperature is 800˚C. In this temperature interval the samples show more or less stable behaviour. It is predicted that the samples only react with oxygen. The amount of oxygen gained can be calculated. The results from the measurements from room temperature to the maximum point of curve are listed in table 3.1:

Experiment name	Weight change (mg)	Calculated oxygen content
$CaMnO_{2.5}$ TG I	2.14	2.96
$CaMnO_{2.5}$ TG II	2.13	2.83
$CaMnO_{2.5}$ TG III	1.93	2.99

Table 3.1: List of the results for the TGA reoxidation experiments for the $Ca_2Mn_2O_5$ phase from start to the maximum value.

The results derived from the measurements from start to after the small weight loss (approximately 600˚C) are listed in table 3.2:

Experiment name	Weight change (mg)	Calculated oxygen content
$CaMnO_{2.5}$ TG I	2.07	2.94
$CaMnO_{2.5}$ TG II	2.02	2.81
$CaMnO_{2.5}$ TG III	1.87	2.97

Table 3.2: List of the results for the TGA reoxidation experiments for the $Ca_2Mn_2O_5$ phase from start to after weight loss.

Some comments must be made in regard to the TGA experiments reported in tables 3.1 and 3.2. First of all, the plot of the experiment $CaMnO_{2.5}$ TG I, shows a small jump (0.04mg, at the temperature of 407˚C) in the continuous curve. After discussing this with instrument experts, that weigh difference was subtracted from the weight recorded at higher temperatures. Secondly the oxygen content obtained is not always consistent with the predicted value of $CaMnO_3$. Also the second temperature interval indicates only slightly lower oxygen content than $CaMnO_3$. A possibility is that this step is due to impurities. Likely impurities might be $CaCO_3$ or $(Ca,Mn)CO_3$. These issues will be discussed in detail in discussion 4.1

The other reduced samples with oxygen content of $CaMnO_{2.665}$ and $CaMnO_{2.8}$ have also been reoxidized with this technique. Their plots are shown in figure 3.2.

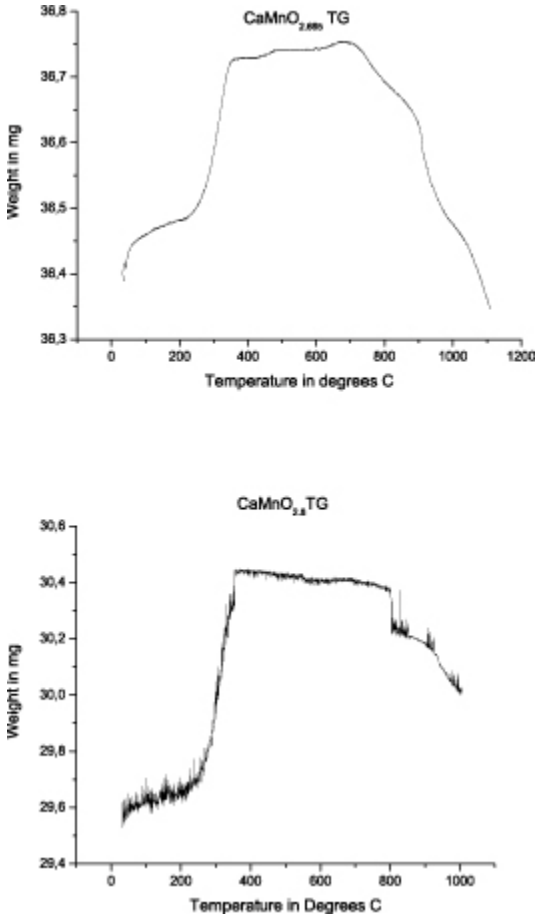

Figure 3.2: TGA reoxidation experiments in air for $CaMnO_{2.665}$ and $CaMnO_{2.8}$

The oxygen content is calculated from the maximum weight value of the TGA curve in both experiments. The results derived from the measurements are listed in table 3.3

Experiment name	Weight change (mg)	Calculated oxygen content
$CaMnO_{2.665}$	0.38	2.77 (3)
$CaMnO_{2.8}$	0.87	3.05 (4)

Table 3.3: List of results for the TGA reoxidation experiments in air for $CaMnO_{2.8}$ and $CaMnO_{2.665}$.

The results from these experiments show that the samples react with oxygen until about 300˚C. From here the sample is more or less stable until 800˚C, after which it rapidly loses oxygen. The oxygen content calculated for the $CaMnO_{2.665}$ sample was 2.77 where it was predicted to be 3.0. The $CaMnO_{2.8}$ result of 3.05 is more consistent with that predicted value. The results will be discussed in chapter 4.1.

The totally reduced sample $Sr_2Mn_2O_5$ was also heated in the TGA oven. The experiment can be seen in figure 3.3

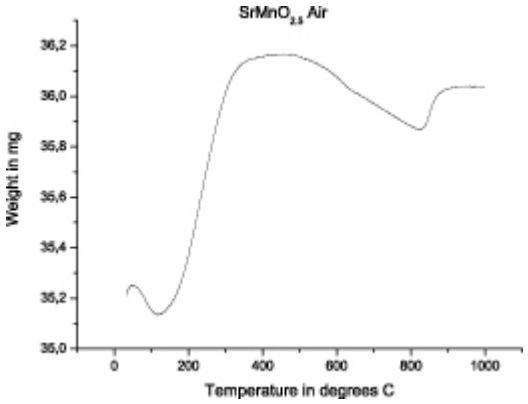

Figure 3.3: TGA curve of $Sr_2Mn_2O_5$ heated in air.

The TGA curve shows that $Sr_2Mn_2O_5$ gains weight until about 430˚C, before weight loss commences. The calculated oxygen content and weight difference is listed in table 3.4.

Experiment name	Weight change (mg)	Calculated oxygen content
$Sr_2Mn_2O_5$ air	0.94 mg	2.80 (4)

Table 3.4: Results for TGA reoxidation of $Sr_2Mn_2O_5$ in air.

$Sr_2Mn_2O_5$ reaches its top peak at about 450˚C and the calculated oxygen content of 2.80 is below the expected value. This is discussed in chapter 4.1. The reoxidation of $Sr_2Mn_2O_5$ in TGA is completed at about 450˚C, but also a discontinuity in the curve occurs at 800˚C. In order to find what compounds exited at these temperatures, two different samples of $Sr_2Mn_2O_5$ were therefore heated to the actual temperature. The first was heated to 450˚C and the other to 800˚C. The x-ray diffraction pattern of the sample heated to 450˚C yielded a mixture between hexagonal and cubic $SrMnO_3$. The sample

heated to 800˚C yielded the hexagonal $SrMnO_3$. These results are in good agreement with that reported in literature [13]. The results are discussed in detail in chapter 4.1.

Some samples were heated in inert atmosphere. Nitrogen gas is used as inert gas. One such experiment, a sample with composition $CaMnO_{2.667}$, was heated in nitrogen atmosphere. The TGA curve is shown in figure 3.4.

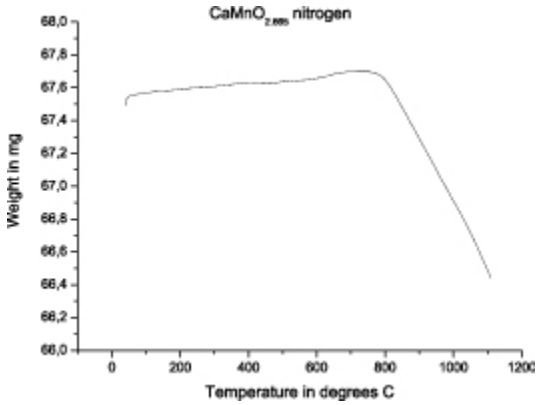

Figure 3.4: TGA curve of $CaMnO_{2.667}$ heated in nitrogen.

The $CaMnO_{2.667}$ heated in nitrogen atmosphere shows a small weight gain before weight loss starts at about 800˚C. Since nitrogen atmosphere is used this weight gain was not expected. A possibility is that some oxygen is present in the sample holder or on the sample as an oxidized layer. The weight gain and calculated composition at 800˚C is listed in table 3.5.

Experiment name	Weight change (mg)	Calculated oxygen content
$CaMnO_{2.665}$ nitrogen	0.21 (0)	2.69 (1)

Table 3.5: Results from $CaMnO_{2.667}$ heated in nitrogen.

The weight gain is very small, and the oxygen content at 800˚C is 2.69. The sample loses oxygen from this temperature steadily up to 1100˚C. No signs of any intermediate stable area that can be interpreted as a stable phase can be observed above this temperature.

3.3 Obtained Diffraction Patterns and GSAS Calculations:

In order to get a systematic overview of the structures in the $CaMnO_3$ and $SrMnO_3$ some of the already described structures were refined and compared with earlier reported values. These are $CaMnO_3$, $Ca_2Mn_2O_5$, $SrMnO_3$ and $Sr_2Mn_2O_5$. Promising compositions that had been observed earlier were synthesized using the methods described in chapter 2.1 and chapter 2.2. The phases observed in HREM by Reller et al [1] where $CaMnO_{2.8}$, $CaMnO_{2.75}$, $CaMnO_{2.655}$, and $Ca_2Mn_2O_5$. In addition the phase $CaMnO_{2.556}$ was described theoretically but not observed. Taguchi et al [8] also reported the structures $CaMnO_{2.92}$ and $CaMnO_{2.89}$. Samples of all of these above listed compounds were attempted synthesized. Patterns from the samples that are recorded on the difractometer diff3 (as described in chapter 2.3.1, page 26) are used to compare different samples of the same composition. These patterns prove how good the reproducibility is. The patterns used for refinements are recorded on the difractometer diff1 as transmission x-ray patterns. Some diffraction patterns are recorded with synchrotron radiation at the SNBL (chapter 2.3.3) in Grenoble. The General Structure Analysis System (GSAS) is used for Rietveld refinement. The GSAS programmes calculate a theoretical pattern that can be compared to the obtained pattern from the different diffractometers. The quality factors for structure modelling R_p, wR_p and χ^2 values are minimized as the calculated pattern fits better with the measured pattern. This is described thoroughly in Chapter 2.5.

In the oxygen deficient samples there will be changes in the diffraction pattern compared to that of the $CaMnO_3$ structure. The new reflections that appear, or changes to them, are likely to have their origin in the vacant oxygen positions and tilting of the octahedra/ square pyramids. The scattering factor of x-ray diffraction relies on the number of electrons and some of the new reflections and changes in the pattern might be difficult to detect by normal x-ray diffraction. Since impurity phases can be present, reflections that belong to these phases must be identified, as their presence greatly affect the refinement process. The impurity phases present in the $CaMnO_{3-x}$ and $SrMnO_{3-x}$ samples must be accounted for in order for the GSAS refinement to be successful. In figure 3.5 x-ray

patterns of the six different $CaMnO_{3-x}$ compositions synthesized are displayed from $CaMnO_3$ (top) to lower oxygen content until $Ca_2Mn_2O_5$ (bottom).

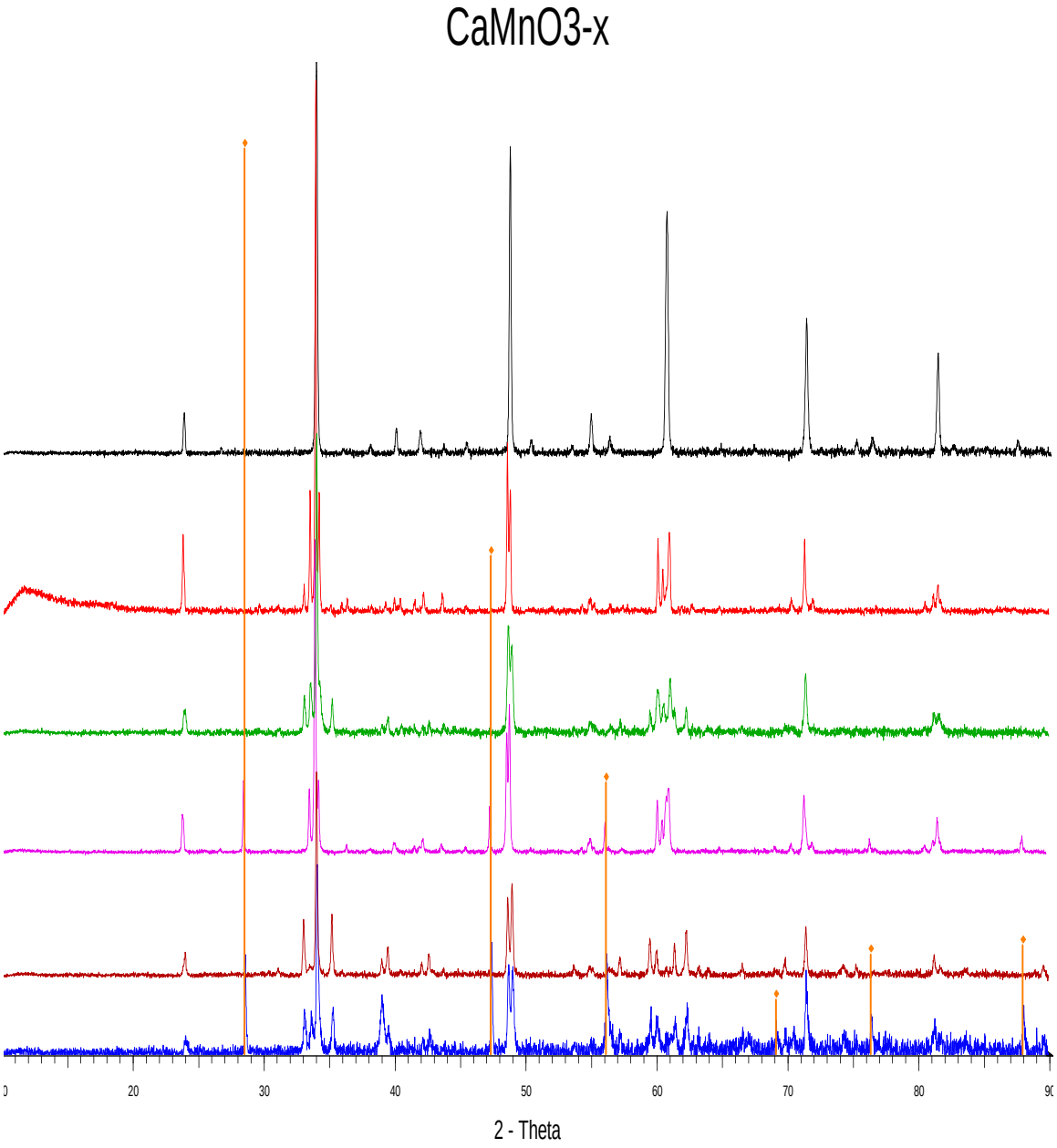

Figure 3.5: Diffraction patterns of the six different $CaMnO_{3-x}$. The compositions are $CaMnO_3$ (black), $CaMnO_{2.8}$ (red), $CaMnO_{2.75}$ (green), $CaMnO_{2.665}$ (purple), $CaMnO_{2.556}$ (brown) and $Ca_2Mn_2O_5$ (blue). The yellow horizontal lines belong to the internal standard Silica that is present in some samples.

3.3.1 $CaMnO_3$, $Ca_2Mn_2O_5$ and $CaMnO_{2.75}$:

3.3.1.1 $CaMnO_3$,

The parent compound $CaMnO_3$ produced diffraction patterns that show great resemblance to those reported by Poeppelmeier et al [4]. Since the structure of $CaMnO_3$ is quite well described in this publication the suggested space group, atom positions and unit cell dimensions of Poeppelmeier [4] were used in GSAS refinement. The x-ray patterns of the samples made are identical, and show that the reproducibility of the synthesis method is good. Even though the patterns are similar to the earlier reported ones, the quality of the newer recorded patterns is generally better. Figure 3.6 shows the x-ray patterns of three different samples for $CaMnO_3$.

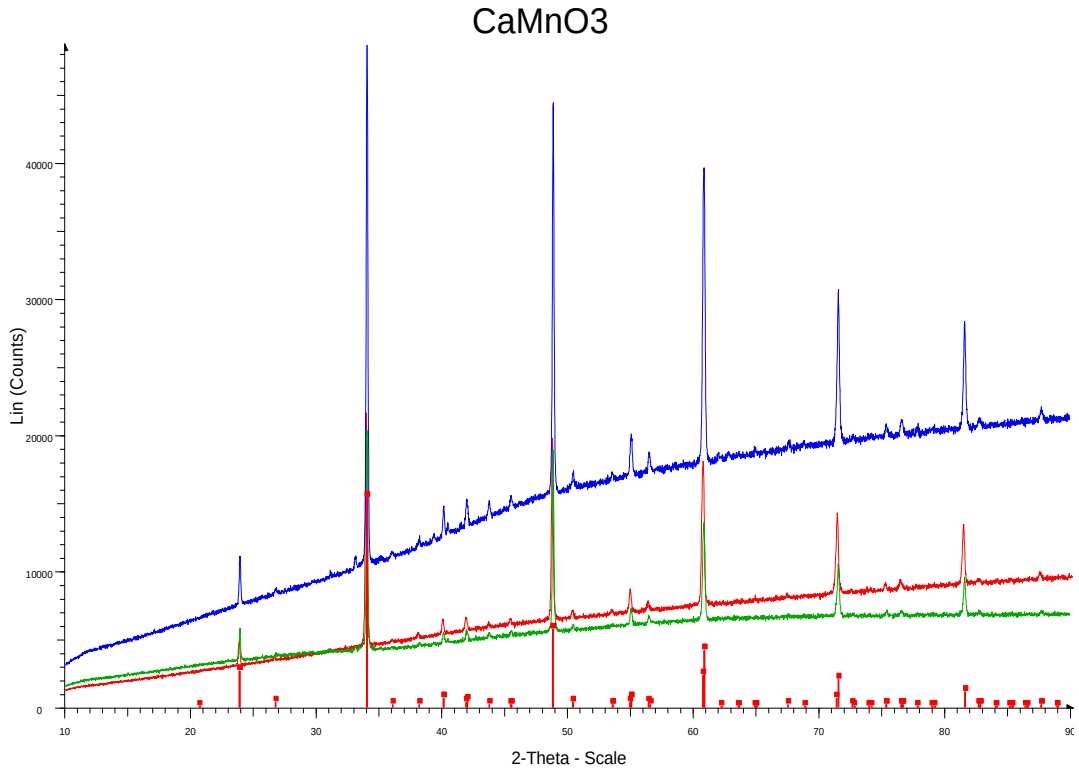

Figure 3.6: X-ray patterns for $CaMnO_3$. Three different scans show the same intensities and relative heights. The vertical red lines at the bottom show the intensities reported by Poeppelmeier.

The refinement for $CaMnO_3$ is based on the unit cell dimensions, atom positions and space group reported by Poeppelmeier et al [4]. The calculated pattern compared to the

diffraction pattern in this refinement to the measured x-ray pattern with GSAS and is shown in figure 3.7.

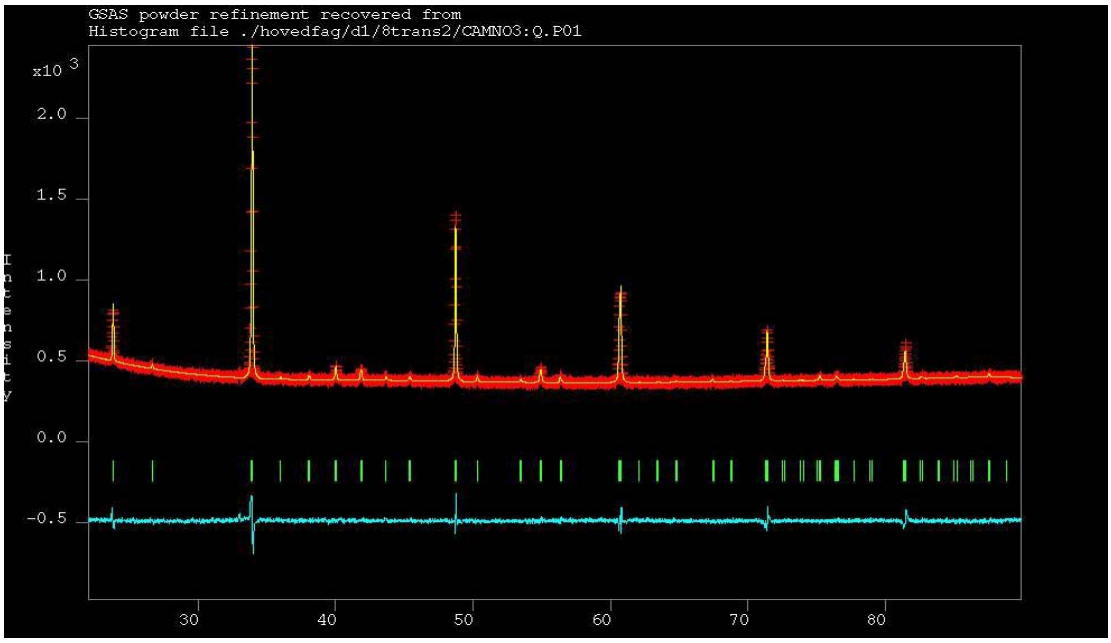

Figure 3.7: The refinement of $CaMnO_3$. The red spotted pattern is the measured pattern from diffractometer 1. The yellow pattern is the calculated pattern and the blue pattern shows the difference between them.

The error factors after the Rietveld refinement are listed in table 3.6

R_p	0.0171
wR_p	0.0255
χ^2	0.2611

Table 3.6 Rietveld error factors from refinement of $CaMnO_3$

The crystallographic information from the refinement of $CaMnO_3$ is listed in table 3.7

Space Group:	Pnma
Symmetry:	Orthorhombic
a (in Ångstrøm)	5.28847 (11)
b (in Ångstrøm)	7.46358 (16)
c (in Ångstrøm)	5.27357 (10)

Table 3.7: Crystallographic information obtained from the refinement of $CaMnO_3$.

Atom positions are listed in table 3.8

	x	y	z
Ca	0.03142	0.025	0.99718
Mn	0	0	0.5
O	0.48986	0.250	0.06593
O	0.28728	0.03358	0.71211

Table 3.8 Atom positions found for $CaMnO_3$. The atom positions were fixed during the refinement.

A schematic representation of the structure is shown in figure 3.8:

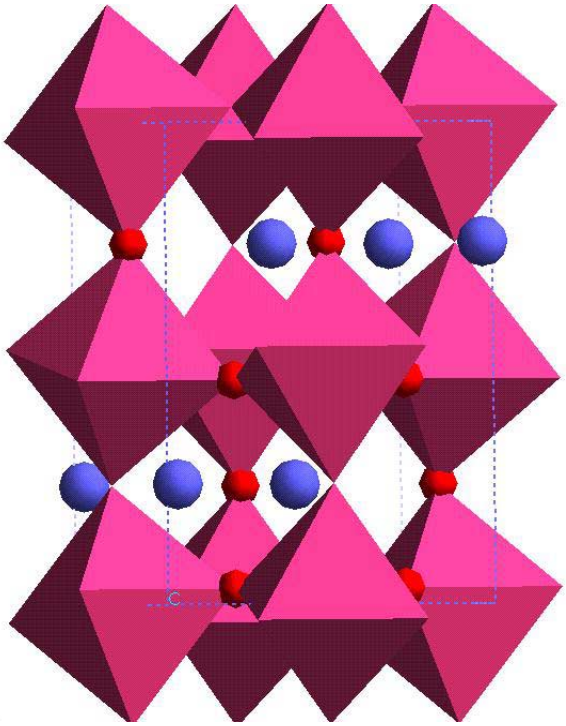

Figure 3.8: Schematical representation of $CaMnO_3$. The unit cell is shown as the blue stippled line. Ca is blue, O is red (Only oxygen atoms that are inside the unit cell are shown) and Mn is purple. The Mn atom positions are in the centres of the octahedra.

The results are in very good agreement with those of Poeppelmeier et al [4]. A list of the d-values can be found in the appendix.

3.3.1.2 $Ca_2Mn_2O_5$:

This phase is obtained when all of the MnO_6 octahedra are turned into MnO_5 square pyramids by the reduction of the Mn^{4+} ions to Mn^{3+} ions. This total reduction of the Mn ions was done with zirconium reduction. Multiple samples where synthesized. Figure 3.9 shows three different $Ca_2Mn_2O_5$ samples made.

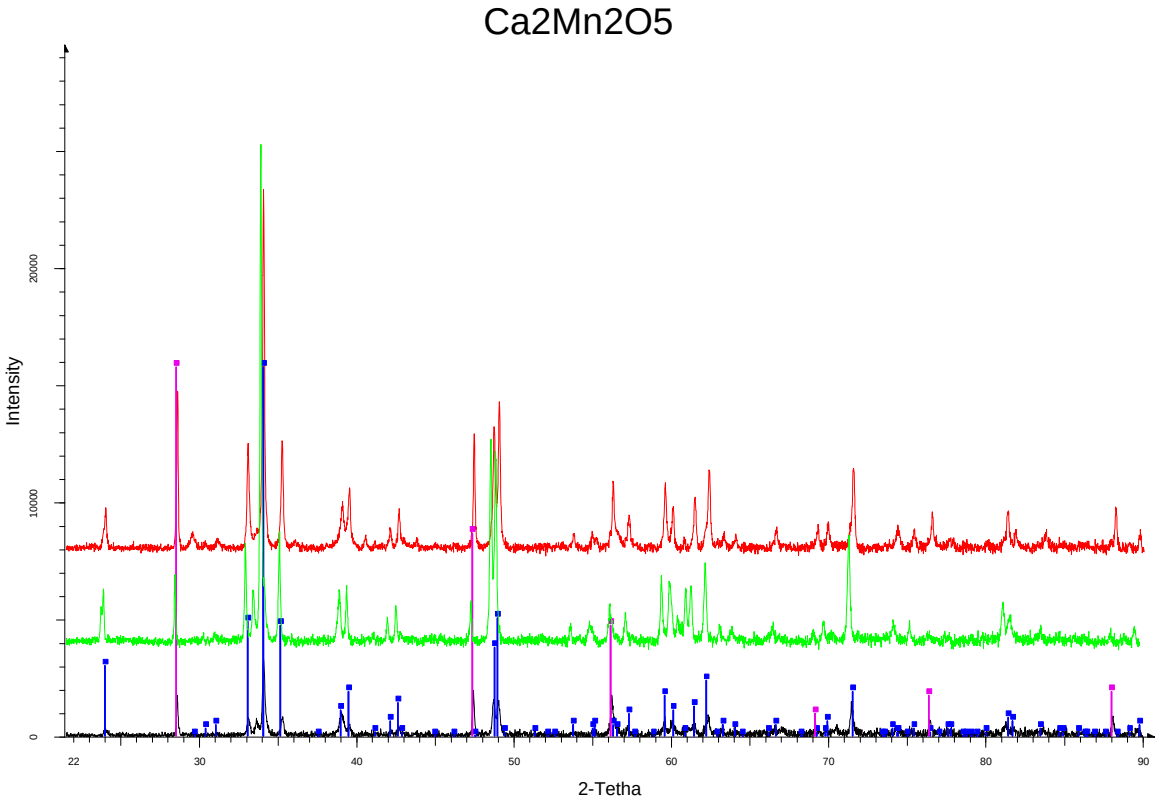

Figure 3.9: X-ray diffraction patterns of three different $Ca_2Mn_2O_5$ samples. The purple lines indicate reflections from the internal standard silica. The blue are the reported reflections by Poeppelmeier [5].

As was the case with the $CaMnO_3$ structure, the refinement for $Ca_2Mn_2O_5$ structure is based on the reported space group, atom positions and unit cell dimensions of Poeppelmeier et al [4] and [5]. The refinement of the x-ray pattern is showed in figure 3.10.

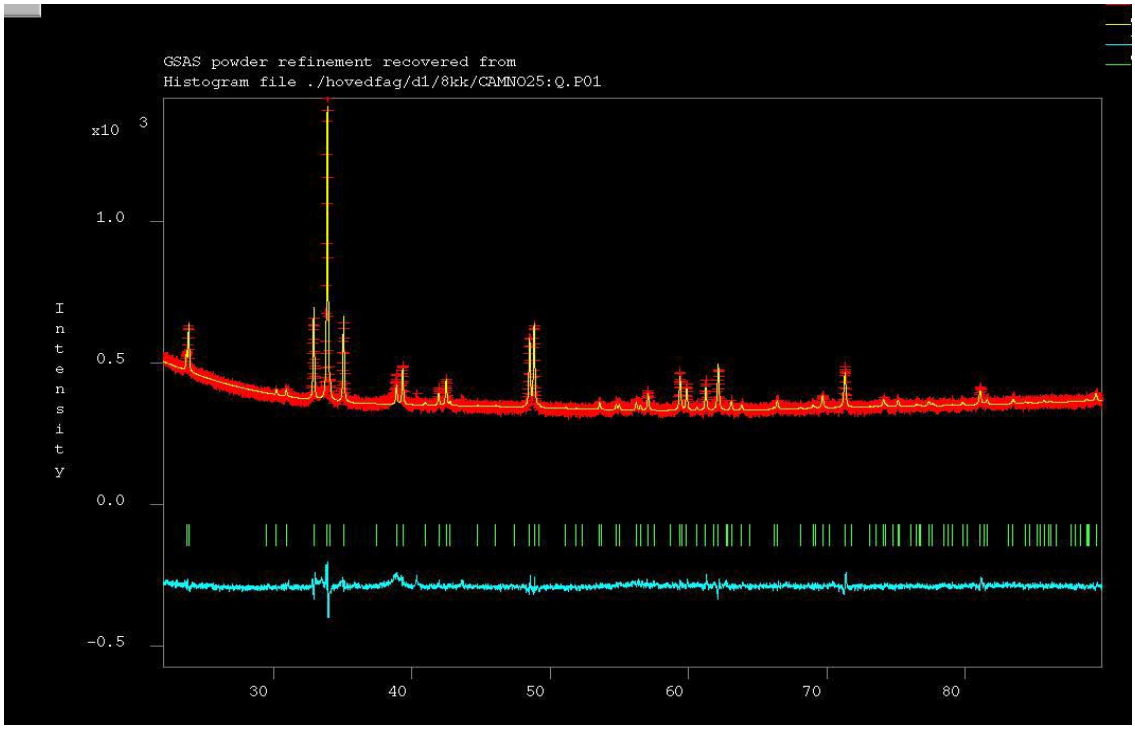

Figure 3.10: The refinement for $CaMnO_{2.5}$ The red pattern shows the experimental scan, while the yellow is the calculated pattern. The blue pattern at the bottom is the difference between the two.

The error factors after the Rietveld refinement found are shown in table 3.9:

R_p	0.0163
wR_p	0.0229
χ^2	0.0163

Table 3.9: Error factors from the refinement of the $Ca_2Mn_2O_5$ structure.

The calculated pattern yielded the crystallographic information listed in table 3.10.

Space Group	Pbam
Symmetry	Orthorhombic
a (in Ångstrøm)	5.43974 (11)
b (in Ångstrøm)	10.22736 (20)
c (in Ångstrøm)	3.75006 (6)

Table 3.10: Crystallographic information obtained from the refinement of the $Ca_2Mn_2O_5$ structure.

Coordinates for the atom positions are listed in table 3.11.

	x	y	z
Ca	0.299	0.3610	0.5
Mn	0.2826	0.12010	0
O	0.0800	0.28240	0
O	0.2875	0.10270	0.5
O	0	0	0

Table 3.11: Atom positions found for the $Ca_2Mn_2O_5$ structure. The atom positions were fixed through the refinement.

A schematic representation of the structure is shown in figure 3.11.:

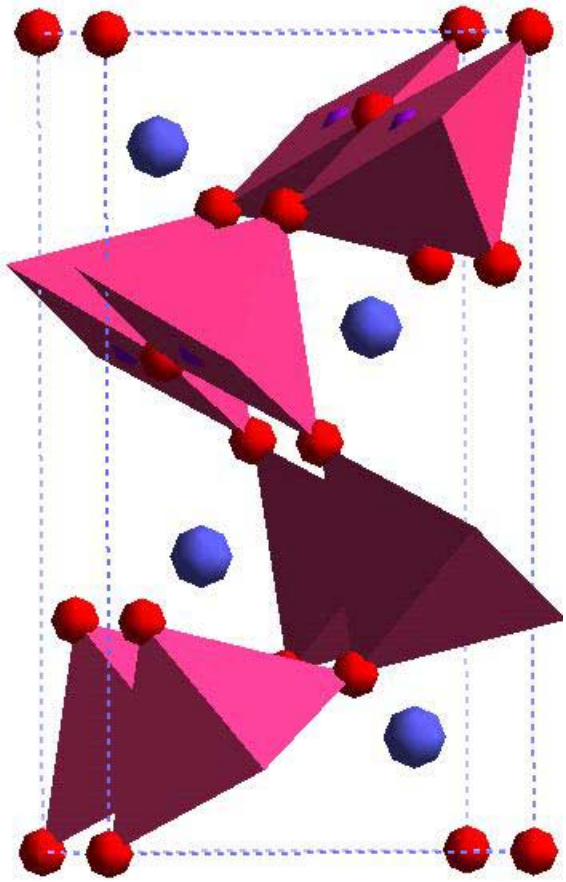

Figure 3.11: Schematic representation of the structure of $Ca_2Mn_2O_5$. Missing oxygen atoms produce square pyramids instead of octahedra. Ca is blue, O is red and Mn is purple.

3.3.1.3 $CaMnO_{2.75}$ ($Ca_4Mn_4O_{11}$):

In the proposed structure model of this composition, 50% of the manganese ions in the original $CaMnO_3$ framework have been reduced. It consists therefore of 50% MnO_6 octahedra and 50% MnO_5 square pyramids. The x-ray patterns of these samples show great likeness to the pattern that Chiang-Poeppelmeier [6] found and studied for this composition. The experiment was carried out several times and good reproducibility was obtained. An evaluation of the patterns in regard to a single phase product was made. At close studies it became clear that most of the $CaMnO_{2.75}$ samples contained the $Ca_2Mn_2O_5$ phase to a variable, but small degree. Even though the amount of the impurity phase is small it can influence the refinement greatly, and must be therefore be accounted for. The d-values of the observed $Ca_2Mn_2O_5$ reflections that where most profound are listed in table 3.12

d-value	2θ- With x-ray λ	2θ- With synchrotron λ
2.71	33.048	14.8
2.55	35.05	15.75
2.28	39.40	17.55

Table 3.12: List of the d-values of the observed reflections belonging to the $Ca_2Mn_2O_5$ impurity phase found in the $CaMnO_{2.75}$ sample.

Multiple samples of the composition $CaMnO_{2.75}$ were synthesized. Figure 3.12 shows the diffraction patterns of three different samples. The lower pattern shows extra reflections due to the internal standard Si that is used.

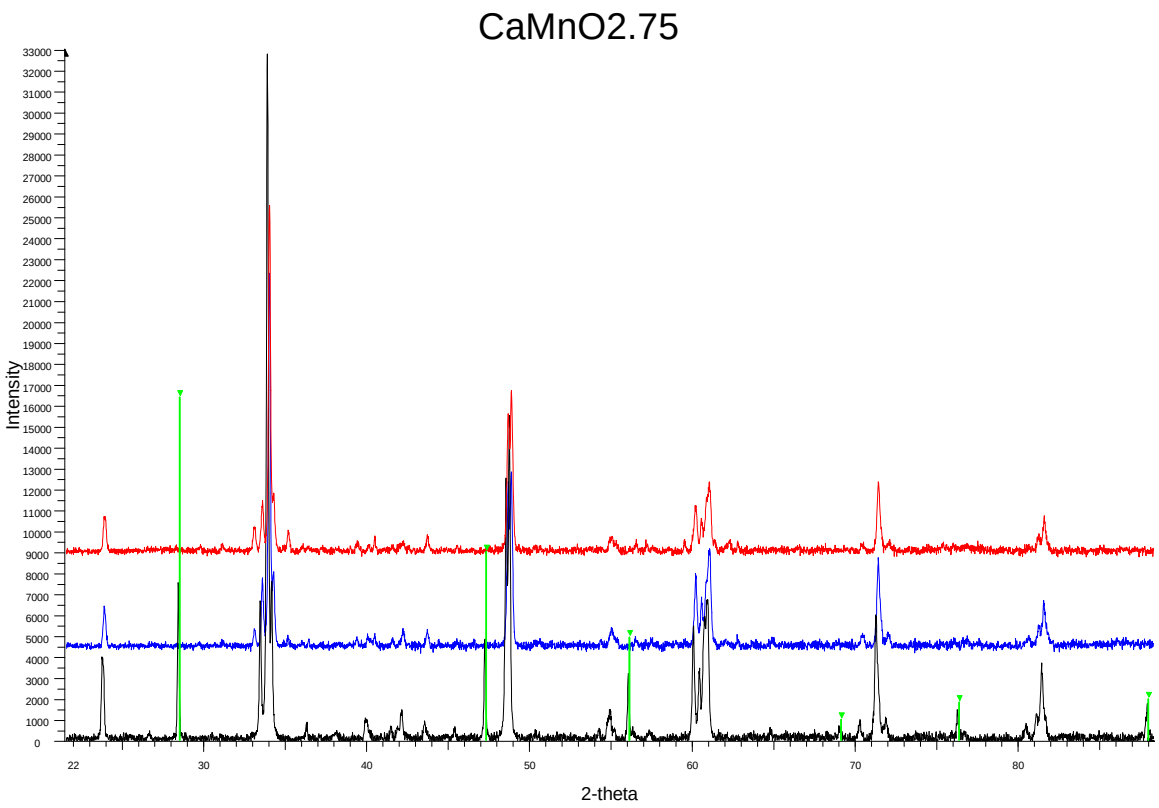

Figure 3.12: Diffraction patterns of three different samples of $CaMnO_{2.75}$. The samples show great likeness. Some of the intensities reported for the phase $Ca_2Mn_2O_5$ are present as impurities. The green vertical lines indicate reflections from the internal standard Si.

Chiang-Poeppelmeier [6] noted that x-ray powder pattern determination of the structure was unrealistic due to the small scattering factor of oxygen atoms and therefore used neutron data to supplement his refinement studies. Never the less an attempt to identify the structure was made using the x-ray pattern from diffractometer 1. The pattern was investigated thoroughly using GSAS refinement, based on the unit cell proposed by Chiang-Poeppelmeier [6]. This is not the same unit cell that Reller et al [1] used, since the b-axis is doubled by in the Chiang Poeppelmeier model. The space group $Pmc2_1$ was used since this space group had been used by Chiang-Poeppelmeier even though they did not conclude that this was the correct space group.

The atom positions were introduced into the model by using the $CaMnO_3$ positions as starting values, except that the b axis and y coordinates were divided by 4. This was done due to the fact that the superstructure proposed by Chiang Poeppelmeier [6] has a b axis

four times as large as $CaMnO_3$. This is when the view of the perovskites is from above with the octahedra into the paper plane as seen in figure 3.13. This gives the $CaMnO_{2.75}$ unit cell with the oxygen content of $CaMnO_3$. Figure 3.13 shoves the unit cell before oxygen has been removed to create vacancies. This represents a $CaMnO_3$ super cell with four normal $CaMnO_3$ units in the y direction.

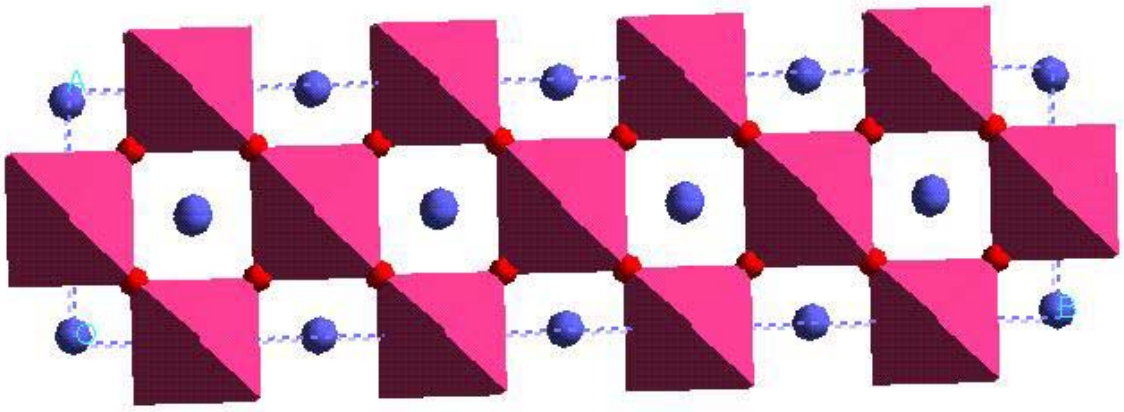

Figure 3.13: $CaMnO_{2.75}$ before removing oxygen from the lattice. The projection is of the ab plane with Ca as blue atoms in the corners. Oxygen is red. Oxygen atoms at the top and bottom of the octahedra are not shown.

In $CaMnO_{2.75}$ every twelfth oxygen atom is missing which corresponds to the condition when half of the Mn ions are reduced. There are six possible oxygen vacancy arrangements that satisfy square pyramid creation and the $CaMnO_{2.75}$ composition. Chiang-Poeppelmeier [6] had predicted these different oxygen orderings. In figure 3.14 these six different orderings of $CaMnO_{2.75}$ are shown. The projections are in the ab plane, the Ca atoms are not included and the oxygen atoms are moved into the origo positions. Oxygen atoms on top and below the Mn ions are not shown.

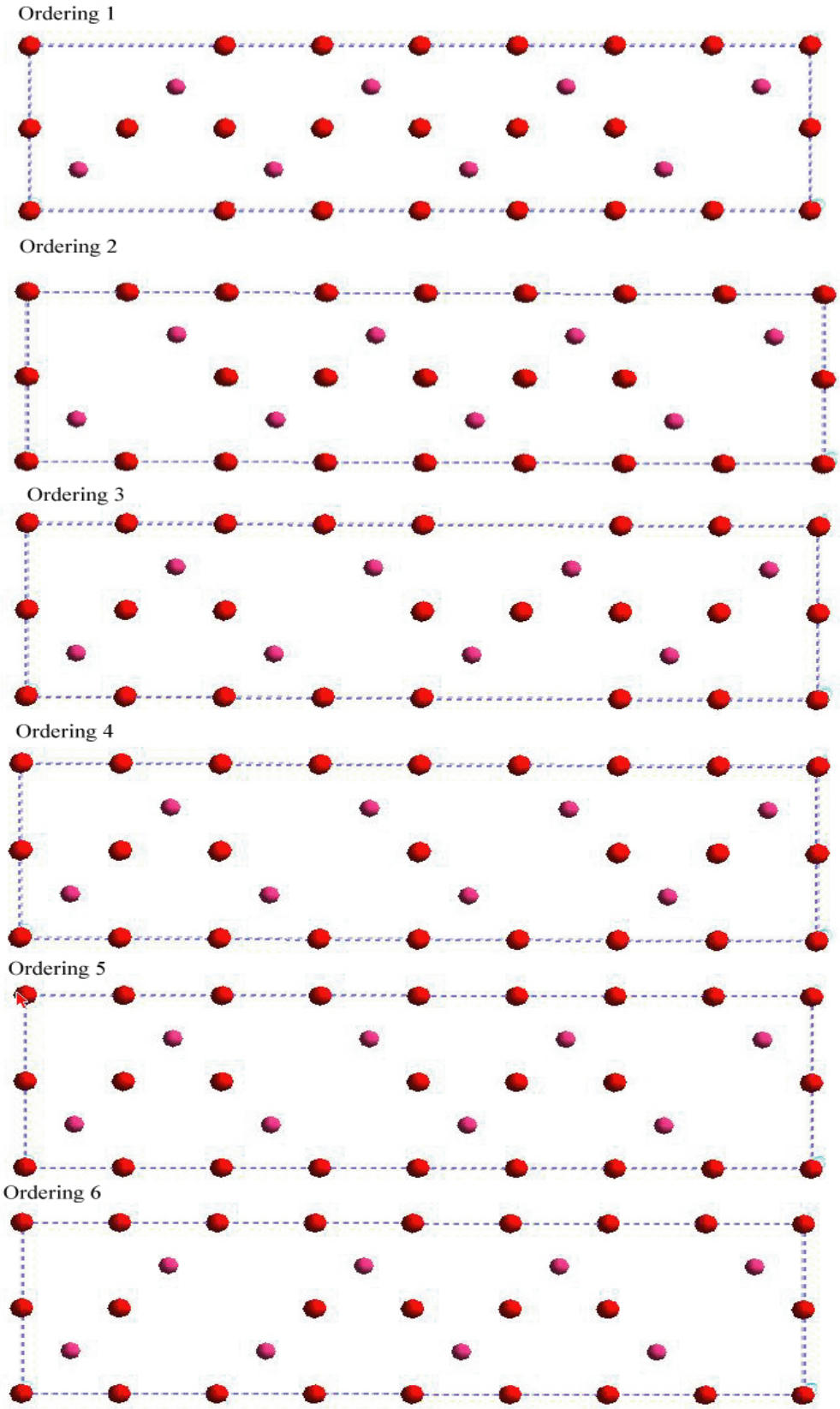

Figure 3.14: Six different orderings of oxygen in $CaMnO_{2.75}$.

A preliminary refinement based on the data and model of Chiang-Poeppelmeier et al [6] was done. It gave a good, but not satisfactory fit with the unit cell dimensions they had reported. The refinement of the pattern can be seen in figure 3.15

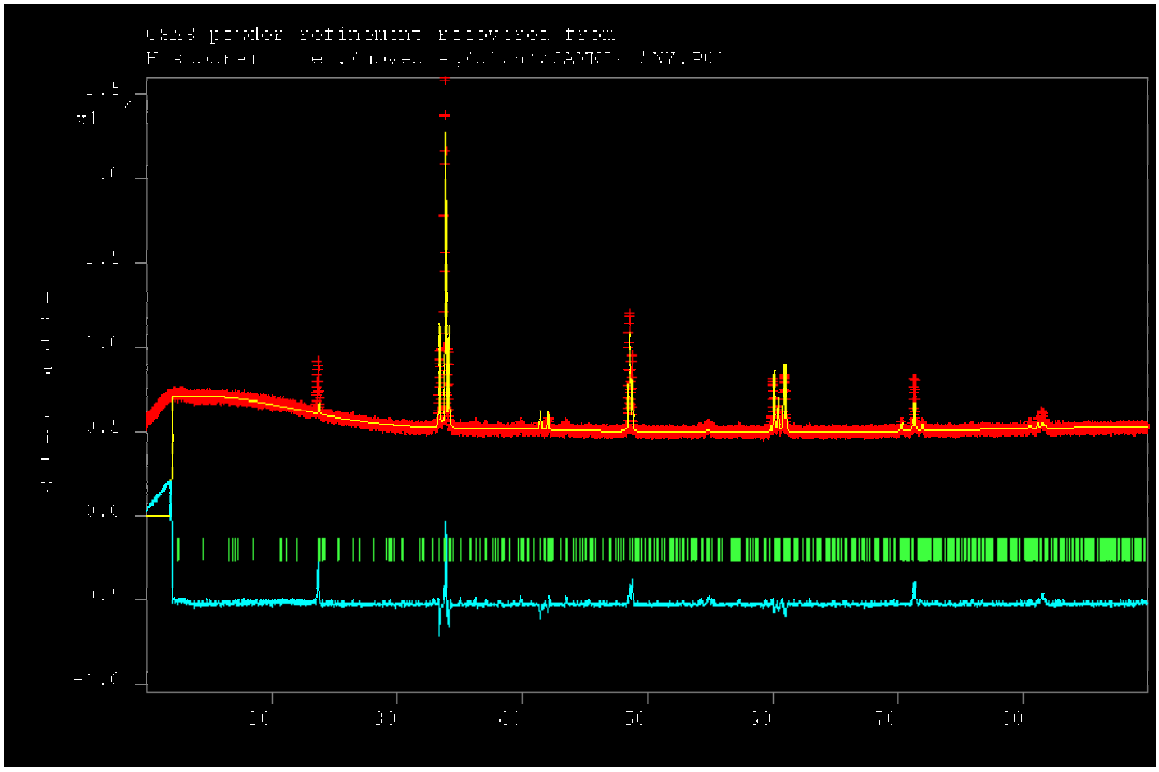

Figure 3.15: Preliminary refinement of x-ray diffraction pattern of $CaMnO_{2.75}$. Background function and most profound peaks are fitted well. The pattern is recorded on home diffractometer 1.

As reported earlier reflections from impurities had been detected during the refinement of the $CaMnO_{2.75}$ pattern recorded on diffractometer 1. The Le Bail method was used with the same structure model as used earlier to study the diffraction pattern. As expected, it became clear that not all reflections could belong to the unit cell of the $CaMnO_{2.75}$ phase. The existence of $Ca_2Mn_2O_5$ was found and that phase was entered into the refinement experiment. This made the Le Bail fitted pattern much better, but it also became evident that there were still some reflections that could not be indexed with either of the two unit cells. It was likely that another impurity phase was present. The positions of the reflections not belonging to $Ca_2Mn_2O_5$ or $CaMnO_{2.75}$ were listed and their d-values found. The list of these reflections is shown in table 3.13

2θ Synchrotron	d-value	2θ Synchrotron	d-value
8.27	4.8460	17.52	2.2957
11.51	3.4834	18.00	2.2343
13.32	3.0128	18.07	2.2251
13.96	2.8762	18.42	2.2048
15.59	2.5769	19.32	2.0757
16.57	2.4257	20.939	1.9238

Table 3.13: The list of reflections that could not be indexed by the unit cells of $CaMnO_{2.75}$ and $Ca_2Mn_2O_5$.

After checking the international database for other $CaMnO_3$ related structures with reflections that did not match either the unit cell of $Ca_2Mn_2O_5$ or $CaMnO_{2.75}$ it became clear that the phase $CaMn_2O_4$ fitted every one of the listed reflections. $CaMn_2O_4$ is the mineral Marokite and is well described [26]. The unit cell and atom positions of Marokite were introduced into the refinement.

This further improved the Le Bail fitted pattern, and except for a few very small reflections every reflection had been assigned to one of these three phases. The pattern from the Le Bail refinement can be seen in figure 3.16.

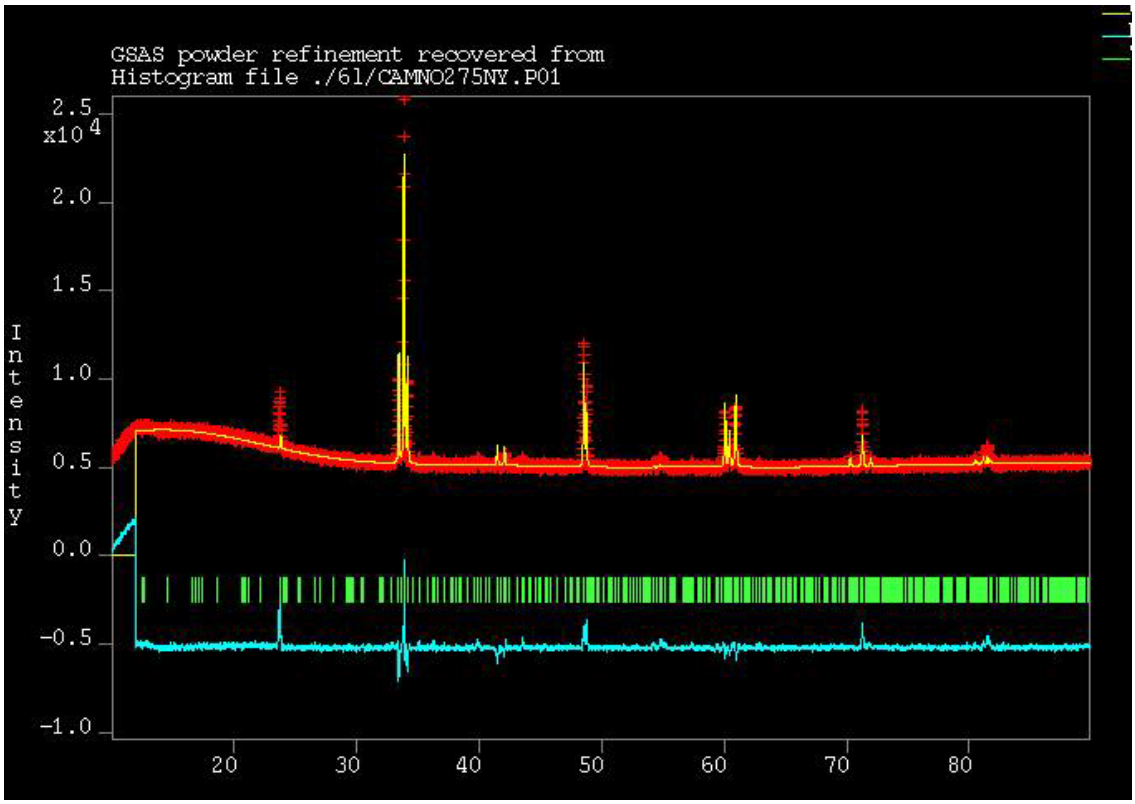

Figure 3.16: Pattern obtained with Le Bail refinement compared with the x-ray diffraction pattern of $CaMnO_{2.75}$.

Neutron data for one $CaMnO_{2.75}$ sample had also been collected. The neutron pattern for this composition was recorded on the pus reactor at IFE, Kjeller. Figure 3.17 shoves the neutron pattern recorded at room temperature refined with the same structural information used for the preliminary refinement of the x-ray pattern in figure 3.15 on page 53.

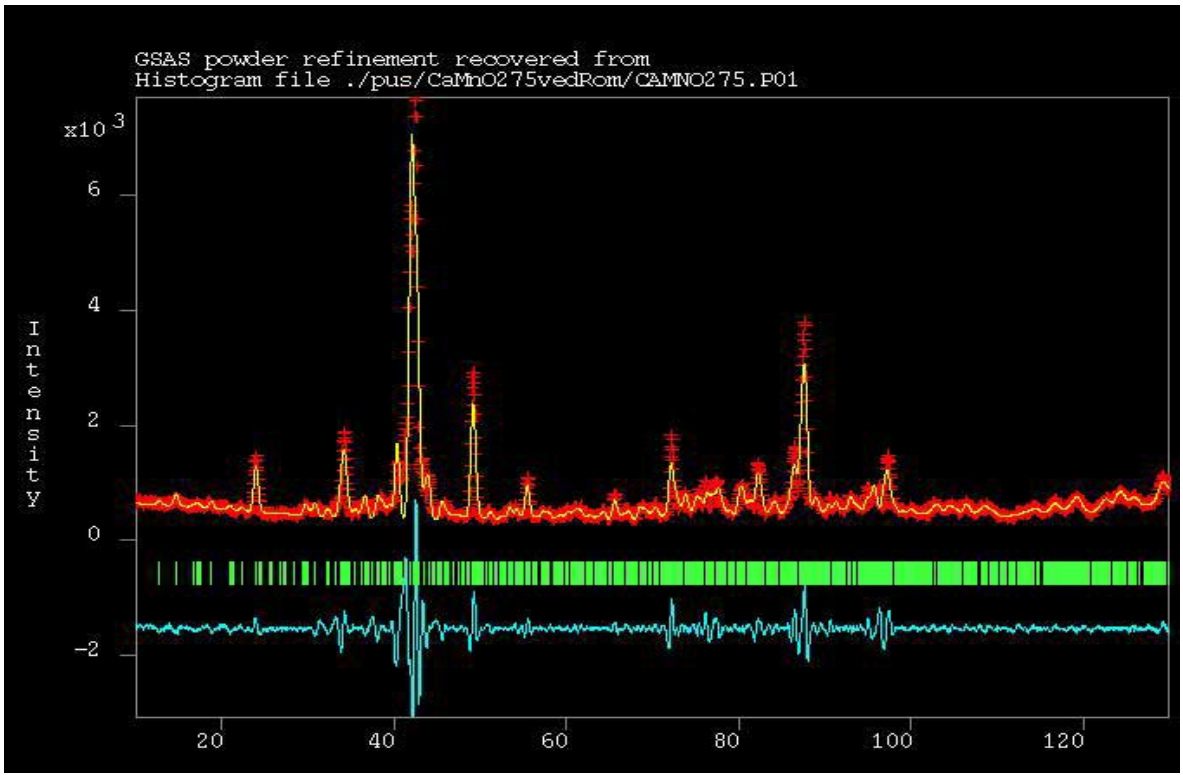

Figure 3.17: Refinement of the neutron diffraction pattern of $CaMnO_{2.75}$.

The error factors found for refinement for the neutron pattern are shown in table 3.14:

R_p	0.1042
wR_p	0.1591
χ^2	17.55

Table 3.14: The error factors from the refinement of the neutron pattern of $CaMnO_{2.75}$.

The neutron pattern refinement gave the crystallographic information listed in table 3.15:

Space Group	$Pmc2_1$
Symmetry	Orthorhombic
a (in Ångstrøm)	5.3507 (4)
b (in Ångstrøm)	20.9718 (5)
c (in Ångstrøm)	7.4587 (4)

Table 3.15: Crystallographic information obtained from the refinement of neutron pattern of $CaMnO_{2.75}$.

In order to determine the exact origin of the reflections present in the diffractogram and to be able to distinguish them better from one another and the background a synchrotron XRD dataset was recorded in Grenoble. The space group that had been used with the x-ray diffraction pattern was $Pmc2_1$, but doubts that this was the actual space group existed as it could not be verified satisfactory. A new orthorhombic space group was sought for since the parent material $CaMnO_3$ is an orthorhombic perovskite and the structure model for $CaMnO_{2.75}$ was derived from that structure. In an attempt to determine the space group manually, the synchrotron diffraction pattern was refined with the same unit cell dimensions that Chiang-Poeppelmeier used and the space group Pmmm. Pmmm is an orthorhombic space group without extinctions. Impurities were not included. Both a LeBail fitting refinement and a normal least squares refinement were performed. The result of the normal least square refinement can be seen in figure 3.18.

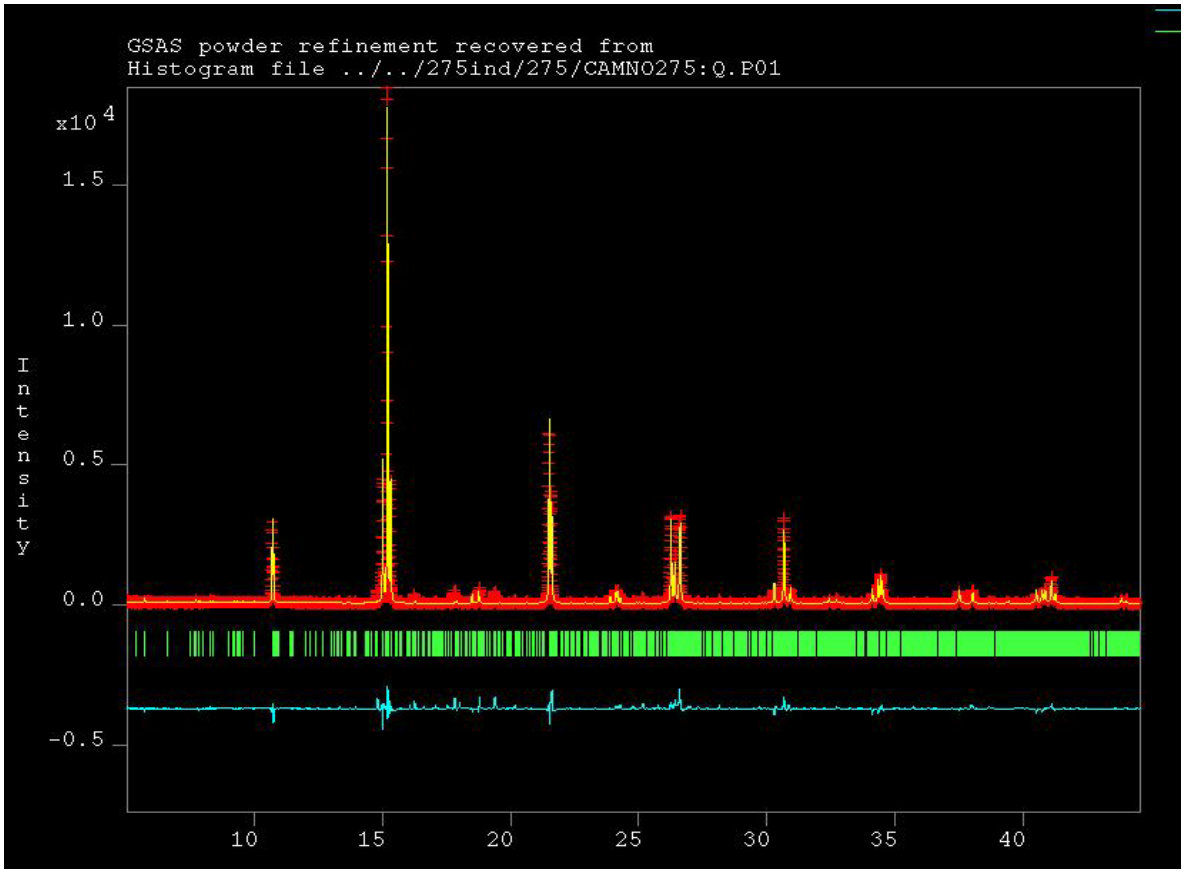

Figure 3.18: Refinement of the synchrotron data recorded for the $CaMnO_{2.75}$ structure.

The data values found after the Rietveld refinement for the synchrotron pattern are shown in table 3.16:

R_p	0.1418
wR_p	0.1959
χ^2	5.248

Table 3.16: Error factors from the refinement of synchrotron pattern of $CaMnO_{2.75}$.

The calculated pattern for the synchrotron pattern yielded the crystallographic information listed in table 3.17:

Space Group	Pmmm
Symmetry	Orthorhombic
a (in Ångstrøm)	5.3496 (1)
b (in Ångstrøm)	20.9719 (1)
c (in Ångstrøm)	7.4586 (9)

Table 3.17: Crystallographic information obtained from the refinement of synchrotron pattern of $CaMnO_{2.75}$.

From the LeBail refinement a list of the first 200 reflections and their corresponding hkl values was produced. These were then compared to the experimental pattern to evaluate where reflections were present. The list can be seen in the appendix. The reflections that could be observed visually in the experimental pattern were listed. Systematic rules of extinction for the reflections not observed and hkl summation rules for the reflections observed were then sought for. As a result only one rule could be found with certainty. This is the condition h0l with h + l = 2n. In addition some other conditions are likely to exist. The condition h00 with h = 2n could be present, but there is only one reflection that fulfils the criteria. This is the reflection from the plane (2 0 0). The condition 0k0 with k = 2n is more likely to be present. In this case there are numerous observed reflections that fulfils the criteria, but on the contrary the reflection from the plane (0 13 0) that disqualifies this condition is also observed. The presence of the reflection from (0 13 0) is uncertain and it is very difficult to evaluate if there truly is a reflection at this angle (2θ = 25.03, d = 1.61318). In the case of the 00l condition with l = 2n only one reflection again

fulfils the condition. In addition the reflection from the plane (0 0 5) that disqualifies the condition is observed. Again it is very difficult to evaluate if these reflections truly are there. These observations gave rise to only one possible space groups. If only the first condition is present, together with the h = 2n and l = 2n then the space group is $Pmn2_1$. Due to the uncertainty in the observations, the indications toward this space group are not very reliable. Another technique was therefore applied.

In an attempt to determine the correct space group once and for all a TEM study of the sample was provided. Electron diffraction pictures from TEM would reveal systematic extinctions and would also verify the unit cell. In figure 3.19 and 3.20 pictures from the TEM study can be seen.

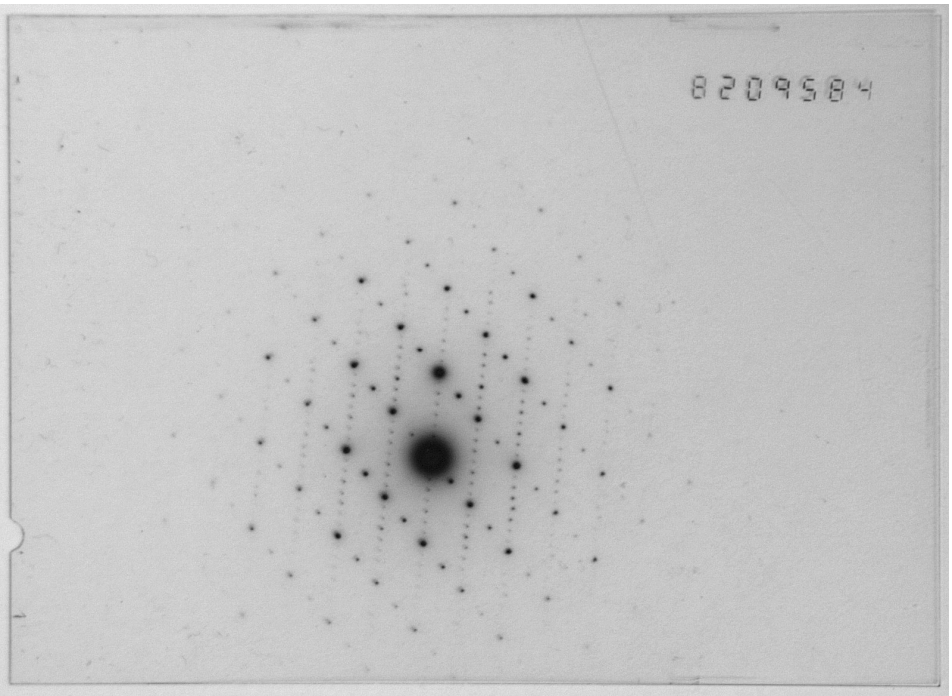

Figure 3.19: TEM electron diffraction picture of the ab plane. If systematic extinctions existed points would be missing systematically. No extinctions can be seen.

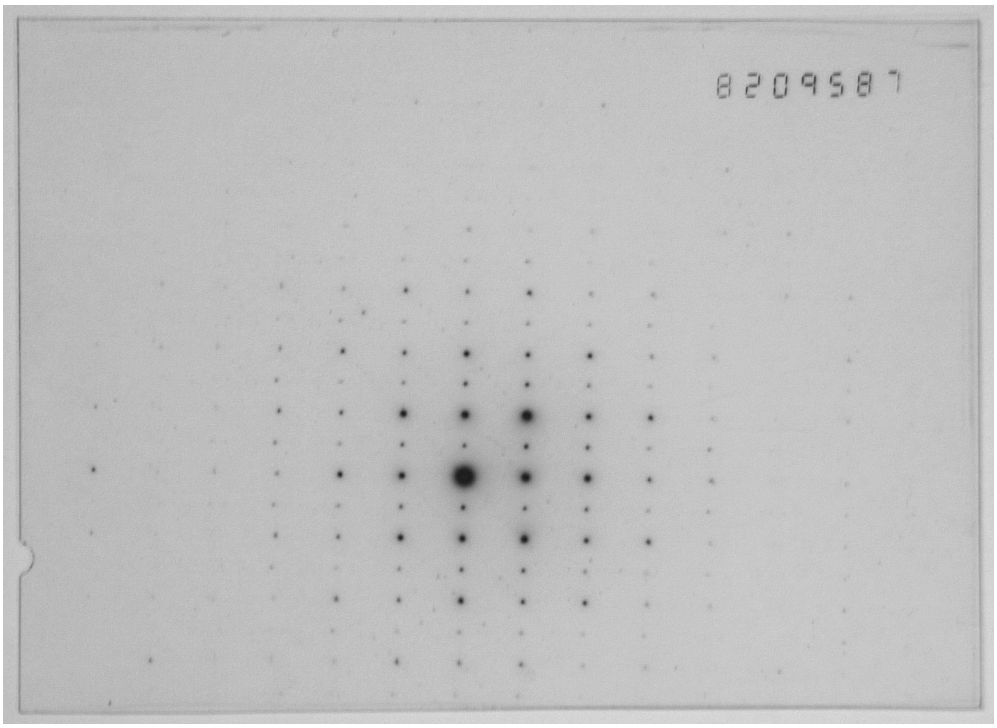

Figure 3.20: TEM electron diffraction picture of the ac plane. No extinctions can be observed.

In the TEM pictures no extinctions can be seen. This means that either the space group is a very simple one or the crystals observed were not the $CaMnO_{2.75}$ phase. What could be deducted from the images after calculation, however, was the unit cell proposed by Chiang –Poeppelmeier [6]. Since the TEM images indicate a simple space group without extinctions, but the oxygen defect structure model was derived from a space group with a screw axis, the results contradict the model.

It is very useful to be able to refine synchrotron XRD, PND and normal x-ray patterns in the same work session. The acquired changes in the parameters can then be applied to all patterns, and a better understanding of the changes can be obtained when they are observed in all scans simultaneously. A refinement that calculates changes in both synchrotron XRD and PND at the same time was commenced. This refinement was done very thoroughly with refining of many small parameter details in the structure model that in many cases contribute only a little to the total refinement. Several refinement experiments that were only slightly different gave rise to numerous calculations, and

minor changes in the structure model could worsen the error Rietveld factors drastically. These parameters include atom temperature factors, atom positions, atom constrains, phase fractions and lattice constants to name some. Even though two impurity phases have been discovered it is clear that minor reflections are not fitted and that traces of other impurities are present. This impurity was sought for, but could not be found among reported $CaMnO_{3-x}$, $CaCO_3$ and $(Ca,Mn)CO_3$ compounds. The d-values of these reflections are listed in table 3.18.

d-value	7.72	13.32	17.53	18.02	24.77	27.00	34.06

Table 3.18: List of d-values of reflections that could not belong to any of the phases entered into the refinement experiment.

The results from the simultaneous experiment are presented here. The refinement of the pattern of $CaMnO_{2.75}$ for synchrotron can be seen in figure 3.21 while the refinement of the neutron pattern can be seen in figure 3.22. The crystallographic information and the error factors from the experiment are listed in table 3.19 to 3.21.

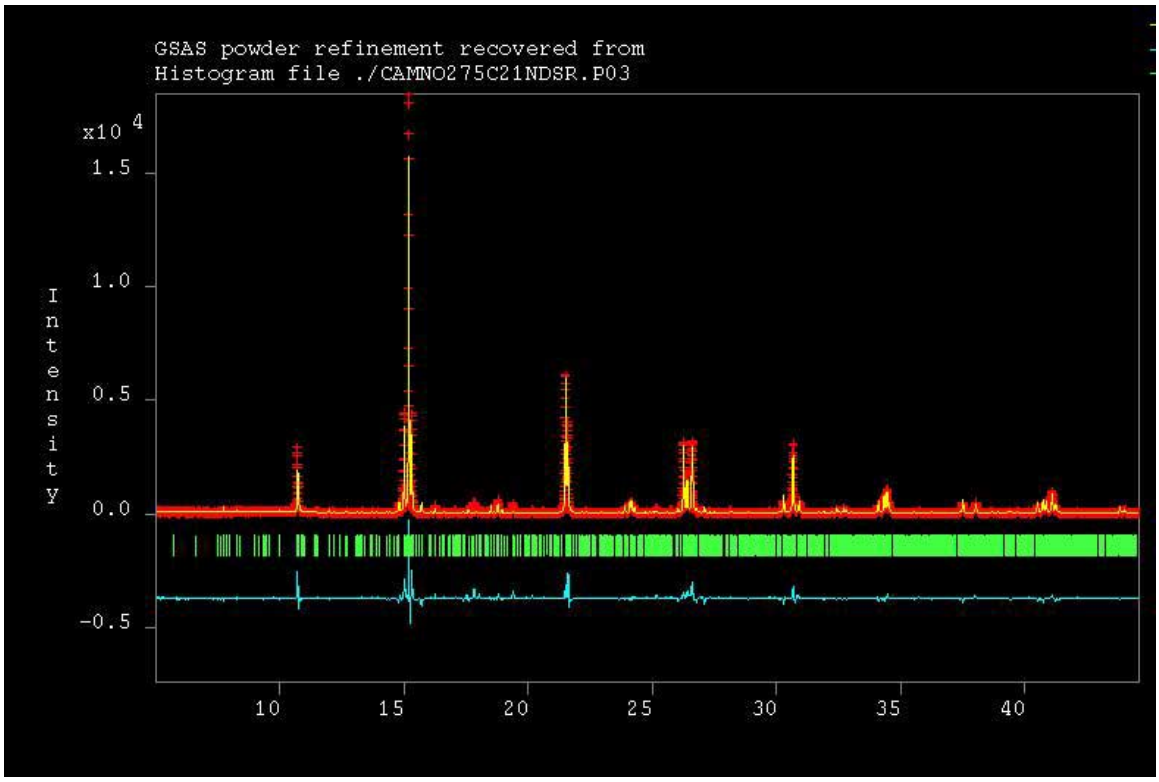

Figure 3.21: Refinement of the synchrotron diffraction pattern together with the neutron diffraction pattern with the space group $Pmc2_1$.

The error factors found in the refinement for the synchrotron pattern when refined with the neutron pattern and space group $Pmc2_1$ are listed in table 3.19.

R_p	0.1778
wR_p	0.2445
χ^2	16.67

Table 3.19: The error factors from the refinement of the synchrotron pattern of $CaMnO_{2.75}$.

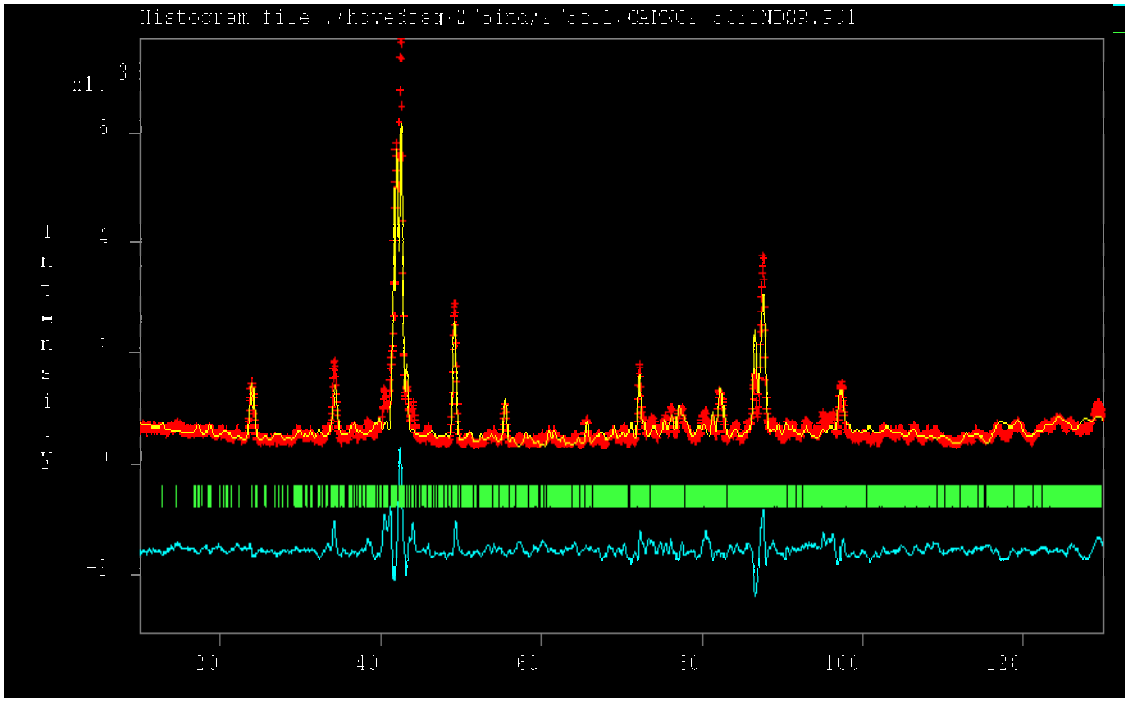

Figure 3.22: Refinement of the neutron diffraction pattern at room temperature when refined together with the synchrotron data set for the space group $Pmc2_1$.

The error factors found after the Rietveld refinement for the neutron pattern with the space group $Pmc2_1$ are shown in table 3.20:

R_p	0.1826
wR_p	0.2491
χ^2	16.67

Table 3.20: The error factors from refinement of the neutron pattern of $CaMnO_{2.75}$.

The refinement for synchrotron yielded the crystallographic information in table 3.21:

Space Group	$Pmc2_1$
Symmetry	Orthorhombic
a (in Ångstrøm)	5.34893 (9)
b (in Ångstrøm)	20.9708 (4)
c (in Ångstrøm)	7.45788 (14)

Table 3.21: Crystallographic information obtained from the refinement of the synchrotron pattern of $CaMnO_{2.75}$.

The space group used in this experiment was $Pmc2_1$ even though indications earlier showed that this space group probably was not correct. The paradox that became clear as the TEM electron pictures showed no extinctions together with the knowledge that the oxygen defect model needs a screw axis or glide plane complicates the experiment. Most of the refinement of this structure was done with the space group $Pmc2_1$ and thus the results from that work are presented here. One orthorhombic space group that has a glide plane is the space group Pmm2. This space group does not have any extinctions and thus fits both criteria. It is clear that it is possible to draw oxygen models with this space group that can correspond to the ones proposed by Poeppelmeier (figure 3.14). Refinement works with this space group (Pmm2) and its alternative settings (Pm2m and P2mm) are however beyond the work limits of this thesis. It is clear that all information concerning the $CaMnO_{2.75}$ phase has not been found. It is in particular the smaller reflections that likely have their origin in oxygen vacancies or the superstructure that are not fitted in the model. The $CaMnO_{2.75}$ results are discussed in chapter 4.2.2.

A study of the $CaMnO_{2.75}$ structure at low temperature was also performed. Low temperature neutron diffraction would reveal possible changes in the diffraction pattern due to magnetic ordering at low temperatures. A pattern was recorded at 9K. All reflections from the room temperature pattern (except the impurity reflections) can be indexed with the unit cell used in the synchrotron refinement of this phase. The extra reflections that appear on the pattern recorded at low temperature are indexed by a unit cell with double c-axis. This indicates a magnetic ordering at low temperature. The

patterns are displayed in figure 3.23. The first half of the neutron diffraction patterns recorded at 9K is compared with the first half of the one recorded at room temperature together with the difference between them.

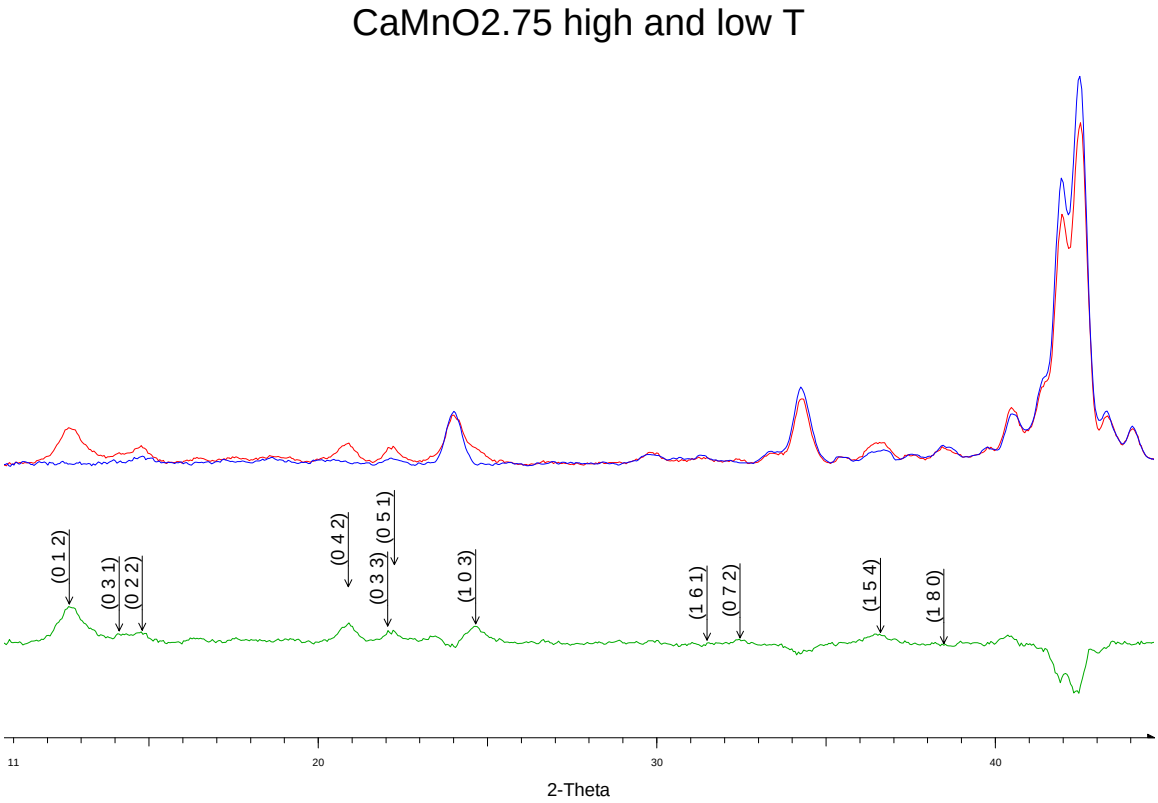

Figure 3.23: The first half of the high (blue) and low (red) temperature neutron diffraction pattern of $CaMnO_{2.75}$ and the difference between them with the (hkl) values of the extra reflections caused by the enlarged unit cell.

3.3.2 Other $CaMnO_{3-x}$ compositions investigated:

3.3.2.1 $CaMnO_{2.8}$:

In this composition 40% of the MnO_6 octahedra have been turned into MnO_5 square pyramids. The phase was described by Reller et al [1], but only the unit cell was presented and no further structure determination was performed. The samples were made by standard zirconium reduction as described in chapter 2.2.1.

The unit cell Reller et al [1] observed by HREM has tetragonal symmetry with the unit cell dimensions a = b = 8.34 Ångstrøm and c = 7.46 Ångstrøm, or in terms of the cubic perovskite $a = \sqrt{5}\ a_c$, $b = \sqrt{5}\ a_c$ and $c = 2\ a_c$ where a_c = 3.73 Ångstrøm and rotation angle R = 26.5˚. Reller et al described the unit cell as pseudo tetragonal. This indicates that it in reality is an orthorhombic unit cell with the a and b axis slightly different. Derived from the structure of $CaMnO_3$ the supercell of the $CaMnO_{2.8}$ structure that Reller et al observed is shown in figure 3.24:

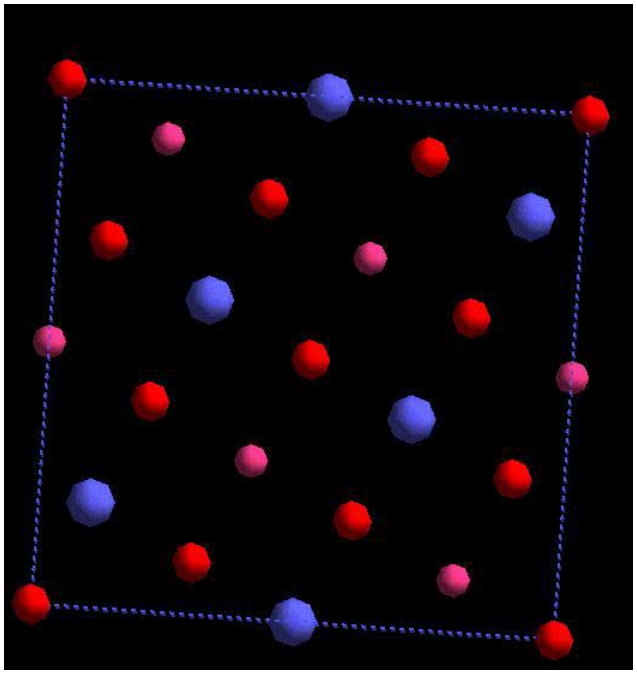

Figure 3.24: Supercell of $CaMnO_{2.8}$ with the dimensions $a = \sqrt{5}\ a_c$, $b = \sqrt{5}\ a_c$ before removing oxygen from the lattice. Oxygen atoms at top and bottom octahedra (above and below Mn ions) are not drawn. Ca is blue, O red and Mn purple.

There are two different oxygen vacancy ordering schemes that satisfies the condition where 40% of the Mn^{4+} ions in the MnO_6 octahedra have been reduced to Mn^{3+} in MnO_5 square pyramids. These two conditions are shown in figure 3.25.

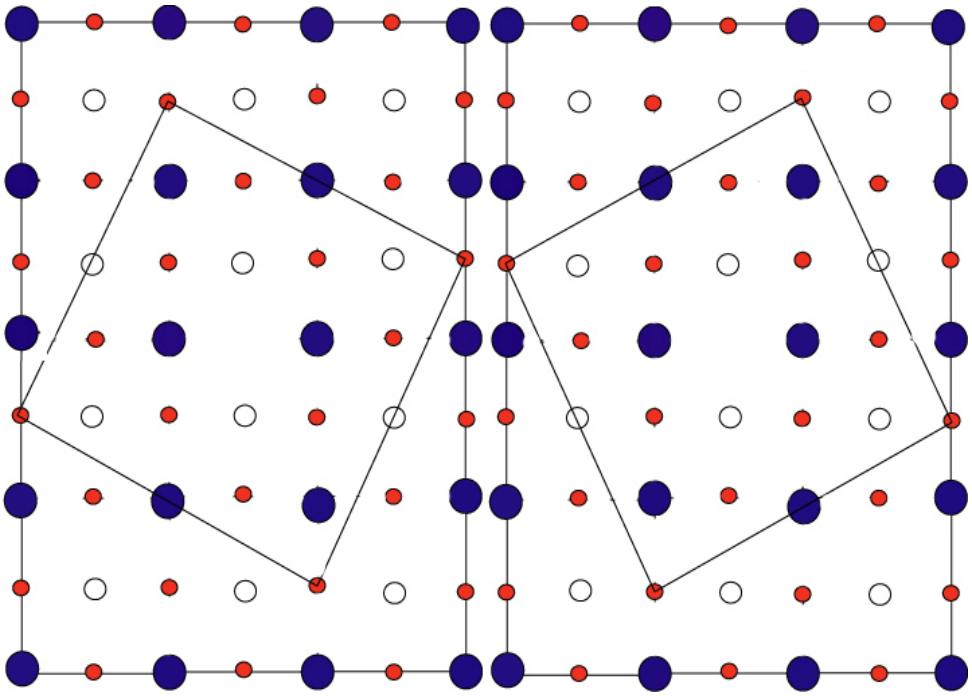

Figure 3.25: To possible oxygen vacancy orderings for $CaMnO_{2.8}$.

Numerous samples with the $CaMnO_{2.8}$ composition were made by zirconium reduction. Five different samples are shown in figure 3.26.

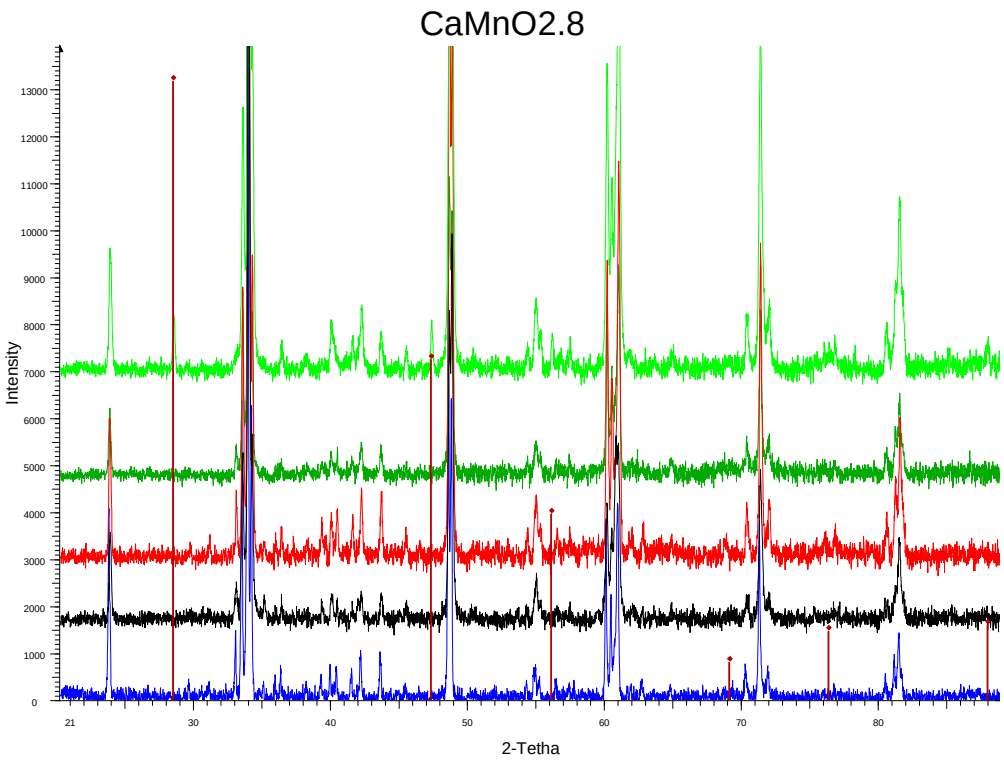

Figure 3.26: Five patterns for the composition $CaMnO_{2.8}$. The brown vertical lines are the reflections of Si.

Standard indexing methods were used in order to verify the unit cell dimensions proposed by Reller et al [1] from the diffraction patterns of the $CaMnO_{2.8}$ samples. These unit cell dimensions could not be reproduced. Impurity phases were sought for, and as was the case for the $CaMnO_{2.75}$ phase, reflections from both $CaMnO_{2.5}$ and Ca_2MnO_4 were found. These were considered impurity phases, and reflections belonging to these phases were removed before indexing once more. This produced no confirmation of the suggested unit cell. In order to obtain better data, a sample was sent to Grenoble and a synchrotron x-ray pattern for this composition was recorded.

At the start of the refinement of this phase, possible space groups had to be discussed. The synchrotron x-ray pattern was indexed using a programme named Material Studios. It has an indexing programme (Le Bail method) implemented that calculates error values for every possible space group. This was done for every orthorhombic space group. A satisfactory fit that could reveal the space group was not found for any of the space groups. Instead a GSAS refinement with an orthorhombic space group without systematic

extinctions was done. The space group Pmmm was chosen. The synchrotron pattern obtained for the $CaMnO_{2.8}$ composition structure was then modelled using Rietveld-GSAS LeBail refinement. It became clear that the proposed unit cell of the phase Reller et al [1] have described could not belong to the $CaMnO_{2.8}$ sample.

When compared the pattern of the $CaMnO_{2.8}$ composition shows great likeness to the pattern observed for the $CaMnO_{2.75}$ phase, and only minor differences can be seen. Since the differences between the scans of $CaMnO_{2.75}$ and $CaMnO_{2.8}$ are so small it is possible that the phase is either not stable in air or that the diffraction patterns are so alike in nature that they cannot be distinguished by this technique and experimental methods. The fact that $CaMnO_{2.5}$ and $CaMn_2O_4$ are present to a small degree is also a factor that contributes to make it harder to distinguish the phases if a $CaMnO_{2.8}$ phase truly exists. This is discussed further in chapter 4.2. No further refinement work was performed with this composition. In figure 3.27 a comparison of the $CaMnO_{2.8}$ and $CaMnO_{2.75}$ synchrotron patterns can be seen.

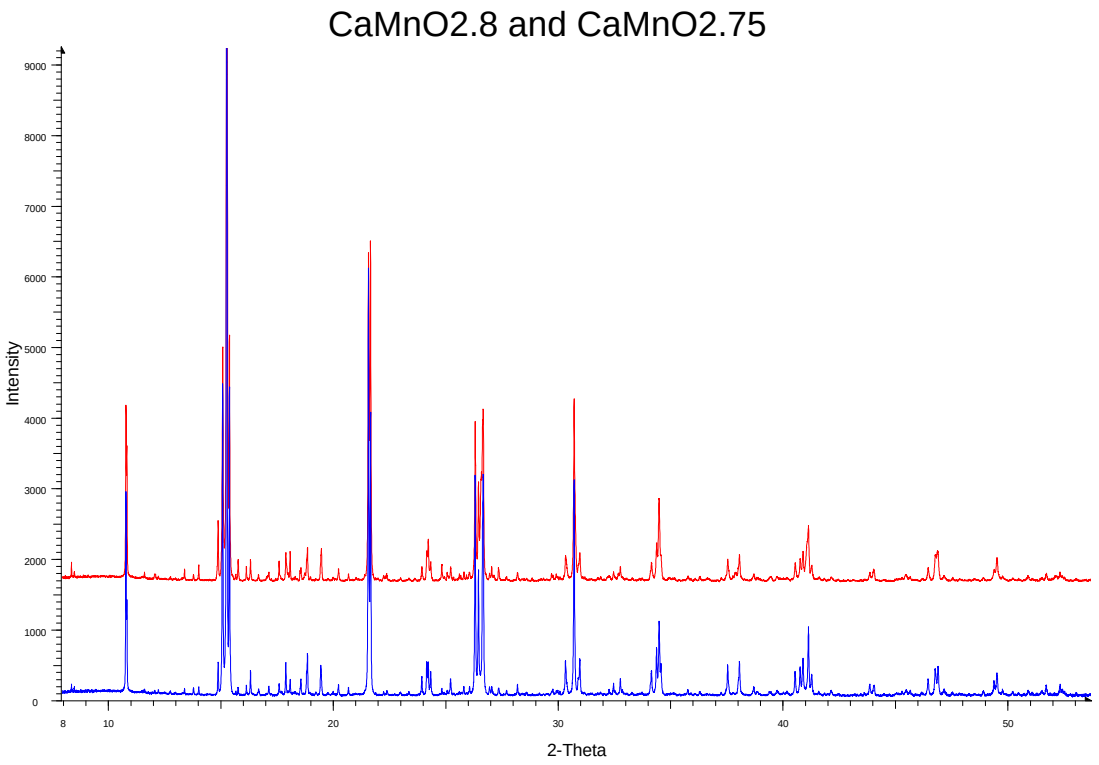

Figure 3.27: Synchrotron patterns of $CaMnO_{2.8}$ (red) and $CaMnO_{2.75}$ (blue). Only minor differences can be distinguished between them.

3.3.2.2 $CaMnO_{2.667}$:

This composition is obtained when 66.7% of MnO_6 octahedra are turned into MnO_5 square pyramids. It was described by Reller et al [1] as an intermediate phase with unit cell dimensions expressed in terms of the cubic perovskite, but no further structure determination has been reported for this composition. The samples were made by zirconium reduction. It was measured for high quality x-ray data on the diffractometer 1. Figure 3.28 below shows four scans for $CaMnO_{2.667}$:

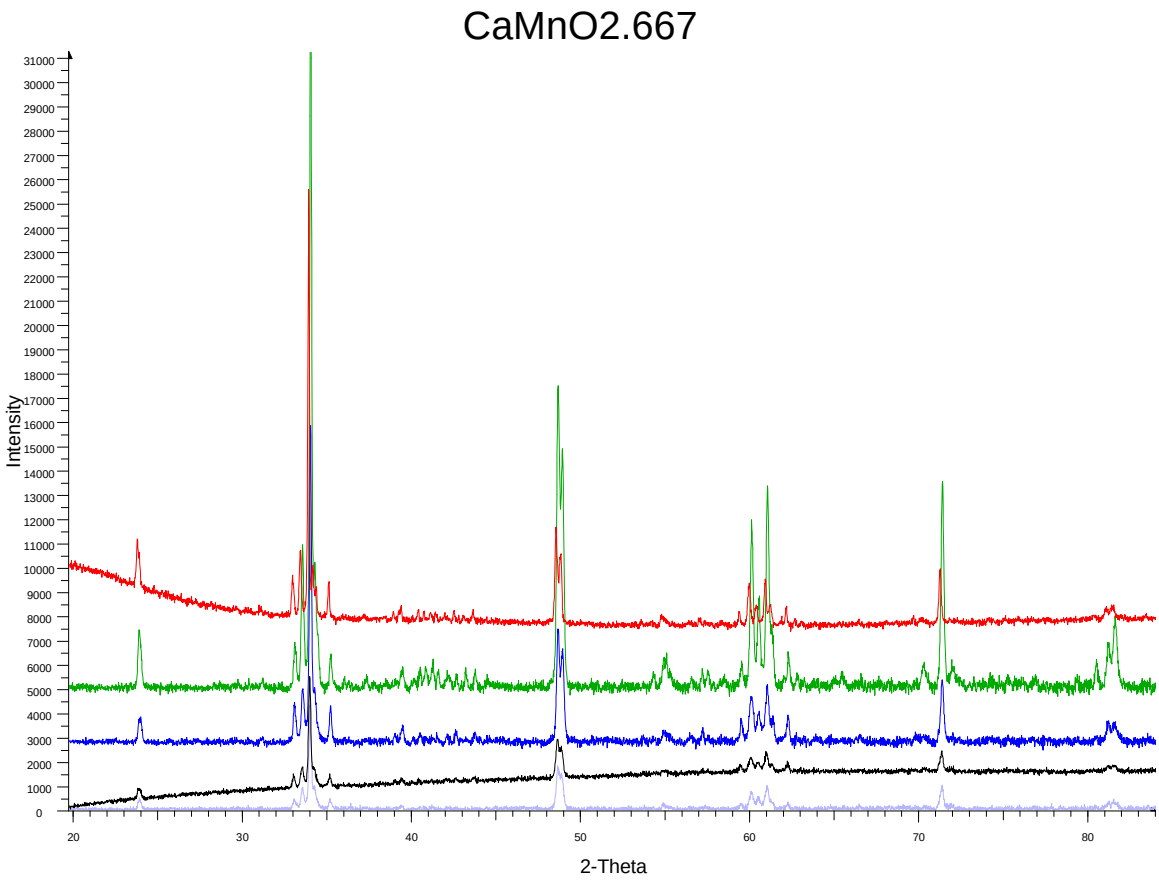

Figure 3.28: Diffraction patterns of four samples with the composition of $CaMnO_{2.667}$.

The unit cell suggested by Reller et al [1] had orthorhombic crystal symmetry with the unit cell dimensions a = 5.43 Å, b = 16.29 Å and c = 3.74 Å or in terms of the cubic unit cell $\sqrt{2}\ a_c$ x $3\sqrt{2}\ a_c$ x a_c where a_c = 3.73 Ångstrøm and rotation angle R = 45˚. In figure 3.29 an illustration of the unit cell is shown:

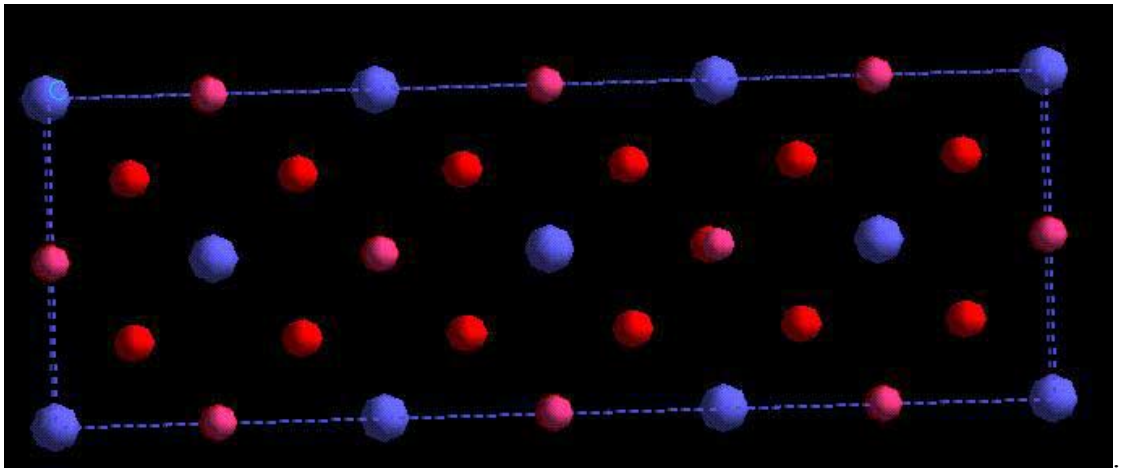

Figure 3.29: Super cell based on the $CaMnO_3$ structure described for the phase $CaMnO_{2.667}$.

There are two different oxygen vacancy orderings that satisfy this composition. These orderings are shown in figure 3.30.

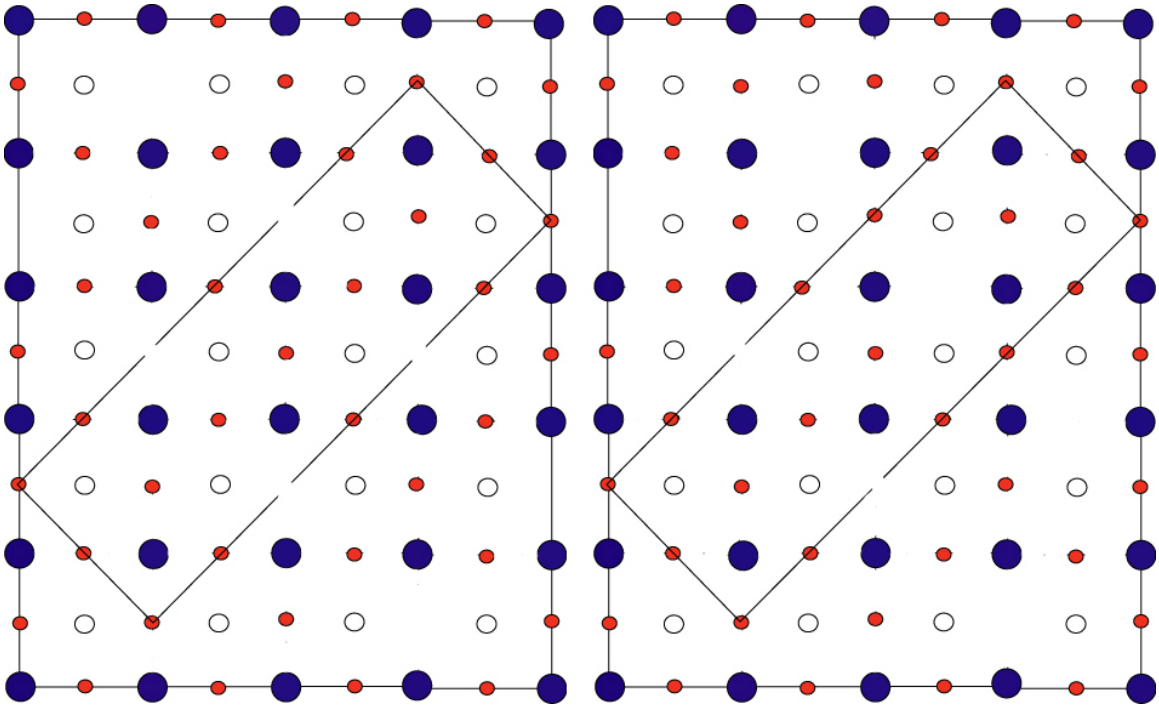

Figure 3.30: Two possible ordering schemes of oxygen vacancies for the $CaMnO_{2.667}$ structure. Ca is blue, Mn is white and O is red.

The pattern of a $CaMnO_{2.665}$ composition sample was tested with the LeBail method against the proposed unit cell. It was not possible to refine the unit cell dimensions proposed in literature [1] with the diffraction pattern of this composition. The x-ray pattern was checked for impurities of the phases $CaMnO_3$, $CaMnO_{2.5}$, $CaMnO_{2.75}$ and $CaMn_2O_4$. All of these were present in the pattern. The pattern was then, as was done with the $CaMnO_{2.8}$ composition samples, checked against the pattern of $CaMnO_{2.75}$. The reflections were at the same positions as in the $CaMnO_{2.75}$ composition. The patterns look very similar except that the $CaMnO_{2.5}$ phase is present to a much larger degree in these samples. No further structural work was performed with samples of this composition.

3.3.2.3: $CaMnO_{2.556}$:

The composition of $CaMnO_{2.556}$ is obtained when 88.9% of the MnO_6 octahedra have become MnO_5 square-pyramids. This was a phase described by Reller et al [1] that they did not observe. However, they found it most likely to exist. The suggested unit cell was described with orthorhombic symmetry with the unit cell dimensions a = 5.43 Å, b = 10.24 Å and c = 3.74 Å. The first sample was made by standard zirconium reduction. A second sample was made in the same manner and shows the same intensities, but with what seemed to be impurities of the phases $CaMnO_3$ and $CaMnO_{2.5}$. A third sample was therefore made. This sample looked very much alike the second one, and not single phase. A fourth sample was made. The scan of the fourth sample was identical to the latter samples made and these where taken as the representative patterns for this composition. All four scans can be seen in figure 3.31:

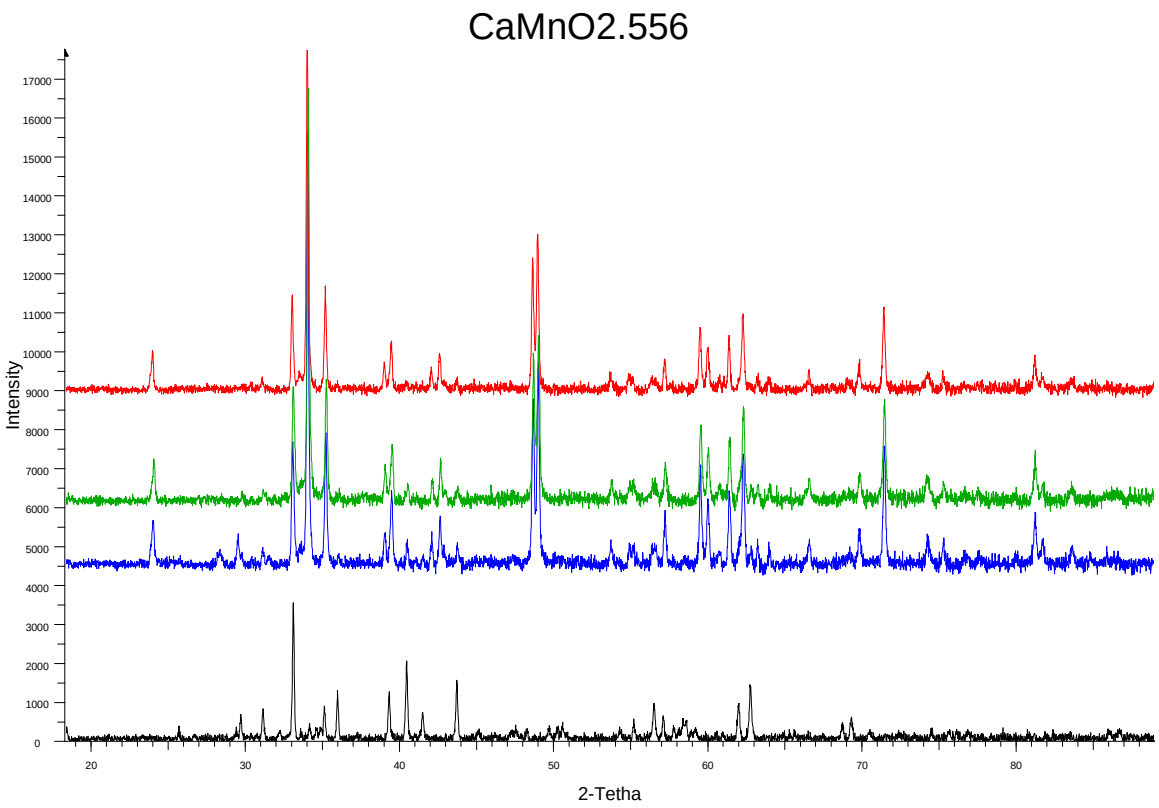

Figure 3.31: Three scans with the composition $CaMnO_{2.556}$. The black one at the bottom is the first sample made that did resemble the others. This pattern has been found to contain mainly Marokite but also $Ca_2Mn_2O_5$.

Even though this phase was not observed by Reller et al [1], the proposed unit cell based on HREM observations indicated microdomains of $CaMnO_{2.556}$ in the intergrowth of $CaMnO_{2.667}$ and $CaMnO_{2.5}$. The theorized unit cell proposed was $3\sqrt{3}\ a_c$ x $3\sqrt{3}\ a_c$ x a_c. A projection of the $CaMnO_3$ supercell can be can be seen in figure 3.32.

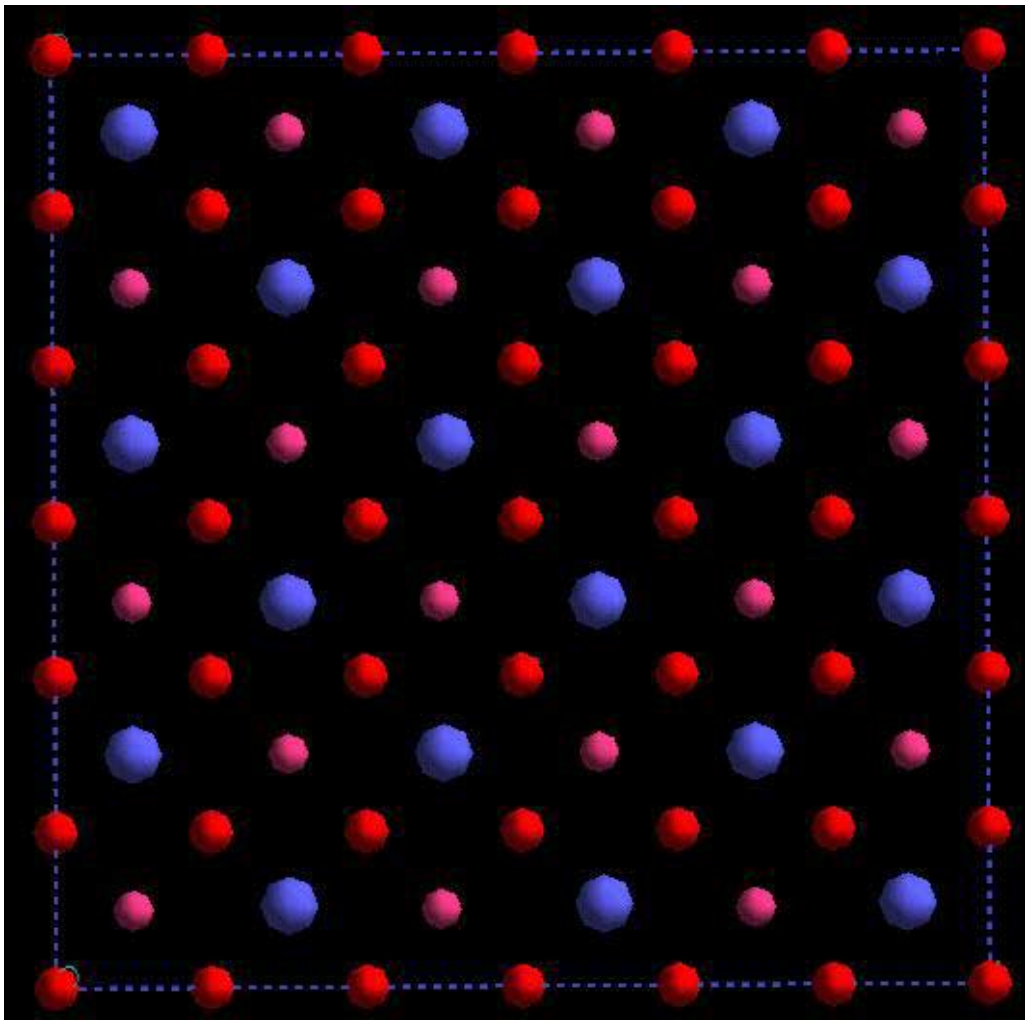

Figure 3.32: The supercell of $CaMnO_3$ with the proposed dimensions for $CaMnO_{2.556}$. Ca is blue, O red and Mn purple.

To reach the $CaMnO_{2.556}$ composition 88.9% of the MnO_6 octahedra must be changed into MnO_5 square pyramids. The figure 3.33 shows the supercell with the oxygen vacancies that satisfies the composition of $CaMnO_{2.556}$.

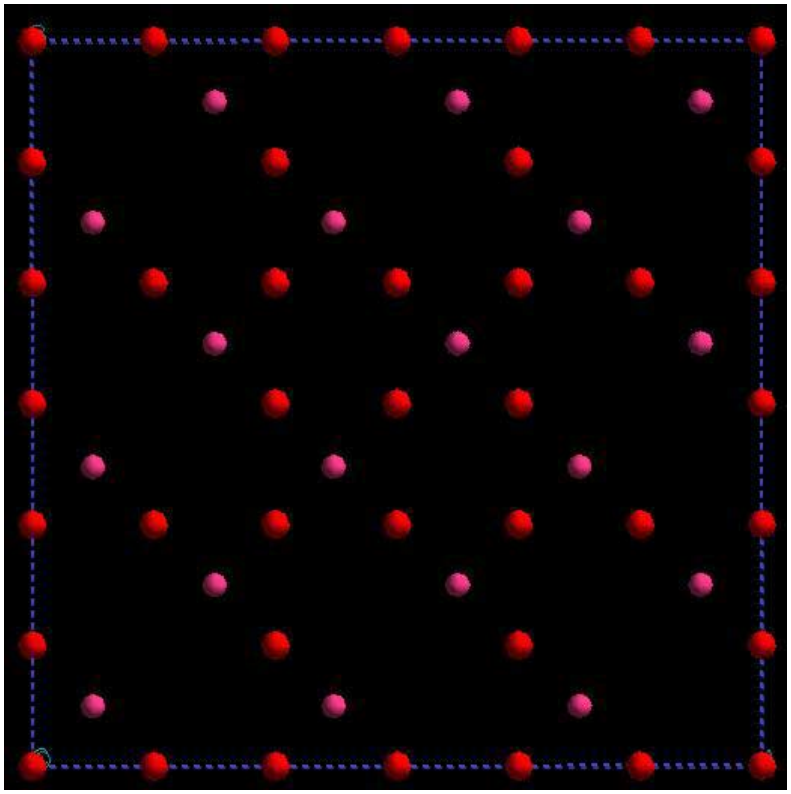

Figure 3.33: Supercell with oxygen vacancies of the theoretically described $CaMnO_{2.556}$. Mn is purple and Oxygen is red. Ca is not included.

The diffraction pattern was like the others reported by Reller et al [1] tested with the proposed unit cell. Again the unit cell did not match the reflections at all. The patterns of $CaMnO_{2.556}$ show only minor differences to that of $Ca_2Mn_2O_5$. If in reality the sample shows a separate phase, the reflections caused by the ordering of the oxygen vacancies and enlarged supercell cannot be distinguished from $Ca_2Mn_2O_5$ by these methods. It is also possible that the phase is not stable and turns into $Ca_2Mn_2O_5$. A comparison of $Ca_2Mn_2O_5$ and $CaMnO_{2.556}$ can be seen in figure 3.34.

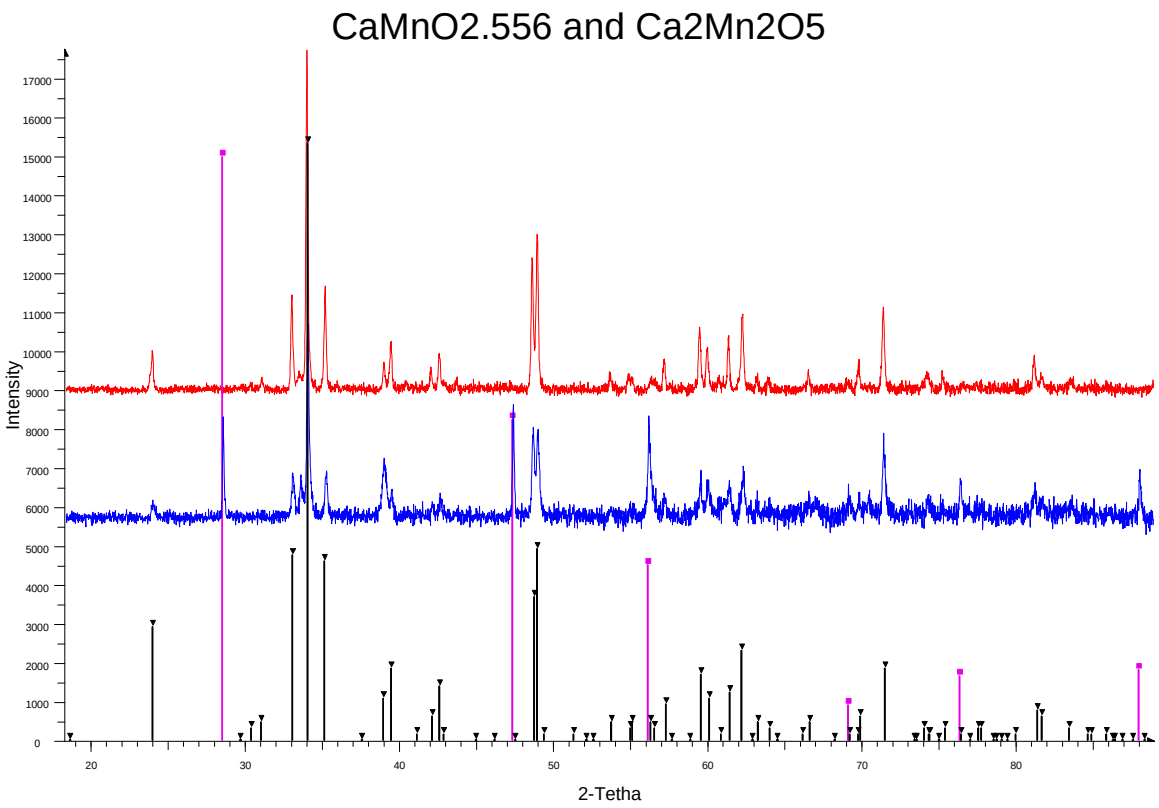

Figure 3.34: $Ca_2Mn_2O_5$ (blue) and $CaMnO_{2.556}$ (red) with the reported intensities of $Ca_2Mn_2O_5$ (black) and the internal standard Si (green).

3.2 Results from other techniques used for creating reduced $CaMnO_{3-x}$ samples:

3.2.1 Quenching experiments:

$CaMnO_{2.89}$ and $CaMnO_{2.94}$ are two compositions that were reported by Zeng and Greenbladt [10]. They were synthesized by quenching from the temperatures of 1100°C and 1000°C. A quenching from these temperatures was preformed in order to verify the results. The x-ray patterns of quenched samples from the temperatures listed showed no signs of any change and are identical to the patterns found for $CaMnO_3$. The x-ray diffraction patterns are shown in figure 3.35 below.

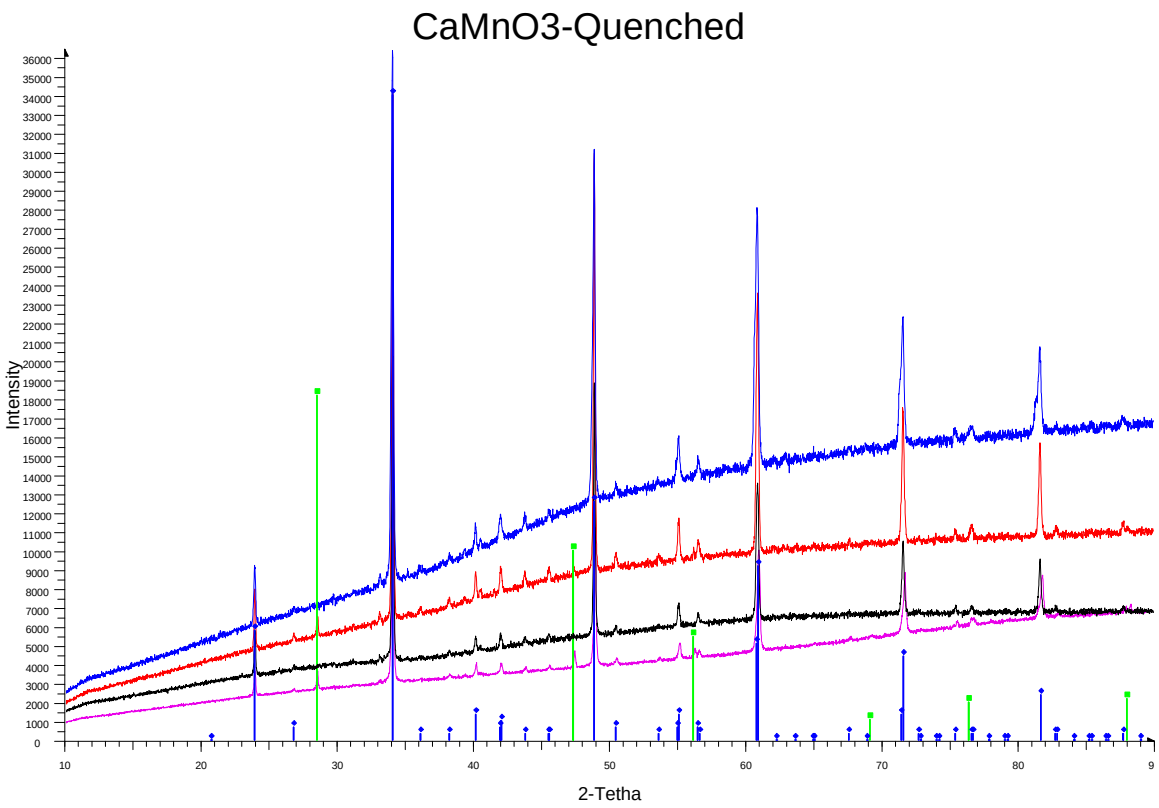

Figure 3.35: The quenched samples from the temperatures 1100°C (blue) and 1000°C (Red) together with two scans for $CaMnO_3$ (black and purple). Disregarding the reflections from silicon (green), the scans are identical. Blue lines at bottom are the reported intensities for $CaMnO_3$.

The conclusion to this experiment is that either no loss of oxygen occurred at these temperatures, the reaction reversed upon quenching or opening of ampoule or the reported phases show so small changes to the x-ray patterns that they cannot be distinguished from the parent $CaMnO_3$.

3.2.2 Mixing of two $CaMnO_{3-x}$ samples with different oxygen content.

A new method for creating reduced phases by mixing of two $CaMnO_{3-x}$ samples with different oxygen content to obtain a third was also attempted. The reduction of $CaMnO_3$ to the composition $CaMnO_{2.667}$ was attempted by mixing adequate amounts of $CaMnO_3$ and $CaMnO_{2.5}$ before heating to 650°C in an inner and outer evacuated closed ampoule (see figure 2.1, page 20). The x-ray pattern of this sample shows great likeness to that

recorded for the phase believed to be $CaMnO_{2.667}$, but with some additional reflections that belong to other calcium manganese oxides. As mentioned the $CaMnO_{2.667}$ samples could not be identified as a phase and the reflections were identical to that found for the phase $CaMnO_{2.75}$ and $Ca_2Mn_2O_5$. Figure 3.36 shows the diffraction pattern of the sample together with that recorded for the conventional $CaMnO_{2.667}$ attempt.

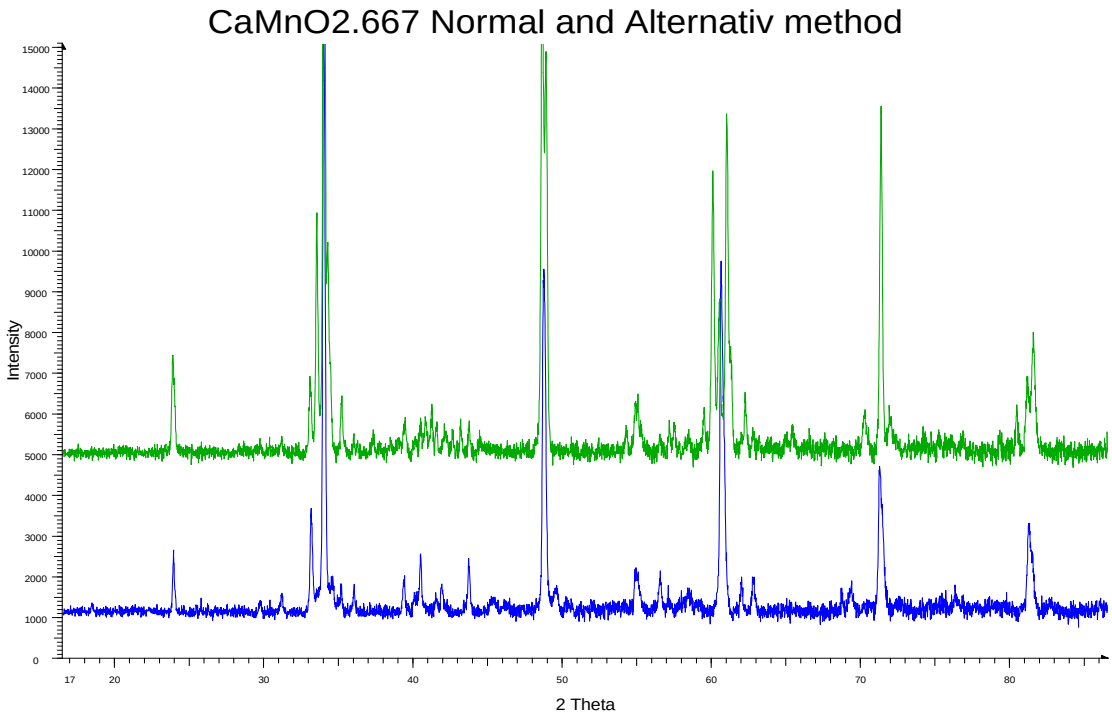

Figure 3.36: Two different attempts to make $CaMnO_{2.667}$. The blue pattern is from the one made with mixture of $CaMnO_3$ and $Ca_2Mn_2O_5$, and the green is from the one made with normal zirconium reduction.

Upon evaluation of the patterns it is clear that both samples contain multiple phases. They both are made mainly up of $CaMnO_{2.75}$, $CaMn_2O_4$ (Marokite) and $CaMnO_{2.5}$. An interesting observation is that it is clear that this technique can be used for creating reduced phases.

3.2.3 $CaMnO_3$ in nitrogen atmosphere heat treatment:

An experiment to prepare reduced $CaMnO_{3-x}$ through heating in nitrogen atmosphere was also done. The sample was heated to 1000°C and held there for one week with continuous nitrogen gas flow. The sample shows signs of reaction. The pattern can be

identified as a mixture of the patterns for $CaMnO_3$, Ca_2MnO_4 (Marokite) and $Ca_2MnO_{3.5}$. The sample was reheated to 1100°C for one week, but this produced no further visible reaction. This reduction process produced multiple phases in the sample and the technique was not used in further sample preparation. The patterns at the two different temperatures can be seen in figure 3.37.

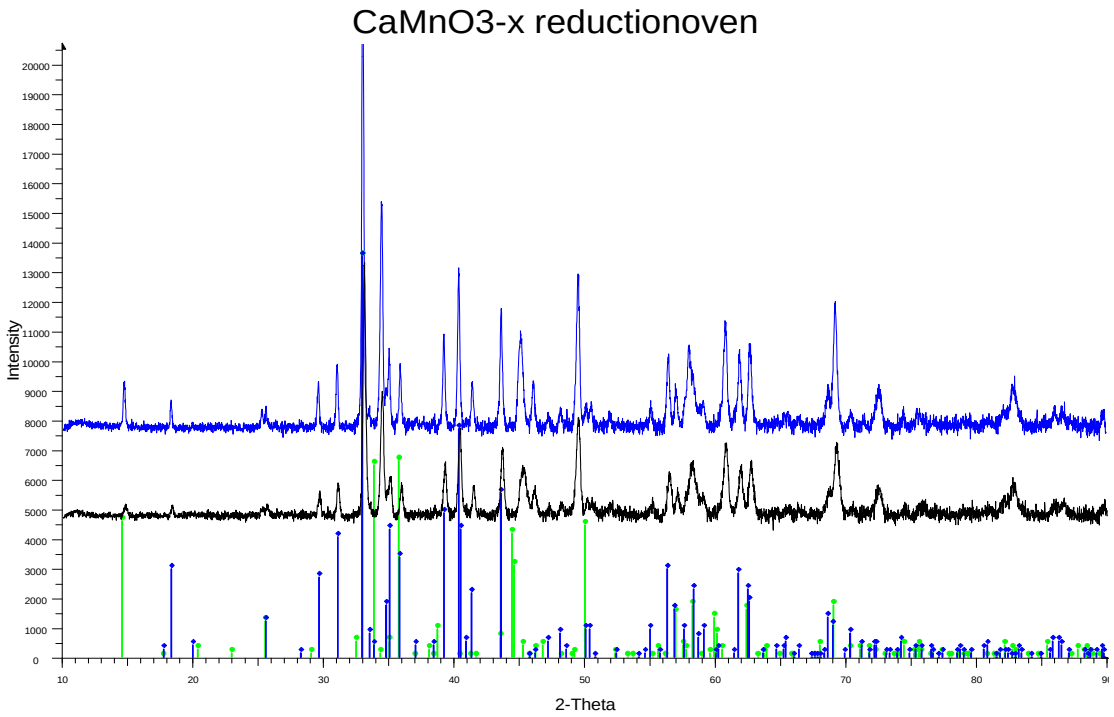

Figure 3.37: Patterns produced from samples heated in reduction oven at 1000˚C (black) and 1100˚C (blue). The vertical lines are the reported reflections of $CaMn_2O_4$ (blue) and $Ca_2MnO_{3.5}$ (green).

3.4 $SrMnO_{3-x}$:

3.4.1 $SrMnO_3$:

The $SrMnO_3$ compound produced from the citric acid synthesis is the hexagonal $SrMnO_3$. Multiple samples were made of hexagonal $SrMnO_3$ and their patterns were identical to the ones reported in earlier publications. The synthesis was reproducible. Figure 3.38 shows three different samples of the hexagonal $SrMnO_3$.

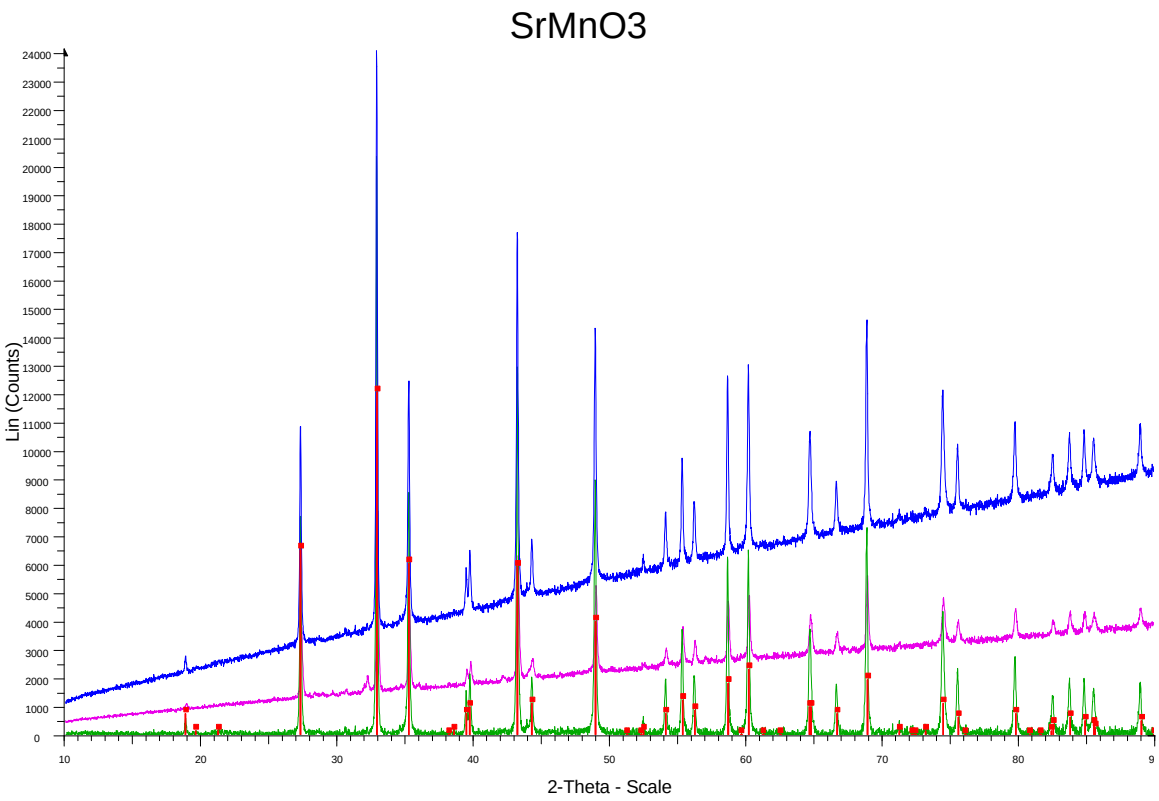

Figure 3.38: Three different samples of $SrMnO_3$. The red lines at the bottom are the reported intensities from earlier literature [16].

The refinement of $SrMnO_3$ is based on the results of Battle and Gibb [16] and the reported data where in good agreement with the experimental patterns obtained. The refinement is showed in figure 3.39:

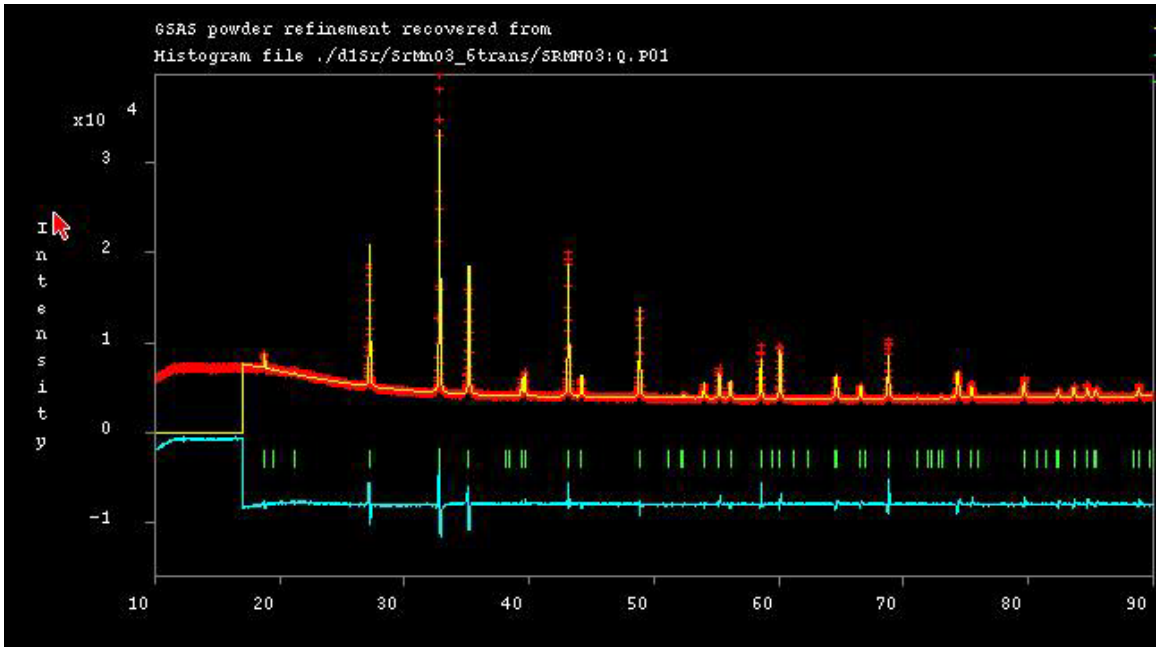

Figure 3.39: Refinement of the hexagonal $SrMnO_3$.

The error factors found after the Rietveld refinement are shown in table 3.22:

R_p	0.0230
wR_p	0.0356
χ^2	5.811

Table 3.22: Error factors for hexagonal $SrMnO_3$.

The obtained crystallographic information for $SrMnO_3$ can be found in table 3.23:

Space Group:	$P6_3/mmc$
Symmetry:	Hexagonal
a (in Ångstrøm)	5.44283 (8)
b (in Ångstrøm)	5.44283 (8)
c (in Ångstrøm)	9.07048 (3)

Table 3.23: Crystallographic information for hexagonal $SrMnO_3$.

The atom positions are shown in table 3.24:

	x	y	z
Sr (1)	0	0	0
Sr (2)	0.3333	0.6667	0.2500
Mn	0.3333	0.6667	0.61220
O	0.5	0	0
O	0.8181	0.6363	0.25

Table 3.24: Atom positions found for hexagonal $SrMnO_3$. The atom positions were fixed during refinement.

A schematic representation of the structure can be seen in figure 3.40:

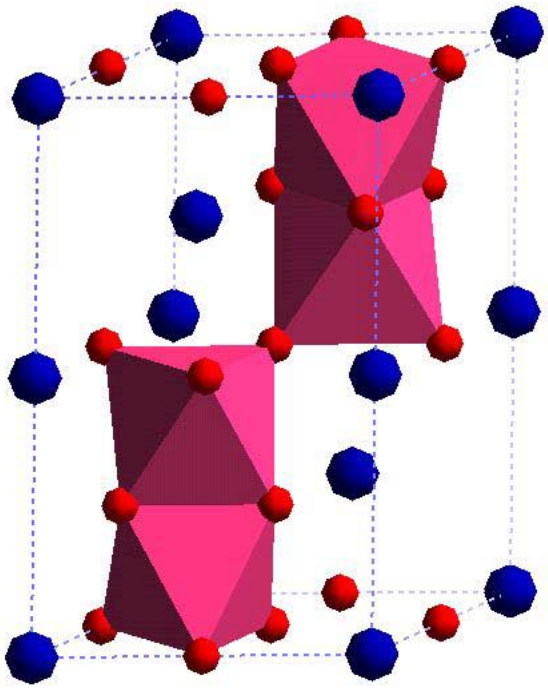

Figure 3.40: Schematic representation of $SrMnO_3$. Mn is displayed as octahedra while Sr is blue and O red.

$SrMnO_3$ also exists as a cubic phase. This phase is obtained if samples are allowed to reoxidize. This phase was also obtained. When an attempt to reoxidize $Sr_2Mn_2O_5$ to 400˚C was performed, the fuse of the oven switched off and the sample was only heated

to about 150˚C. The product was the cubic $SrMnO_3$ which is in good agreement with that reported by Negas and Roth [27]. Another sample was heated to 400˚C and this sample interestingly yielded a mixture of the cubic and hexagonal $SrMnO_3$. A sample was also heated to 800˚C and yielded only the hexagonal $SrMnO_3$ phase. The three diffraction patterns can be seen in figure 3.41.

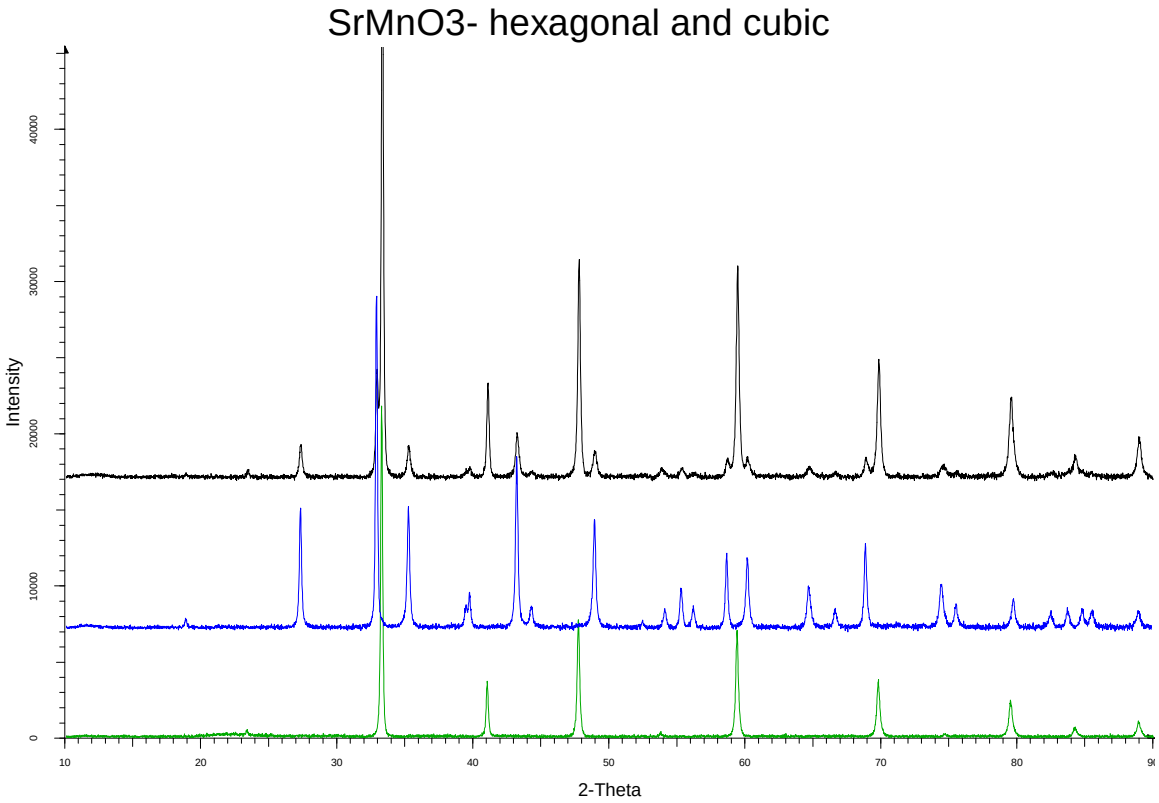

Figure 3.41: The different reoxidized $SrMnO_3$ samples. The green is the cubic from reoxidation at 150˚C, the black is from reoxidation at 400˚C (both hexagonal and cubic) and blue is the hexagonal from reoxidation at 800˚C

Magnetic structure of hexagonal $SrMnO_3$:

Many hexagonal perovskites have magnetic orderings at low temperatures. If $SrMnO_3$ has an ordering of magnetic momentums at lower temperatures, it is likely that changes in the neutron diffraction pattern can be observed as a result of this ordering. The changes can be either in the form of extra reflections and/or different intensities. In figure 3.42 a comparison of $SrMnO_3$ at room temperature and low temperature (9K) is illustrated.

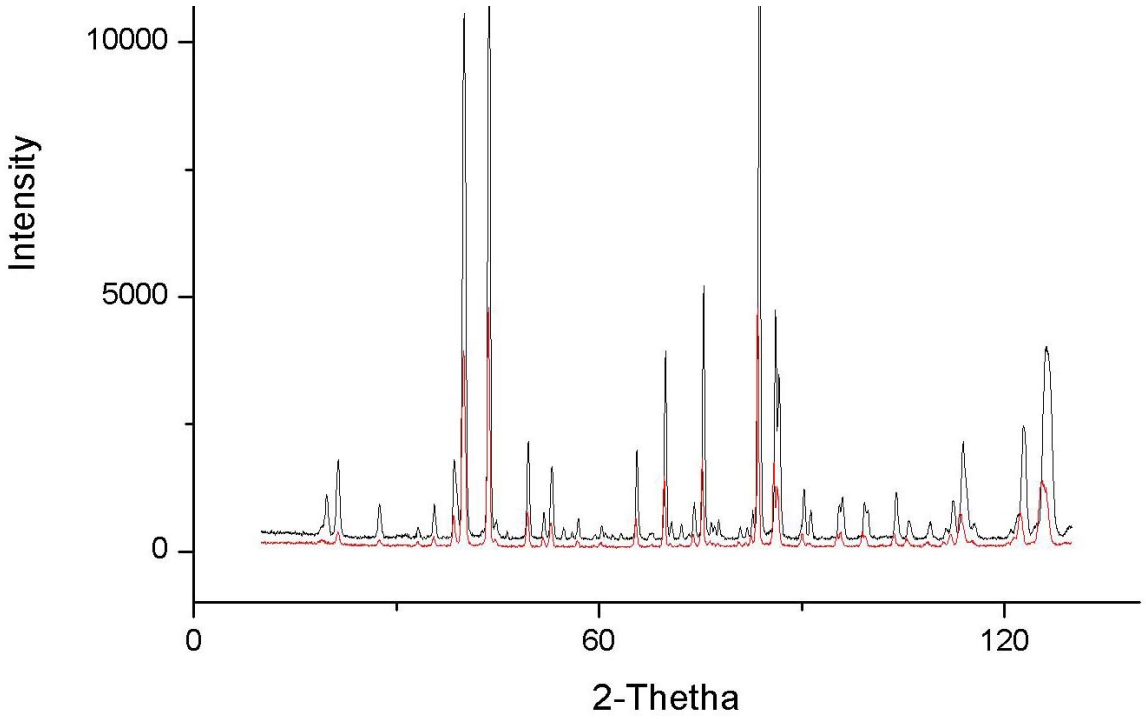

Figure 3.42: Diffraction patterns for $SrMnO_3$ at room temperature (red) and at 9K (black). Extra reflections can be observed in the low temperature pattern as a result of magnetic ordering.

The diffraction pattern containing the magnetic reflections was refined using the programme Fullproof. This programme enables the user to refine with magnetic parameters in addition to Rietveld refinement. Different alignments of the magnetic momentums can be distributed. The refined pattern is shown in figure 3.43.

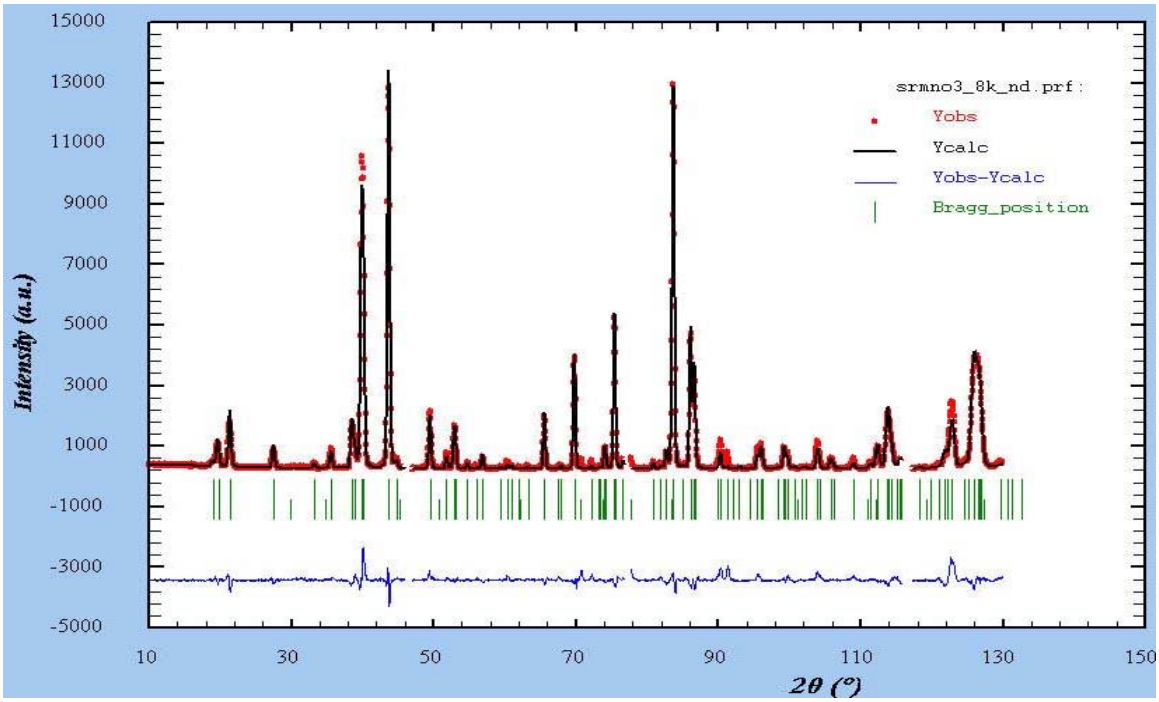

Figure 3.43: Refinement of the low temperature $SrMnO_3$ neutron diffraction pattern. The observed pattern is red, the calculated is black and the difference between them is blue.

The refinement of the magnetic structure yielded an alignment in an antiferromagnetic fashion like shown in figure 3.44. The magnitude of the momentums is M_{ab} is 2.48μβ.

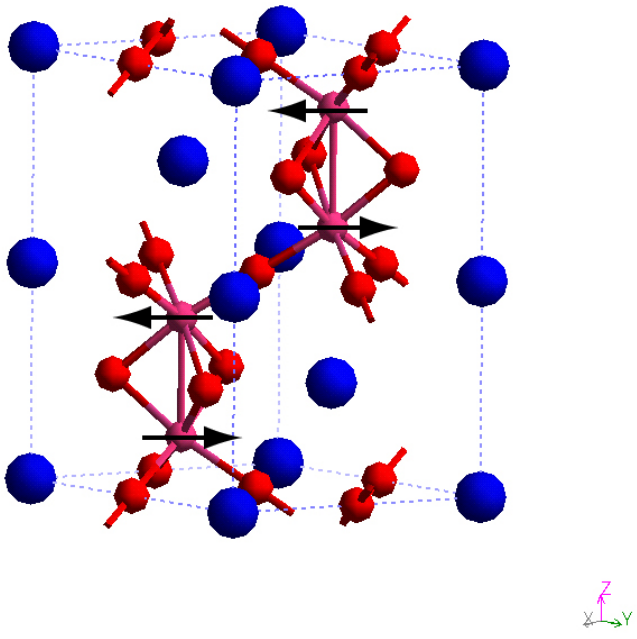

Figure 3.44: Antiferromagnetic ordering of magnetic momentums in hexagonal $SrMnO_3$.

3.4.2 $Sr_2Mn_2O_5$:

This completely reduced phase was made by zirconium reduction of the material hexagonal $SrMnO_3$. The results were reproducible and three samples are shown in figure 3.45.

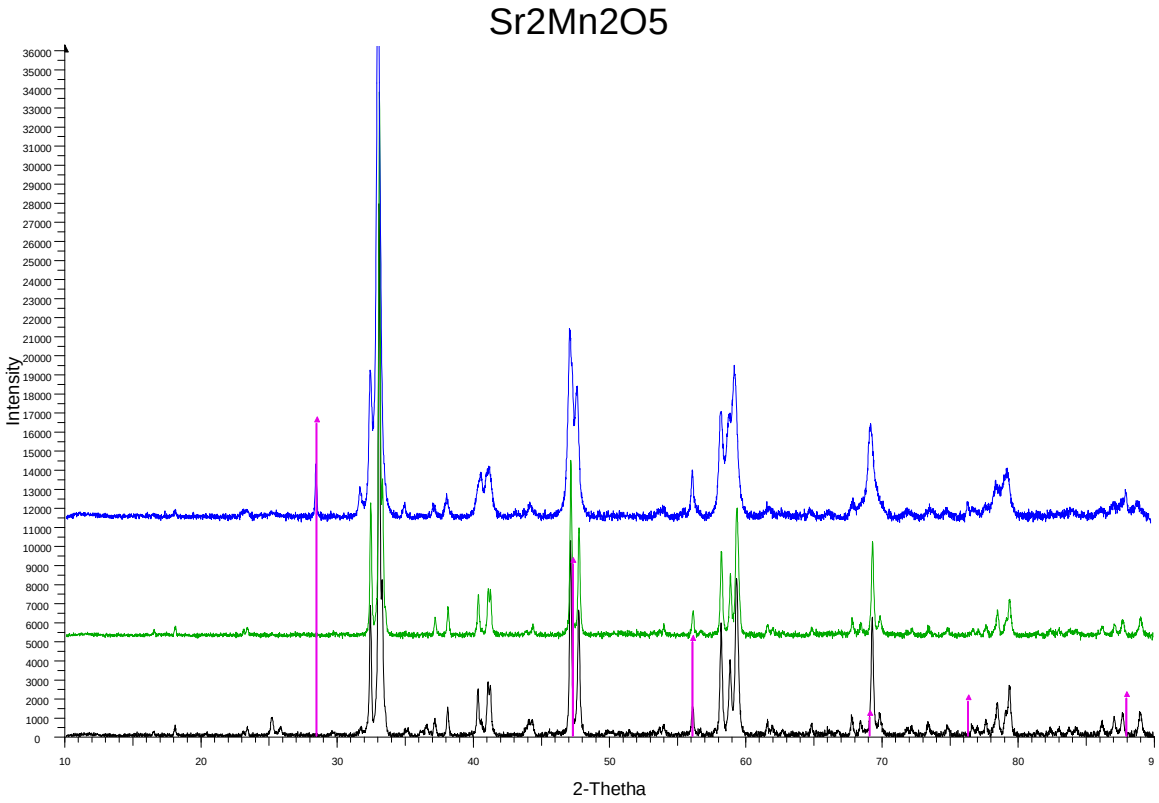

Figure 3.45: Three different scans of $Sr_2Mn_2O_5$. Purple lines indicate reflections from the internal standard Si.

A solution for this structure was proposed by Caignaert et al [19], and their results were tested with GSAS Rietveld refinement. This reported data were in good agreement with the experimental data which is shown in figure 3.46

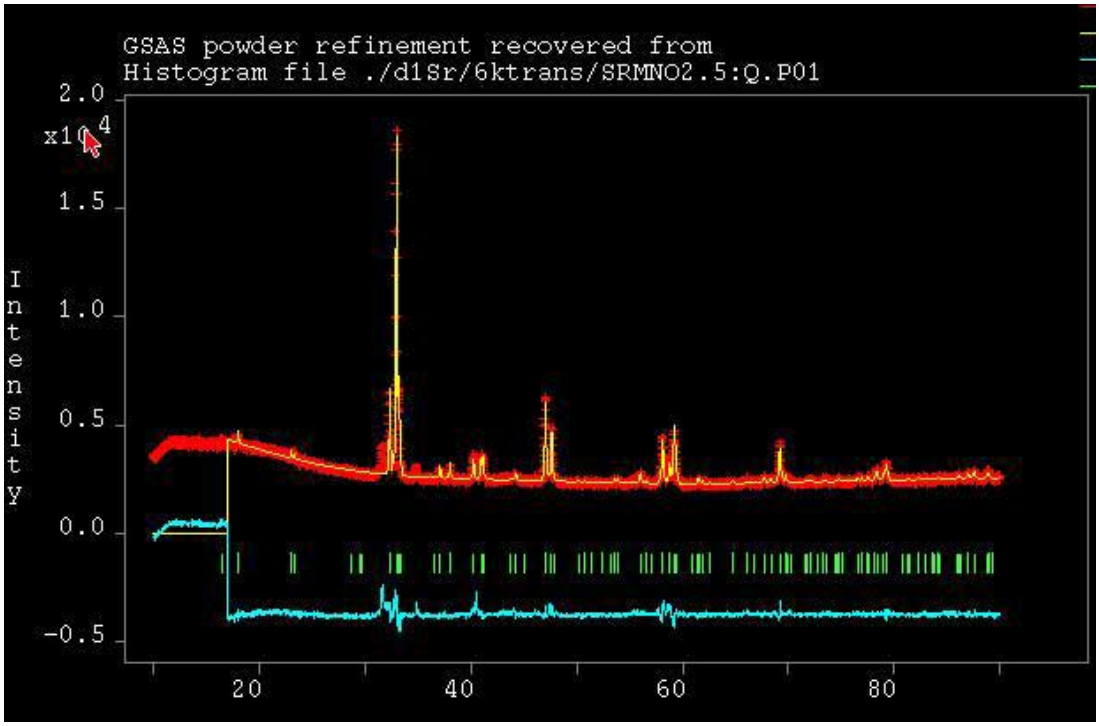

Figure 3.46: Rietveld refinement of the $Sr_2Mn_2O_5$ pattern.

At close studies it is clear that some of the $Sr_2Mn_2O_5$ samples contain some impurities, including the one Rietveld refinement was performed on. Based on observations of the strongest reflection (d = 2.82, 2θ = 31.54) that did not belong to the $Sr_2Mn_2O_5$ phase, $Sr_2MnO_{3.84}$ was a good candidate. This phase is well described by Kriegel et al [28], and was at present the only phase found that could explain this impurity reflection. Caignaert et al [19] also had problems with one or more impurities, but did not find out what the impurities were. When entered into the refinement model, however, $Sr_2MnO_{3.84}$ did not make the refinement any better and $Sr_2MnO_{3.84}$ is not a likely impurity phase. The presence of an impurity phase can contribute to explain low oxygen content in the TGA experiment for $Sr_2Mn_2O_5$.

The error factors found after the Rietveld refinement are shown in table 3.25:

R_p	0.0423
wR_p	0.0278
χ^2	5.76

Table 3.25: Error factors found for the $Sr_2Mn_2O_5$ structure.

The obtained crystallographic information for $Sr_2Mn_2O_5$ is listed in table 3.26:

Space Group:	Pbam
Symmetry:	Orthorhombic
a (in Ångstrøm)	5.53042 (15)
b (in Ångstrøm)	10.77881 (30)
c (in Ångstrøm)	3.81427 (10)

Table 3.26: Crystallographic information for the $Sr_2Mn_2O_5$ structure.

Atom positions are listed in table 3.27

	x	y	z
Sr	0.27986	0.36209	0.5
Mn	0.25571	0.12386	0
O	0	0	0
O	0.27900	0.09120	0.5
O	0.55300	0.2259	0

Table 3.27: Atom positions of $Sr_2Mn_2O_5$. The atom positions were fixed during refinement.

A schematic representation of the structure of $Sr_2Mn_2O_5$ can be seen in figure 3.47:

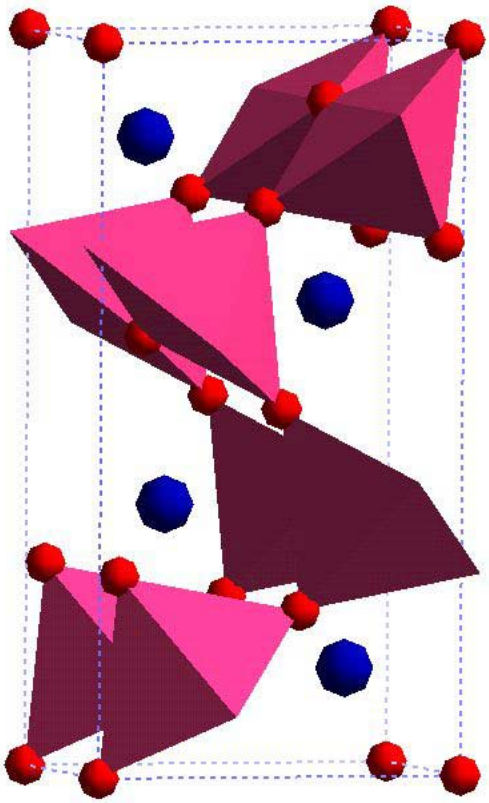

Figure 3.47: Schematic representation of $Sr_2Mn_2O_5$. Mn is displayed as square pyramids while Sr is blue and O red.

3.4.3: $SrMnO_{3-x}$:

This structure is the oxygen deficient orthorhombic distortion of the hexagonal $SrMnO_3$ structure. A homogeneity range exists between $SrMnO_{2.74}$ and $SrMnO_{2.62}$. When made with zirconium reduction it is possible to obtain this phase with other oxygen content. The orthorhombic distortion was described by Negas and Roth [13]. They indexed the structure, but stopped at the 2θ angle of 70˚. Another orthorhombic distortion was also described by Sedmidubsky et al [18]. Three different samples of the phase with composition $SrMnO_{2.8}$ can be seen in figure 3.48.

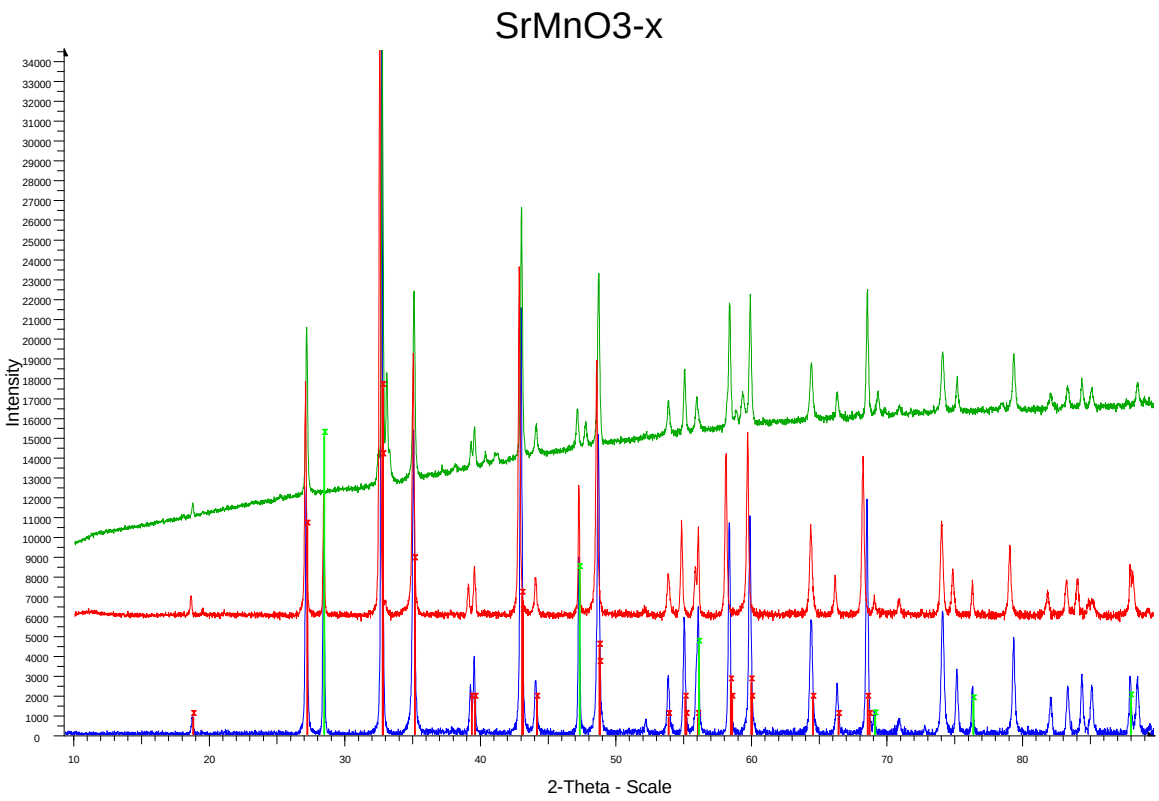

Figure 3.48: Orthorhombic distortion of hexagonal $SrMnO_{3-x}$. The red vertical lines are the earlier reported intensities Negas and Roth, and the green vertical lines are internal standard Si.

Refinement of the diffraction pattern was started with both the unit cell of Negas and Roth [13] and the unit cell of Sedmidubsky et al [18]. None of the unit cells could be verified with the LeBail method. It is clear that this pattern is the same as the one Negas and Roth [13] found for the orthorhombic distortion. No further structural refinement was performed. In figure 3.49 the attempted LeBail refinement can be seen.

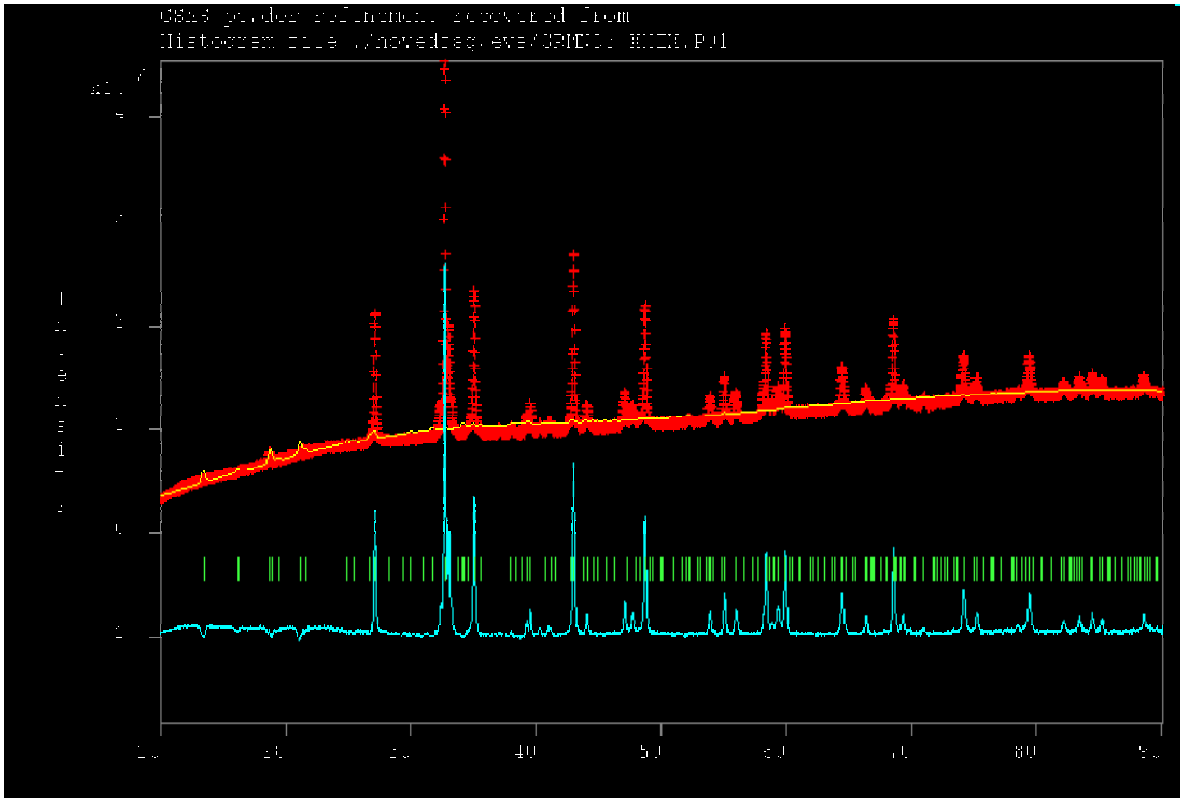

Figure 3.49: Attempted LeBail refinement of $SrMnO_{3-x}$ with the unit cell proposed by Sedmidubsky et al [18]. The intensities cannot be extracted with the LeBail method for the proposed unit cell.

The pattern of $SrMnO_{3-x}$ can described as a mixture of $SrMnO_3$ and $Sr_2Mn_2O_5$. This is shown in figure 3.50. It is not clear that Sedmidubsky et al [18] have been investigating the same phase that Negas and Roth reported. This is discussed in chapter 4.3.

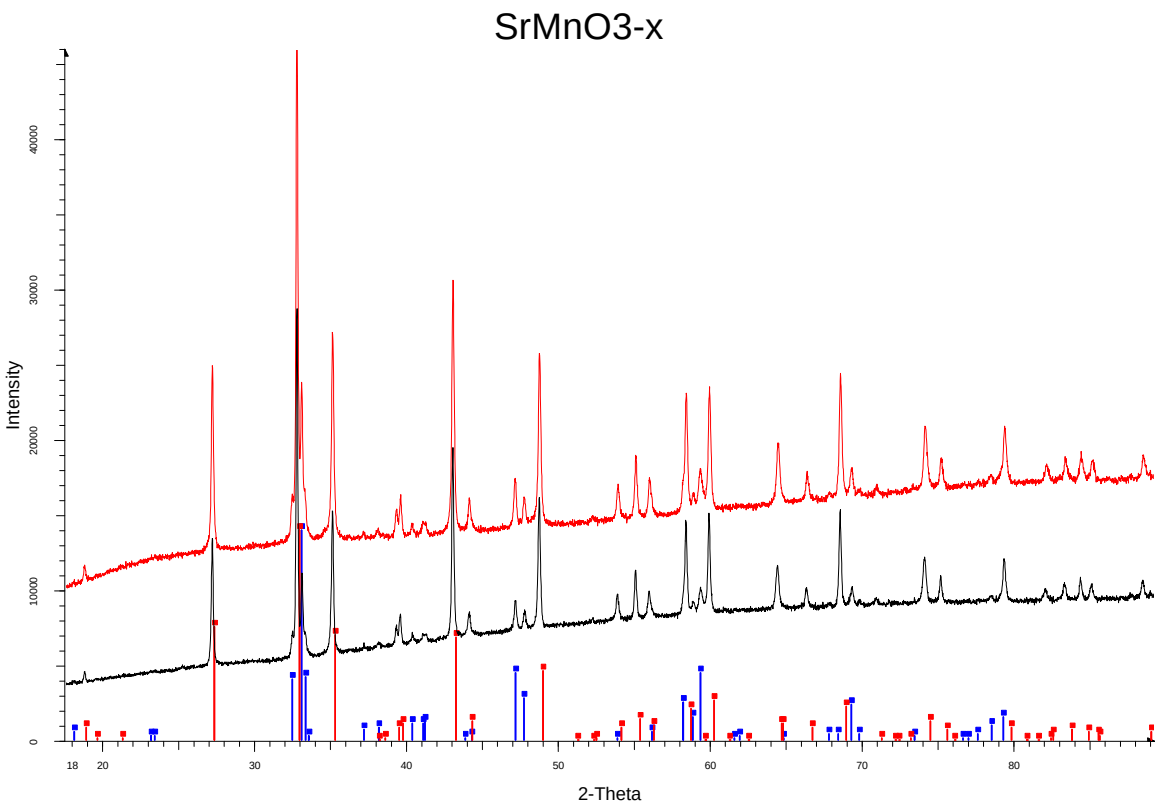

Figure 3.50: Two diffraction patterns of the compound $SrMnO_{3-x}$. The blue vertical lines are reported intensities from $Sr_2Mn_2O_5$ while the red are from $SrMnO_3$. These reported peaks together index the diffraction pattern.

Chapter 4: Discussion

Experimental results on crystal structure, phases and thermal properties are described in chapter 3 for $CaMnO_{3-x}$ and $SrMnO_{3-x}$. Several of the findings require some more detailed considerations and discussions.

4.1 Oxygen non-stoichiometry; TGA-Experiments:

Reoxidation in air of various $CaMnO_{3-x}$ and $Sr_2Mn_2O_5$ samples in TGA oven should theoretically lead to the stable oxygen content of 3.0. The results from the TGA experiments, however, deviate from the expected values. Most commonly the derived oxygen content after reoxidation is less than that expected. Out of three experiments with different $Ca_2Mn_2O_5$ samples as starting materials the measured oxygen content in two of them is found to be close to (2.96, 2.99) and in quite good agreement with the predicted value of 3.0. The third sample shows a significantly lower value (2.81). The reasons for the low values may be as follows: First of all the samples are stored in a desicator. It is possible that they take up oxygen (reoxidize) to a small degree during long time storage. Another possibility is that the powder is not grinded thoroughly enough (too large particles) or has a small oxidized (protective) layer on the surface which does not allow the whole sample to become easily oxidized. Presence of impurities in the samples would also cause a too low oxygen value. Finally it is possible that the oxygen content of the $CaMnO_{3-x}$ compound that is stable at the actual temperature is not 3.0, but less. It is not uncommon for perovskites to lose oxygen as a function of temperature, although this commonly happens above 1000˚C. The above listed possibilities are all factors that can explain too low oxygen content as determined by TGA. Other errors that can produce either too low or too high oxygen contents are weighing errors. The amount of material used in TGA is typically very small (5-100 mg), and an accurate weight is important. This weight error is believed to be negligible.

The possibility of an oxidation reaction of the sample when transferred from the desicator to the TGA set-up was evaluated. X-ray diffraction patterns were compared between one

$Ca_2Mn_2O_5$ sample that had been stored in the desicator for approximately one year and a $Ca_2Mn_2O_5$ sample that had been exposed to air for 24 hours. None of these patterns showed any signs of reaction between the reduced $Ca_2Mn_2O_5$ sample and oxygen. This is quite interesting since some other reduced perovskites show a strong tendency towards reoxidation during storage. It is reasonable to assume that Mn(III) is quite stable in air, like is the case with the binary Mn-oxides (Mn_2O_3). Therefore the $Sr_2Mn_2O_5$ and $Ca_2Mn_2O_5$ phase is also expected to be quite stable in air. X-ray diffraction pattern of a $Sr_2Mn_2O_5$ sample exposed to air in 48 hours showed the same diffraction pattern as before exposure. A schematic illustration of a $Ca_2Mn_2O_5$ TGA-reoxidation curve is shown in figure 4.1.

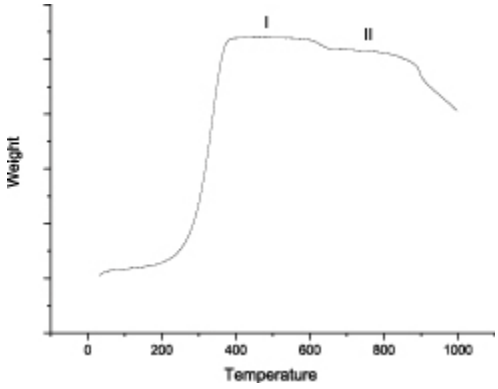

Figure 4.1: Typical TGA reoxidation curve of $Ca_2Mn_2O_5$ sample. The two stable areas are noted I and II.

The TGA experiments (chapter 3.2) show a small weight loss at some 600-650˚C as can be seen on schematic illustration (figure 4.1, between range I and range II). This weight loss would correspond to an x of 0.02 in the formula $CaMnO_{3-x}$.This weight loss is too small for making it likely that there exists a distinct phase with this oxygen content (2.98). However, it may indicate a small intrinsic oxygen non stoichiometry, i.e. $CaMnO_3$-$CaMnO_{2.98}$. On the other hand it is possible that the weight loss is caused by the decomposition of impurities. Two likely candidates are $CaCO_3$ and $(Ca,Mn)CO_3$. In literature the decomposition temperature of $CaCO_3$ is commonly reported between 600˚C and 800˚C. No evidence of $CaCO_3$ was however observed in the x-ray diffraction analysis of the present samples. If it is present as amorphous $CaCO_3$ it would have escaped detection. In the XRD analysis (chapter 3.3) Mn rich impurities like $CaMn_2O_4$

were detected. Amorphous or surface layers of $CaCO_3$ may explain the lack of Ca rich contamination phases. No indications of $(Ca,Mn)CO_3$ or $MnCO_3$ were found in the diffraction pattern. If such carbonate impurities are present in the TGA samples one would expect a weight loss at 650-750˚C due to their thermal decomposition.

MacChesney et al [29] had measured the oxygen content of their $CaMnO_3$ sample to 2.98. They had employed chemical back-titration analysis [30] to determine the tetravalent manganese concentration. This was done by adding a known amount of $CaMnO_3$ into a known amount of Mn^{2+} in solution. Reaction between the Mn^{2+} and Mn^{4+} occurred. The excess Mn^{2+} was then determined with titration. Impurities present in the $CaMnO_3$ sample would produce less tetravalent manganese than expected and could explain the low oxygen content they discovered.

4.2 Phase stability and crystal structure of $CaMnO_{3-x}$:

In the series $CaMnO_3 – Ca_2Mn_2O_5$ Reller et al [1] reported several ordered oxygen deficient structures observed by High Resolution Electron Microscopy ($CaMnO_{2.8}$ $CaMnO_{2.75}$ $CaMnO_{2.667}$ and $Ca_2Mn_2O_5$). The synthesis of these oxygen deficient phases proved presently difficult. In addition to the well described $CaMnO_3$ and $Ca_2Mn_2O_5$ phases the only phase that could be synthesized as a single phase was $CaMnO_{2.75}$.

4.2.1 $CaMnO_3$ and $Ca_2Mn_2O_5$:

The diffraction patterns recorded for $CaMnO_3$ and $Ca_2Mn_2O_5$ were generally of better quality than previously recorded. This is likely due to the development in instrumentation (and also in analysing software). The results of Poeppelmeier et al [4], [5] on crystal structure were satisfactory reproduced. This provides the fundament for evaluating the findings for the non-stoichiometric $CaMnO_{3-x}$ phases.

4.2.2 $CaMnO_{2.75}$ ($Ca_4Mn_4O_{11}$):

The $CaMnO_{2.75}$ phase was extensively studied. The appearance of superstructure reflections in the XRD pattern indicates an O-vacancy ordered structure, consistent with a composition $Ca_4Mn_4O_{11}$ (or multiples). A major issue was presently determination of the crystal structure, and hence the space group. There exists up to now no verified information of the space group of $Ca_4Mn_4O_{11}$ in the literature. Although the space group $Pmc2_1$has been used by Poeppelmeier, it has not been claimed as correct. Synchrotron data and LeBail method refinements did not really give any significant hints for $Pmc2_1$ being wrong. Actually a space group with a screw axis or a glide plane is needed to explain the oxygen defect models that Chiang-Poeppelmeier et al [6] proposed. Structure considerations based on assumptions of square pyramidal Mn-coordination at the oxygen vacant sites were made, consistent with Mn(III) local surroundings in $Ca_2Mn_2O_5$. This implies restrictions to the space group choices. On the other hand the results from the TEM electron diffraction indicated no extinctions and this complicated the process, since no space group that could fulfil both the glide plane induced vacancy distribution and the TEM criteria exists among the orthorhombic space groups. The unit cell (a = 5.35, b = 20.96 and c = 7.47) that had been observed by Reller et al [1] and Chiang-Poeppelmeier [6] could be verified in the TEM pictures and also fitted well in the LeBail refinement. The space groups that were tested were Pmmm, P222, $Pmc2_1$ and $Pmn2_1$. Out of these Pmmm and $Pmc2_1$ were tested thoroughly. Finally the space group Pmm2 and its alternative settings Pm2m and P2mm were considered. This space group fulfils all criteria. Unfortunately refinement works with this space group is beyond the limits of this thesis. An approach to do further investigations into this material should be to thoroughly study the Pmm2 space group. If this is inconclusive the next step could be to search for space groups in lower symmetry. If one or more of the angles deviate from 90˚ one might have a monoclinic unit cell that might explain the model. No indications for monoclinic symmetry like peak broadening for different types of reflections that could indicate angle deviation from 90˚, however, were observed in synchrotron diffraction pattern.

4.2.3 $CaMnO_{2.8}$, $CaMnO_{2.667}$ and $CaMnO_{2.556}$:

$CaMnO_{2.8}$ and $CaMnO_{2.667}$ could not be identified as separate phases contrary to the findings by Reller et al [1]. The HREM pictures reported in literature are not consistent with the recorded XRD data. The x-ray diffraction pattern of $CaMnO_{2.8}$ (nominal), showed great resemblance to that of $CaMnO_{2.75}$. Only minor differences could be distinguished between the two patterns and even with synchrotron data it was impossible to index the pattern with the unit cell proposed by Reller et al [1]. The pattern of the nominal $CaMnO_{2.667}$ composition had many of the same reflections as the $CaMnO_{2.75}$ as well in addition to reflections that could be attributed to $Ca_2Mn_2O_5$. The $Ca_2Mn_2O_5$ phase was in some cases present in the $CaMnO_{2.75}$ sample as well, but only to a very small degree and entered as a contamination phase. In nominal $CaMnO_{2.667}$ it was present to a notably larger degree. Reller et al also proposed another phase for oxygen deficient $CaMnO_{3-x}$. It had the composition $CaMnO_{2.556}$, but without providing strong experimental evidence. It was only described theoretically with a unit cell being a supercell to the $CaMnO_3$ parent structure. Multiple attempts to prepare this phase were made. The pattern of these samples showed only minor differences to that of $Ca_2Mn_2O_5$, and the unit cell proposed by Reller et al can not be said to fit the pattern recorded for the nominal $CaMnO_{2.557}$ composition. A close examination of the XRD patterns of the samples for $Ca_2Mn_2O_5$ and $CaMnO_{2.556}$ show no significant differences.

The oxygen deficient structures of $CaMnO_{2.8}$, $CaMnO_{2.667}$ and $CaMnO_{2.556}$ that Reller et al described could not be produced by the normal zirconium reduction method applied here. It is possible that the synthesis temperature is not correct or that the samples are not stable at normal conditions. It might also not be possible to achieve these phases as bulk samples, but rather as phases that occur as intergrowth between other phases or that are formed during more harsh conditions like vacuum and under electron beam.

There exist also other reports on oxygen deficient $CaMnO_{3-x}$ samples. Zeng and Greenbladt [10] proposed that distinct phases with compositions of $CaMnO_{2.89}$ and $CaMnO_{2.94}$ could be achieved by quenching from high temperature. When an attempt to reproduce the results was performed, no difference form the $CaMnO_3$ sample could be

distinguished. There is presently no evidence that quenching from high temperatures may produce well defined (additional) reduced phases.

Also a new method for producing reduced phases was attempted. It consists of mixing two samples with different oxygen content in an inner and outer ampoule to obtain a third oxygen deficient sample. The results show that the product from this method bears great resemblance to the product achieved from conventional zirconium reduction. Unfortunately the target oxygen deficient sample was $CaMnO_{2.667}$ that could not be distinguished as a separate phase. Therefore it is not easy to compare the two methods against each other and concluding which one is the better. The method has its limitations as it cannot be used to produce totally reduced phases. This method can rather be used as an alternative when synthesis problems occur in the more traditional method.

4.3 Phase stability and crystal structure of $SrMnO_{3-x}$:

Both the cubic and the hexagonal $SrMnO_3$ were produced. The hexagonal one was shown the main attention. Since Sr is more electropositive than Ca, one can presume that it should stabilize Mn(IV) better. No intermediate structures between $SrMnO_3$ and $Sr_2Mn_2O_5$ are verified however. Upon reoxidation of $Sr_2Mn_2O_5$ in air an interesting result is found. Synthesis of cubic $SrMnO_3$ from $Sr_2Mn_2O_5$ occurs when heated at low temperatures in the region of 100-200˚C. Samples heated to 400˚C yield a mixture of the cubic and hexagonal $SrMnO_3$ phases, while the samples heated to 800˚C yield only the hexagonal $SrMnO_3$ phase. From this one can assume that from 400-450˚C the $SrMnO_{3-x}$ sample is fully reoxidized but is a mixture of the two different $SrMnO_3$ phases. At 800˚C only the hexagonal $SrMnO_3$ exists.

Low temperature neutron diffraction studies of the hexagonal $SrMnO_3$ phase revealed a magnetic structure with opposite spins inside the dimmers of face sharing octahedra. Battle and Gibb [16] reported antiferromagnetic behaviour, and their results are in agreement with the result in this study. $SrMnO_3$ is a four layered hexagonal perovskite (denoted 4H). Very few compounds adopt this four layer arrangement. Two examples are

$BaRuO_3$ [31] and $CsMnF_3$ [32]. The magnetic ordering of 4H $BaRuO_3$ is not reported at present, but $CsMnF_3$ is reported to have an antiferromagnetic ordering [33]. No distribution of the momentums, however, is mentioned here. Other stacking sequences than 4H are common. In figure 4.2 different hexagonal perovskite structures can be seen.

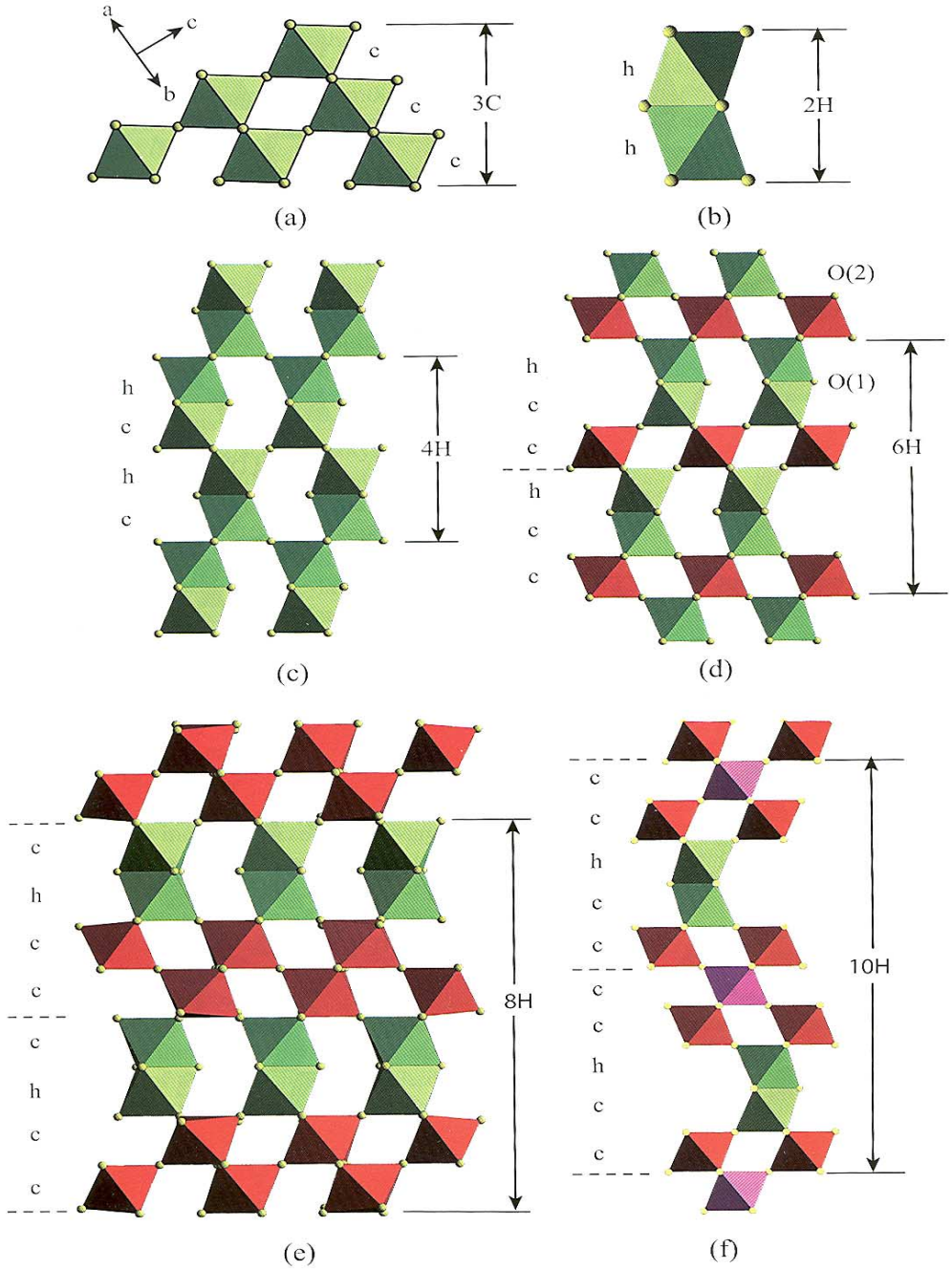

Figure 4.2: Projections along [010] of the structures of hexagonal perovskites produced by stacking of layers of corner-sharing octahedra were cubic stacking (c) and face-sharing octahedra were hexagonal stacking (h) occurs.

It is not unusual that hexagonal perovskite structures with face sharing dimmers have antiferromagnetic arrangements of the magnetic momentums. Examples are $BaMnO_3$ [34] and $BaIr_{0.2}Fe_{0.8}O_{2.932}$ [35]. The $BaMnO_3$ has a two layered hexagonal structure while the $BaIr_{0.2}Fe_{0.8}O_{2.932}$ has a six layered hexagonal structure (2H and 6H respectively). The alignment of the momentums and the structures are not identical. In figure 4.3 the ordering in $BaMnO_3$ is shown.

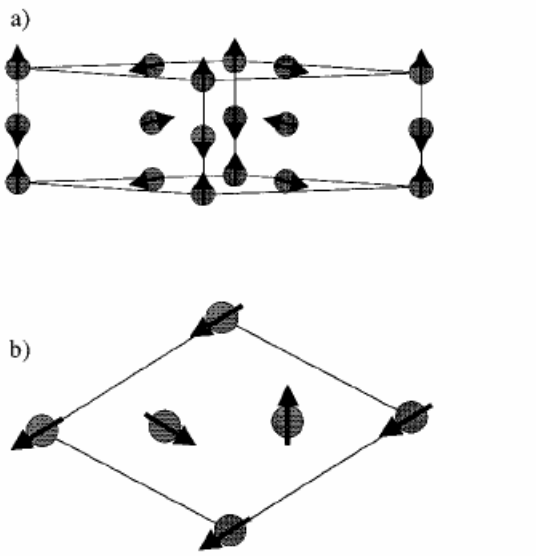

Figure 4.3: Antiferromagnetic ordering in $BaMnO_3$. The figure is taken from Cussen and Battle [34]. Figure a) shows the structure viewed perpendicular to [001] while figure b) is viewed along [001] with arrows indicating the actual spin directions of Mn with z= 0.

Sedmidubsky et al [18] collected both HREM and x-ray from single crystal of the phase $SrMnO_{3-x}$. Their x-ray diffraction pattern is not shown, and it may have differences from the pattern Negas and Roth [13] used for indexing. The pattern obtained the samples synthesized for this thesis show indications that the sample is in fact a mixture of $SrMnO_3$ and $Sr_2Mn_2O_5$. It can in future be interesting to attempt to use new methods for creating stable $SrMnO_{3-x}$ phases like i.e. $SrMnO_{2.75}$. One such method could be heating of $Sr_2Mn_2O_5$ together with a less stable oxide like Ag_2O in a closed ampoule to see if this could increase the stability of possible oxygen deficient compounds.

Chapter 5: Future investigations

There are still unclear features in respect to the oxygen deficient samples of $SrMnO_{3-x}$ and $CaMnO_{3-x}$. It is in clear that the synthesis did not always produce single phase products and that the characterisation methods used here did not solve the oxygen deficient structures except the end members $CaMnO_{2.5}$ and $Sr_2Mn_2O_5$. The problem with the presence of impurity phases could be solved if the phases could be isolated in single crystals, and single crystal x-ray could be obtained. This would especially be useful for the $CaMnO_{3-x}$ samples. Electron diffraction (from TEM) is a single crystal method that requires very small crystals. The challenge however is to ensure that the crystals truly have the oxygen content desired. A combination between TEM electron diffraction and single crystal x-ray could give more information.

For the phases $CaMnO_{2.8}$, $CaMnO_{2.665}$ and $CaMnO_{2.556}$ clearer information regarding the stability is needed before further refinement work can be performed. For these phases alternative ways of synthesis should also be tested. It may also be necessary to store the samples under inert conditions. In the case of $CaMnO_{2.75}$ the unit cell dimensions have been determined, but further refinement work with the space group Pmm2 should be performed. Also a search for space groups in the monoclinic symmetry could perhaps lead to a better match with both the structural model and the patterns obtained from refinements.

For the $SrMnO_{3-x}$ phase it also seems necessary to obtain single crystal data. The earlier reported structural information concerning this phase could be identified as a mixture of the parent compound $SrMnO_3$ and $Sr_2Mn_2O_5$. Again alternative methods of synthesis for the oxygen deficient samples should be applied. The method of heating the totally reduced compound with a less stable oxide (i.e. Ag_2O) in an ampoule to obtain more oxygen rich compounds might be successful.

Appendix:

Here a list of the first 150 hkl values and the corresponding d-values of the reflections obtained from the refinements are presented. Only the reflections from the refinements of the samples that could be identified as phases are listed in appendix table A.1 through A.5. For the refinement of $SrMnO_3$ only 125 reflections are present.

A.1 $CaMnO_3$:

I-reference	H	K	L	Multiplicity	D-value
1	0	1	1	4	4.30695
2	1	0	1	4	3.73423
3	0	2	0	2	3.73179
4	1	1	1	8	3.33956
5	2	0	0	2	2.64423
6	1	2	1	8	2.63964
7	0	0	2	2	2.63678
8	2	1	0	4	2.49243
9	2	0	1	4	2.36374
10	1	0	2	4	2.35974
11	2	1	1	8	2.25343
12	0	3	1	4	2.25005
13	1	1	2	8	2.24996
14	2	2	0	4	2.15752
15	0	2	2	4	2.15347
16	1	3	1	8	2.07044
17	2	2	1	8	1.99687
18	1	2	2	8	1.99445
19	2	0	2	4	1.86712
20	0	4	0	2	1.8659
21	2	3	0	4	1.81194
22	2	1	2	8	1.8113
23	2	3	1	8	1.71362
24	1	3	2	8	1.71209
25	0	1	3	4	1.71104
26	3	0	1	4	1.67189
27	2	2	2	8	1.66978
28	1	4	1	8	1.66913
29	1	0	3	4	1.66812
30	3	1	1	8	1.63146
31	1	1	3	8	1.62795
32	3	2	1	8	1.52576
33	2	4	0	4	1.52455
34	0	4	2	4	1.52311
35	1	2	3	8	1.5229
36	2	3	2	8	1.49334
37	3	0	2	4	1.46548
38	2	4	1	8	1.46457
39	2	0	3	4	1.46389

40	1	4	2	8	1.46362
41	3	1	2	8	1.43802
42	2	1	3	8	1.43652
43	0	5	1	4	1.43629
44	0	3	3	4	1.43564
45	3	3	1	8	1.38766
46	1	5	1	8	1.38608
47	1	3	3	8	1.3855
48	3	2	2	8	1.36407
49	2	2	3	8	1.36279
50	4	0	0	2	1.32212
51	2	4	2	8	1.31982
52	0	0	4	2	1.31839
53	4	1	0	4	1.30185
54	2	5	0	4	1.29989
55	4	0	1	4	1.28243
56	1	0	4	4	1.27924
57	4	1	1	8	1.26391
58	3	3	2	8	1.2627
59	2	5	1	8	1.26212
60	2	3	3	8	1.26168
61	1	5	2	8	1.26151
62	1	1	4	8	1.26085
63	4	2	0	4	1.24622
64	3	4	1	8	1.24516
65	3	0	3	4	1.24474
66	0	6	0	2	1.24393
67	1	4	3	8	1.2436
68	0	2	4	4	1.2431
69	3	1	3	8	1.22779
70	4	2	1	8	1.21281
71	1	2	4	8	1.21011
72	4	0	2	4	1.18187
73	3	2	3	8	1.18079
74	1	6	1	8	1.18017
75	2	0	4	4	1.17987
76	4	3	0	4	1.1675
77	4	1	2	8	1.16732
78	2	5	2	8	1.16591
79	2	1	4	8	1.1654
80	3	4	2	8	1.15251
81	2	4	3	8	1.15174
82	4	3	1	8	1.1399
83	0	5	3	4	1.13783
84	1	3	4	8	1.13766
85	4	2	2	8	1.12671
86	2	6	0	4	1.1256
87	0	6	2	4	1.12502
88	2	2	4	8	1.12498
89	3	5	1	8	1.11349
90	3	3	3	8	1.11319
91	1	5	3	8	1.11237
92	2	6	1	8	1.1008

93	1	6	2	8	1.1004
94	4	4	0	4	1.07876
95	0	4	4	4	1.07674
96	4	3	2	8	1.06754
97	2	3	4	8	1.06606
98	4	4	1	8	1.05688
99	4	0	3	4	1.05662
100	3	0	4	4	1.05579
101	1	4	4	8	1.05509
102	4	1	3	8	1.04619
103	3	5	2	8	1.04575
104	3	1	4	8	1.04538
105	2	5	3	8	1.04517
106	0	7	1	4	1.04508
107	0	1	5	4	1.04434
108	5	0	1	4	1.03704
109	3	4	3	8	1.03548
110	2	6	2	8	1.03522
111	1	0	5	4	1.03435
112	5	1	1	8	1.02717
113	1	7	1	8	1.02526
114	1	1	5	8	1.02455
115	4	2	3	8	1.01665
116	3	2	4	8	1.01591
117	5	2	1	8	0.99918
118	2	4	4	8	0.99723
119	1	6	3	8	0.9972
120	4	4	2	8	0.99843
121	1	2	5	8	0.99677
122	3	6	1	8	0.998
123	4	5	0	4	0.98972
124	2	7	0	4	0.98887
125	5	0	2	4	0.98166
126	2	0	5	4	0.97966
127	5	1	2	8	0.97328
128	4	5	1	8	0.97274
129	4	3	3	8	0.97254
130	2	7	1	8	0.97193
131	3	3	4	8	0.97189
132	1	7	2	8	0.97165
133	1	5	4	8	0.97135
134	2	1	5	8	0.97133
135	0	3	5	4	0.97106
136	5	3	1	8	0.95721
137	3	5	3	8	0.95599
138	1	3	5	8	0.95509
139	5	2	2	8	0.94937
140	3	6	2	8	0.94835
141	2	6	3	8	0.94792
142	2	2	5	8	0.94755
143	4	0	4	4	0.93356
144	0	8	0	2	0.93295
145	4	5	2	8	0.9266

146	4	1	4	8	0.92634
147	2	7	2	8	0.9259
148	2	5	4	8	0.92564
149	4	4	3	8	0.91944
150	3	4	4	8	0.91889

Table A.1: The d-values and hkl numbers from the first 150 reflections of $CaMnO_3$.

A.2 $Ca_2Mn_2O_5$:

I-reference	H	K	L	Multiplicity	D-value
1	0	2	0	2	5.11368
2	1	1	0	4	4.80266
3	0	0	1	2	3.75006
4	1	2	0	4	3.72586
5	0	2	1	4	3.02406
6	1	1	1	8	2.95574
7	1	3	0	4	2.88871
8	2	0	0	2	2.71987
9	1	2	1	8	2.64309
10	2	1	0	4	2.62851
11	0	4	0	2	2.55684
12	2	2	0	4	2.40133
13	1	4	0	4	2.31397
14	1	3	1	8	2.28847
15	2	0	1	4	2.20173
16	2	1	1	8	2.15242
17	2	3	0	4	2.12612
18	0	4	1	4	2.11254
19	2	2	1	8	2.02226
20	1	4	1	8	1.96925
21	1	5	0	4	1.91459
22	0	0	2	2	1.87503
23	2	4	0	4	1.86293
24	2	3	1	8	1.84954
25	3	1	0	4	1.7854
26	0	2	2	4	1.76042
27	1	1	2	8	1.74663
28	3	2	0	4	1.70899
29	1	5	1	8	1.70521
30	0	6	0	2	1.70456
31	1	2	2	8	1.67489
32	2	4	1	8	1.6684
33	2	5	0	4	1.63477
34	1	6	0	4	1.62657
35	3	1	1	8	1.61203
36	3	3	0	4	1.60089
37	1	3	2	8	1.57276
38	3	2	1	8	1.55512
39	0	6	1	4	1.55178
40	2	0	2	4	1.54374
41	2	1	2	8	1.52645
42	0	4	2	4	1.51203

43	2	5	1	8	1.49857
44	1	6	1	8	1.49225
45	3	4	0	4	1.47907
46	2	2	2	8	1.47787
47	3	3	1	8	1.47234
48	1	4	2	8	1.4568
49	2	6	0	4	1.44436
50	1	7	0	4	1.41104
51	2	3	2	8	1.40628
52	3	4	1	8	1.37591
53	4	0	0	2	1.35994
54	3	5	0	4	1.35687
55	4	1	0	4	1.34807
56	2	6	1	8	1.34784
57	1	5	2	8	1.33961
58	2	4	2	8	1.32155
59	1	7	1	8	1.32065
60	4	2	0	4	1.31425
61	3	1	2	8	1.29299
62	2	7	0	4	1.2871
63	4	0	1	4	1.27847
64	0	8	0	2	1.27842
65	3	5	1	8	1.27592
66	4	1	1	8	1.26859
67	4	3	0	4	1.26314
68	3	2	2	8	1.26307
69	0	6	2	4	1.26128
70	0	0	3	2	1.25002
71	1	8	0	4	1.24451
72	3	6	0	4	1.24195
73	4	2	1	8	1.24029
74	2	5	2	8	1.2322
75	1	6	2	8	1.22868
76	3	3	2	8	1.2175
77	2	7	1	8	1.21739
78	0	2	3	4	1.21427
79	0	8	1	4	1.21004
80	1	1	3	8	1.20971
81	4	4	0	4	1.20067
82	4	3	1	8	1.19706
83	1	2	3	8	1.1851
84	1	8	1	8	1.18117
85	3	6	1	8	1.17898
86	3	4	2	8	1.16126
87	2	8	0	4	1.15699
88	1	3	3	8	1.14722
89	2	6	2	8	1.14423
90	4	4	1	8	1.14349
91	3	7	0	4	1.13768
92	2	0	3	4	1.13581
93	4	5	0	4	1.13248
94	2	1	3	8	1.12887
95	1	7	2	8	1.12745

96	0	4	3	4	1.123
97	1	9	0	4	1.11236
98	2	2	3	8	1.10879
99	2	8	1	8	1.10557
100	4	0	2	4	1.10087
101	1	4	3	8	1.0998
102	3	5	2	8	1.09924
103	4	1	2	8	1.09454
104	3	7	1	8	1.08869
105	4	5	1	8	1.08413
106	5	1	0	4	1.08184
107	2	3	3	8	1.07758
108	4	2	2	8	1.07621
109	1	9	1	8	1.06643
110	5	2	0	4	1.06413
111	4	6	0	4	1.06306
112	2	7	2	8	1.06115
113	0	8	2	4	1.05627
114	2	9	0	4	1.04854
115	4	3	2	8	1.0476
116	1	5	3	8	1.04669
117	3	8	0	4	1.04484
118	5	1	1	8	1.03945
119	2	4	3	8	1.038
120	1	8	2	8	1.0369
121	5	3	0	4	1.03645
122	3	6	2	8	1.03542
123	3	1	3	8	1.02399
124	5	2	1	8	1.02371
125	4	6	1	8	1.02276
126	0	10	0	2	1.02274
127	4	4	2	8	1.01113
128	2	9	1	8	1.00981
129	3	2	3	8	1.00893
130	0	6	3	4	1.00802
131	3	8	1	8	1.0065
132	1	10	0	4	1.00513
133	5	4	0	4	1.00109
134	5	3	1	8	0.999
135	4	7	0	4	0.99545
136	2	5	3	8	0.99299
137	1	6	3	8	0.99115
138	0	10	1	4	0.9867
139	3	3	3	8	0.98525
140	2	8	2	8	0.98462
141	3	7	2	8	0.97264
142	1	10	1	8	0.97086
143	4	5	2	8	0.96939
144	5	4	1	8	0.96722
145	3	9	0	4	0.9629
146	4	7	1	8	0.96213
147	5	5	0	4	0.96053
148	2	10	0	4	0.9573

149	1	9	2	8	0.95668
150	3	4	3	8	0.95472

Table A.2: The d-values and hkl numbers from the first 150 reflections of $Ca_2Mn_2O_5$.

A.3 $CaMnO_{2.75}$:

I-reference	H	K	L	Multiplicity	D-value
1	0	1	0	2	0
2	0	2	0	2	0
3	0	0	1	2	7.45818
4	0	1	1	4	7.02702
5	0	3	0	2	6.99044
6	0	2	1	4	6.07761
7	1	0	0	2	5.34953
8	0	4	0	2	5.24283
9	1	1	0	4	5.18354
10	0	3	1	4	5.10033
11	1	2	0	4	4.76521
12	1	0	1	4	4.34695
13	0	4	1	4	4.28911
14	1	1	1	8	4.25647
15	1	3	0	4	4.2483
16	0	5	0	2	4.19427
17	1	2	1	8	4.01556
18	1	4	0	4	3.7444
19	0	0	2	2	3.72909
20	1	3	1	8	3.69143
21	0	1	2	4	3.67149
22	0	5	1	4	3.65582
23	0	2	2	4	3.51351
24	0	6	0	2	3.49522
25	1	4	1	8	3.34634
26	1	5	0	4	3.30071
27	0	3	2	4	3.29021
28	0	6	1	4	3.16491
29	1	0	2	4	3.05917
30	0	4	2	4	3.03881
31	1	1	2	8	3.02713
32	1	5	1	8	3.01833
33	0	7	0	2	2.9959
34	1	2	2	8	2.93674
35	1	6	0	4	2.92603
36	1	3	2	8	2.80255
37	0	5	2	4	2.78687
38	0	7	1	4	2.78
39	1	6	1	8	2.7239
40	2	0	0	2	2.67477
41	2	1	0	4	2.65327
42	1	4	2	8	2.64226
43	0	8	0	2	2.62142
44	1	7	0	4	2.61391
45	2	2	0	4	2.59177

46	0	6	2	4	2.55017
47	2	0	1	4	2.51775
48	2	1	1	8	2.49979
49	2	3	0	4	2.49814
50	0	0	3	2	2.48606
51	0	8	1	4	2.4731
52	1	5	2	8	2.47159
53	0	1	3	4	2.46877
54	1	7	1	8	2.46679
55	2	2	1	8	2.44816
56	0	2	3	4	2.419
57	2	4	0	4	2.38261
58	2	3	1	8	2.36879
59	1	8	0	4	2.35398
60	0	3	3	4	2.34234
61	0	7	2	4	2.33554
62	0	9	0	2	2.33015
63	1	6	2	8	2.30198
64	2	4	1	8	2.26961
65	2	5	0	4	2.25521
66	1	0	3	4	2.2545
67	0	4	3	4	2.24631
68	1	8	1	8	2.24482
69	1	1	3	8	2.24158
70	0	9	1	4	2.22412
71	1	2	3	8	2.20413
72	2	0	2	4	2.17347
73	2	1	2	8	2.16189
74	2	5	1	8	2.15868
75	1	3	3	8	2.14567
76	0	8	2	4	2.14456
77	1	7	2	8	2.14044
78	0	5	3	4	2.13861
79	1	9	0	4	2.13629
80	2	2	2	8	2.12823
81	2	6	0	4	2.12415
82	0	10	0	2	2.09713
83	2	3	2	8	2.07547
84	1	4	3	8	2.07113
85	2	6	1	8	2.04291
86	1	9	1	8	2.0537
87	0	6	3	4	2.02587
88	0	10	1	4	2.01884
89	2	4	2	8	2.00778
90	2	7	0	4	1.99526
91	1	8	2	8	1.99056
92	1	5	3	8	1.9858
93	0	9	2	4	1.97609
94	1	10	0	4	1.95246
95	2	5	2	8	1.92976
96	2	7	1	8	1.92747
97	0	7	3	4	1.91315
98	0	11	0	2	1.90648

99	1	6	3	8	1.89457
100	1	10	1	8	1.88881
101	2	8	0	4	1.8722
102	0	0	4	2	1.86454
103	0	1	4	4	1.85722
104	1	9	2	8	1.85366
105	0	11	1	4	1.84709
106	2	6	2	8	1.84572
107	0	2	4	4	1.83575
108	0	10	2	4	1.82791
109	2	0	3	4	1.82097
110	2	8	1	8	1.81586
111	2	1	3	8	1.81414
112	0	8	3	4	1.80386
113	0	3	4	4	1.80156
114	1	7	3	8	1.80141
115	1	11	0	4	1.79585
116	2	2	3	8	1.79412
117	3	0	0	2	1.78318
118	3	1	0	4	1.77677
119	2	3	3	8	1.76216
120	1	0	4	4	1.76066
121	2	7	2	8	1.75926
122	3	2	0	4	1.75794
123	2	9	0	4	1.75695
124	0	4	4	4	1.75676
125	1	1	4	8	1.75449
126	0	12	0	2	1.74761
127	1	11	1	8	1.74595
128	1	2	4	8	1.73636
129	3	0	1	4	1.7343
130	1	10	2	8	1.72972
131	3	1	1	8	1.7284
132	3	3	0	4	1.72785
133	2	4	3	8	1.72017
134	3	2	1	8	1.71105
135	2	9	1	8	1.71014
136	1	8	3	8	1.7093
137	1	3	4	8	1.70734
138	0	5	4	4	1.70378
139	0	12	1	4	1.70152
140	0	9	3	4	1.70011
141	0	11	2	4	1.69751
142	3	4	0	4	1.6882
143	3	3	1	8	1.68327
144	2	8	2	8	1.67317
145	2	5	3	8	1.67034
146	1	4	4	8	1.66906
147	1	12	0	4	1.66121
148	2	10	0	4	1.65035
149	3	4	1	8	1.64655
150	0	6	4	4	1.6451

Table A.3: The d-values and hkl numbers from the first 150 reflections of $CaMnO_{2.75}$.

A.4 $SrMnO_3$:

I-reference	H	K	L	Multiplicity	D-value
1	1	0	0	6	4.71364
2	0	0	2	2	4.53424
3	1	0	1	12	4.18239
4	1	0	2	12	3.26777
5	1	1	0	6	2.72142
6	1	0	3	12	2.54454
7	2	0	0	6	2.35682
8	1	1	2	12	2.3334
9	2	0	1	12	2.28104
10	0	0	4	2	2.26712
11	2	0	2	12	2.09119
12	1	0	4	12	2.04309
13	2	0	3	12	1.85865
14	2	1	0	12	1.78159
15	2	1	1	24	1.74817
16	1	1	4	12	1.74188
17	1	0	5	12	1.69271
18	2	1	2	24	1.65818
19	2	0	4	12	1.63389
20	3	0	0	6	1.57121
21	3	0	1	12	1.54815
22	2	1	3	24	1.53484
23	0	0	6	2	1.51141
24	3	0	2	12	1.4846
25	1	0	6	12	1.43923
26	2	0	5	12	1.43735
27	2	1	4	24	1.40081
28	3	0	3	12	1.39413
29	2	2	0	6	1.36071
30	1	1	6	12	1.32131
31	3	1	0	12	1.30733
32	2	2	2	12	1.30329
33	3	1	1	24	1.29395
34	3	0	4	12	1.29139
35	2	0	6	12	1.27227
36	2	1	5	24	1.27097
37	3	1	2	24	1.25616
38	1	0	7	12	1.24918
39	3	1	3	24	1.19992
40	3	0	5	12	1.18756
41	4	0	0	6	1.17841
42	4	0	1	12	1.16858
43	2	2	4	12	1.1667
44	2	1	6	24	1.15254
45	4	0	2	12	1.14052
46	2	0	7	12	1.13529
47	0	0	8	2	1.13356
48	3	1	4	24	1.13252
49	1	0	8	12	1.10214
50	4	0	3	12	1.09793

51	3	0	6	12	1.08926
52	3	2	0	12	1.08138
53	3	2	1	24	1.07389
54	3	1	5	24	1.06064
55	3	2	2	24	1.05199
56	2	1	7	24	1.04788
57	1	1	8	12	1.04652
58	4	0	4	12	1.04571
59	4	1	0	12	1.02871
60	4	1	1	24	1.02216
61	2	0	8	12	1.02165
62	3	2	3	24	1.0183
63	2	2	6	12	1.01137
64	4	1	2	24	1.00322
65	3	0	7	12	0.99965
66	3	1	6	24	0.98887
67	4	0	5	12	0.98826
68	1	0	9	12	0.98545
69	3	2	4	24	0.97614
70	4	1	3	24	0.97387
71	2	1	8	24	0.95648
72	5	0	0	6	0.94283
73	5	0	1	12	0.93777
74	4	1	4	24	0.9368
75	4	0	6	12	0.92942
76	3	2	5	24	0.92892
77	2	0	9	12	0.92658
78	5	0	2	12	0.92309
79	3	1	7	24	0.9203
80	3	0	8	12	0.91938
81	3	3	0	6	0.90724
82	0	0	10	2	0.90694
83	5	0	3	12	0.90007
84	4	1	5	24	0.89482
85	4	2	0	12	0.89089
86	1	0	10	12	0.89061
87	3	3	2	12	0.88961
88	4	2	1	24	0.88662
89	3	2	6	24	0.87955
90	2	1	9	24	0.87714
91	4	2	2	24	0.87418
92	4	0	7	12	0.87181
93	2	2	8	12	0.87103
94	5	0	4	12	0.87056
95	1	1	10	12	0.86042
96	3	1	8	24	0.85653
97	4	2	3	24	0.85456
98	4	1	6	24	0.85045
99	3	0	9	12	0.84827
100	5	1	0	12	0.84668
101	2	0	10	12	0.84644
102	5	1	1	24	0.84302
103	3	3	4	12	0.84231

104	5	0	5	12	0.83657
105	5	1	2	24	0.8323
106	3	2	7	24	0.83026
107	4	2	4	24	0.82918
108	4	0	8	12	0.81703
109	5	1	3	24	0.81531
110	1	0	11	12	0.81216
111	2	1	10	24	0.80826
112	4	1	7	24	0.80565
113	5	0	6	12	0.79997
114	4	2	5	24	0.79965
115	3	1	9	24	0.79815
116	5	1	4	24	0.79319
117	3	0	10	12	0.7855
118	6	0	0	6	0.78569
119	6	0	1	12	0.78276
120	3	2	8	24	0.78253
121	2	0	11	12	0.77825
122	3	3	6	12	0.77788
123	4	3	0	12	0.775
124	6	0	2	12	0.77416
125	4	3	1	24	0.77219

Table A.4: The d-values and hkl numbers from the first 150 reflections of $SrMnO_3$.

A.5 $Sr_2Mn_2O_5$:

I-reference	H	K	L	Multiplicity	D-value
1	0	0	2	2	6.26595
2	0	2	0	2	5.38967
3	1	1	0	4	4.92049
4	1	2	0	4	3.85982
5	0	0	1	2	3.81433
6	1	0	1	8	3.64158
7	0	2	1	4	3.1135
8	0	0	4	2	3.13298
9	1	1	1	8	3.01462
10	1	3	0	4	3.01301
11	1	0	3	8	2.8133
12	2	0	0	2	2.76514
13	1	2	1	8	2.71308
14	0	4	0	2	2.69483
15	2	1	0	4	2.67842
16	1	1	0	4	2.69111
17	2	2	0	4	2.46025
18	1	1	2	8	2.4727
19	1	4	0	4	2.42253
20	1	3	1	8	2.36435
21	2	0	1	4	2.23876
22	0	4	1	4	2.20095
23	2	1	1	8	2.19198
24	2	3	0	4	2.19136

25	2	2	1	8	2.06749
26	1	0	5	8	2.09322
27	0	0	6	2	2.08865
28	1	4	1	8	2.04495
29	1	1	4	8	2.0414
30	1	5	0	4	2.00864
31	2	4	0	4	1.92991
32	0	0	2	2	1.90717
33	2	3	1	8	1.90011
34	2	0	0	4	1.9029
35	3	1	0	4	1.81705
36	0	2	2	4	1.79792
37	0	6	0	2	1.79656
38	2	0	2	8	1.82079
39	1	1	2	8	1.77826
40	1	5	1	8	1.77727
41	3	2	0	4	1.74422
42	2	4	1	8	1.72204
43	1	2	2	8	1.70983
44	1	6	0	4	1.70866
45	2	5	0	4	1.70019
46	2	1	1	16	1.68652
47	3	1	1	8	1.64042
48	3	3	0	4	1.64016
49	1	1	6	8	1.65
50	0	6	1	4	1.6253
51	1	3	2	8	1.61147
52	2	0	4	8	1.62641
53	1	0	7	8	1.61998
54	3	2	1	8	1.58624
55	2	0	2	4	1.56996
56	1	6	1	8	1.55935
57	0	4	2	4	1.55675
58	2	1	2	8	1.55357
59	2	5	1	8	1.55291
60	2	1	3	16	1.5762
61	0	0	8	2	1.56649
62	3	4	0	4	1.5215
63	2	2	2	8	1.50731
64	3	3	1	8	1.50677
65	2	6	0	4	1.50651
66	1	4	2	8	1.49851
67	1	7	0	4	1.48347
68	2	3	2	8	1.43863
69	3	4	1	8	1.41322
70	2	6	1	8	1.40118
71	3	5	0	4	1.40106
72	2	1	5	16	1.40804
73	2	0	6	8	1.40665
74	1	5	2	8	1.38305
75	4	0	0	2	1.38257
76	1	7	1	8	1.38259
77	4	1	0	4	1.37134

78	2	4	2	8	1.35654
79	0	8	0	2	1.34742
80	2	7	0	4	1.34535
81	4	2	0	4	1.33921
82	1	1	8	8	1.35383
83	2	2	0	4	1.34555
84	3	1	2	8	1.31555
85	3	5	1	8	1.31515
86	1	8	0	4	1.30912
87	0	6	2	4	1.30771
88	4	0	1	4	1.29982
89	2	2	2	8	1.31556
90	4	1	1	8	1.29047
91	4	3	0	4	1.29034
92	1	0	9	8	1.30766
93	3	2	2	8	1.28711
94	3	6	0	4	1.28661
95	1	6	2	8	1.27262
96	0	0	3	2	1.27144
97	0	8	1	4	1.27048
98	2	5	2	8	1.26911
99	2	7	1	8	1.26875
100	4	2	1	8	1.26359
101	3	0	1	8	1.26215
102	3	3	2	8	1.24355
103	1	8	1	8	1.23822
104	0	2	3	4	1.23748
105	0	0	10	2	1.25319
106	1	1	3	8	1.23101
107	4	4	0	4	1.23012
108	4	3	1	8	1.2223
109	2	2	4	8	1.23635
110	3	6	1	8	1.21912
111	2	1	7	16	1.23352
112	2	8	0	4	1.21126
113	1	2	3	8	1.20761
114	3	0	3	8	1.21386
115	2	0	8	8	1.20941
116	3	4	2	8	1.18938
117	3	1	0	8	1.2035
118	2	6	2	8	1.18218
119	3	7	0	4	1.18182
120	1	3	3	8	1.17142
121	1	7	2	8	1.17094
122	4	4	1	8	1.17075
123	1	9	0	4	1.17057
124	3	1	2	16	1.1819
125	4	5	0	4	1.16381
126	2	0	3	4	1.15518
127	2	8	1	8	1.15445
128	0	4	3	4	1.14989
129	2	1	3	8	1.1486
130	2	2	3	8	1.12952

131	3	5	2	8	1.12913
132	3	7	1	8	1.12887
133	1	4	3	8	1.12581
134	1	1	10	8	1.13605
135	4	0	2	4	1.11938
136	1	9	1	8	1.11906
137	3	0	5	8	1.13187
138	2	2	6	8	1.13115
139	4	1	2	8	1.11339
140	4	5	1	8	1.11315
141	3	1	4	16	1.12346
142	0	8	2	4	1.10048
143	5	1	0	4	1.10028
144	2	3	3	8	1.09974
145	2	7	2	8	1.09935
146	2	9	0	4	1.09904
147	4	2	2	8	1.09599
148	4	6	0	4	1.09568
149	3	8	0	4	1.08781
150	5	2	0	4	1.08348

Table A.5: The d-values and hkl numbers from the first 150 reflections of $Sr_2Mn_2O_5$.

References

1. Reller, A., *Superstructures formed by the ordering of vacancies in a selective oxidation catalyst.* Proc. Royal Society London A, 1984. **394**: p. 223-241.
2. Jonker and van Saten, *Ferromagnetic Compounds of Manganese with Perovskite Structure.* Physica XVI, 1950. **No3**.
3. MacChessney, *Magnetic Study of Manganate phases.* Physical Review, 1967. **164**(No 2).
4. Poeppelmeier, K., *Structure Determination of CaMnO3 and CaMnO2.5 by x-ray and Neutron methods.* Journal of Solid State Chemistry, 1982. **45**: p. 71-79.
5. Poeppelmeier, K., *CaMnO2.5 and Ca2MnO3.5: New Oxygen-Defect Perovskite Type Oxides.* Journal of Solid State Chemistry, 1982. **44**: p. 89-98.
6. Chiang, P., *Structural investigation of oxygen-deficient perovskite CaMnO2.75.* Material Letters, 1991. **12**: p. 102-108.
7. Taguchi, *Electrical properties of $CaMnO_{3-x}$.* Phys Stat Solidi, 1985. **(a) 88**(K 79).
8. Taguchi, *High-Temperature Phase Transition of $CaMnO_{3-\delta}$.* Journal of Solid State Chemistry, 1989(78): p. 312-313.
9. Britatico, *Double-Exchange interaction in electron-doped $CaMnO_{3-\delta}$ perovskites.* Physical Review, 1996. **53**(No 21): p. 14020-14023.
10. Zeng and Greenbladt, *Large Magneto resistance in antiferromagnetic $CaMnO_{3-\delta}$.* Physical Review B, 1999. **59**(No 13): p. 8784 - 8788.
11. Syono, Y., *Structural Relations of Hexagonal Perovskite-Like ABX_3 at High Pressure.* Journal of Physical Society of Japan, 1969. **26**(No 4).
12. Chamberland, *Preperation and Characterization of $BamNO_3$ and $SrMnO_3$ Polytypes.* Journal of Solid State Chemistry, 1970(1): p. 506 - 511.
13. Negas, T. and R. Roth, *The System of $SrMnO_{3-x}$.* Journal of Solid State Chemistry, 1970(1): p. 409 - 418.
14. Kuroda, *The Crystal Structure of α-$SrMnO_3$.* Journal of Solid State Chemistry, 1981(1): p. 297 - 299.

15. Kriegel and Preuss, *Dilatometric determination of phase transition temperatures and oxidation temperatures on the compounds $SrMnO_{3-y}$ and Sr_2MnO_{4-y}.* Thermochimica Acta, 1996(285): p. 91 - 98.
16. Battle and Gibb, *The Structural and Magnetic Properties of $SrMnO_3$: A Reinvestigation.* Journal of Solid State Chemistry, 1988(74): p. 60 - 66.
17. Shibahara, *Electron microscope study of the structure of $SrMnO_{3-x}$ with planar defect.* Journal of Material Research, 1991. **6**(3): p. 565 - 573.
18. Sedmidubsky, D., *Structural and Phase Relations in the Sr-Mn-O System.* Solid State Phenomena, 2003. **90-91**: p. 427 - 432.
19. Caignaert, V., *$Sr_2Mn_2O_{2.5}$, An Oxygen-Defect Perovskite with Mn(III) In Square Pyramidal Coordination.* Material Research Bulletin, 1985. **20**: p. 479 - 484.
20. Caignaert, V., *The Oxygen Defect Perovskite $Sr_2Mn_2O_{2.5}$: HREM Study.* Journal of Solid State Chemistry, 1986(62): p. 281 - 289.
21. Mori, T., *Neutron Diffraction Study of $Sr_2Mn_2O_{2.5}$.* Journal of Alloys and Compounds, 2000(296): p. 92 - 97.
22. Rietveld H, M., *Line profiles of Neutron powder-diffraction peaks for structure refinements.* Acta Crystalographica, 1967. **22**: p. 151-152.
23. Rietveld H, M., *A profile refinement method for nuclear and magnetic structures.* Journal of Applied Crystalography, 1969. **2**: p. 65 - 71.
24. Kisi, *Rietveld Analysis of Powder Diffraction Patterns.* Materials Forum, 1994. **18**: p. 135 - 153.
25. Le Bail, A., *The ab-initio structure determination of LiSbWO6 by X-ray powder diffraction.* Material Research Bulletin, 1988(23): p. 447-452.
26. Ling, C., J.J. Neimeier, and D. Argyriou, *Observation of Antiferromagnetism in Marokite $CaMn_2O_4$.* Journal of Solid State Chemistry, 2001(160): p. 167-173.
27. Negas, T. and R. Roth, *Strontium Manganese Oxide (cubic).* National Bureau of Standards monograph, 1972. **10**: p. 58.
28. Kriegel, R., *Untersuchung zur Aniondefektverteilung in Sr_2MnO_{4-y}.* Zeitung Naturforchung, 1992. **48**: p. 15-18.
29. MacChesney, *Magnetic Study of Manganate phases.* Physical Review, 1967. **164**(No 2).

30. MacChesney, *Electric and Magnetic Properties of the Strontium Ferrates.* Journal of Chemical Physics, 1965. **43**: p. 1907-1913.
31. Hong, S. and S. A., *Crystal Structure of 4H $BaRuO_3$: High Pressure phase Prepared at Ambient Pressure.* Journal of Solid State Chemistry, 1997. **12**: p. 251-255.
32. Zalkin, A., *Crystal structure of $CsMnF_3$.* Journal of Chemical Physics, 1962. **37**: p. 697-699.
33. Shapira, Y., *Magnetic phase boundaries of $CsMnF_3$.* Physical Review B, 1980. **21**(3): p. 1271-1274.
34. Cussen, E.J. and P.D. Battle, *Crystal and Magnetic Structures of 2H $BaMnO_3$.* Chemical Materials, 2000. **12**(3).
35. Jordan, N.A., *Structural chemistry and magnetic properties of 6H and 15R hexagonal perovskites $BaIr_xFe_{1-x}O_{3-\delta}$.* Journal of Materials Chemistry, 2003. **13**: p. 2617-2625.